NASA Contractor Report 182126

Cyclic Fatigue Damage Characteristics Observed for Simple Loadings Extended to Multiaxial Life Prediction

David J. Jones and Peter Kurath
University of Illinois
Urbana, Illinois

June 1988

Prepared for
Lewis Research Center
Under Grant NAG3-465

National Aeronautics and
Space Administration

Cyclic Fatigue Damage Characteristics Observed for Simple Loadings Extended to Multiaxial Life Prediction

David J. Jones and Peter Kurath
University of Illinois
Department of Mechanical Engineering
Urbana, Illinois

SUMMARY

Fully reversed uniaxial strain controlled fatigue tests were performed on smooth cylindrical specimens made of 304 stainless steel. Fatigue life data and cracking observations for uniaxial tests were compared with life data and cracking behavior observed in fully reversed torsional tests. It was determined that the product of maximum principal strain amplitude and maximum principal stress (Smith, Watson, Topper parameter) provided the best correlation of fatigue lives for these two loading conditions. Implementation of this parameter is in agreement with observed physical damage and it accounts for the variation of stress-strain response, which is unique to specific loading conditions.

Biaxial fatigue tests were conducted on tubular specimens employing both in-phase and out-of-phase tension-torsion cyclic strain paths. Cracking observations indicated that the physical damage which occurred in the biaxial tests was similar to the damage observed in uniaxial and torsional tests. The Smith, Watson, Topper parameter was then extended to predict the fatigue lives resulting from the more complex loading conditions. The correlation of the biaxial fatigue lives with experimental data was within a factor of 2½, when strain hardening due to out-of-phase loading was incorporated into the life estimation analysis.

ACKNOWLEDGMENTS

Funding for this research was provided by N.A.S.A under Grant No. NAG 3-465. Julie Bannantine is thanked for her insightful advice stemming from her previous research. Kent Elam expertly machined all specimens. Matt Bohnert is thanked for his assistance in examining the replica data.

TABLE OF CONTENTS

Page

SUMMARY i
ACKNOWLEDGMENTS ii
LIST OF SYMBOLS v
1. INTRODUCTION 1
1.1 Background 1
1.1.1 Material 1
1.1.2 Fatigue Testing 2
1.1.3 Purpose and Scope 6

2. EXPERIMENTAL PROGRAM 8
2.1 Test System 8
2.2 Specimen Description 8
2.3 Test Program 9
2.4 Crack Observations 9

3. DISCUSSION 11
3.1 Uniaxial and Torsional Results 11
3.1.1 Surface Crack Observations 11
3.1.2 Fracture Surface Observations 12
3.1.3 Selection of Damage Parameter 13
3.2 Multiaxial Results 17
3.2.1 Analysis of Biaxial Paths 17
3.2.2 Biaxial Surface Crack Observations 19
3.2.3 Biaxial Fatigue Life Predictions 21

4. CONCLUSIONS 24

LIST OF REFERENCES 26

TABLES 29

FIGURES 34

APPENDIX A 64

APPENDIX B 81

LIST OF SYMBOLS

b	Fatigue strength
C	Smith, Watson, Topper Coefficient
c	Fatigue ductility exponent
m	Material constant
E	Linear elastic modulus
G	Shear modulus
K, K'	Monotonic, cyclic strength coefficient
$2N_f, N_f$	Number of reversals cycles to failure
N_t	Transition fatigue life, cycles
n, n'	Monotonic, cyclic strain hardening exponent
β	Smith, Watson, Topper exponent
γ	Torsional strain
$\hat{\gamma}$	Maximum shear strain amplitude
γ_f'	Torsional fatigue shear ductility coefficient
$\Delta\varepsilon_1^{max}$	Maximum principal strain amplitude
$\Delta\varepsilon_e$	Elastic strain amplitude
$\Delta\varepsilon_p$	Plastic strain amplitude
$\Delta\varepsilon_t$	Total strain amplitude
ε	Axial strain
$\Delta\varepsilon_1'$	Principal strain amplitude on secondary plane
$\varepsilon_1, \varepsilon_2, \varepsilon_3$	Principal strains
ε_f'	Fatigue ductility coefficient
$\hat{\varepsilon}_n$	Strain amplitude normal to the plane of maximum shear strain amplitude
σ	Axial stress
$\Delta\sigma_a$	Cyclic axial stress range
σ_1^{max}	Maximum principal stress on plane of maximum principal strain amplitude

σ_f'	Fatigue strength coefficient
$\hat{\sigma}_{no}$	Mean stress normal to the plane of maximum shear strain amplitude
τ	Torsional stress

INTRODUCTION

Fatigue due to cyclic loading must often be considered when designing components for structures and machinery. Accurate fatigue life predictions are imperative to insure safety and component reliability. Often a component subjected to a multiaxial state of stress and/or strain which may radically alter the fatigue life for a given material. Uniaxial cyclic loading is a common test procedure. Correlation of uniaxial fatigue data to other stress or strain states is useful in the development of multiaxial life prediction models. In order to develop a relation between fatigue lives under uniaxial and multiaxial stress states, it would be useful to first correlate uniaxial and torsional test data.

Cyclic biaxial tension-torsion loading has been categorized as either in-phase or out-of-phase. In-phase loading occurs when the axial and torsional loading signals are applied such that no phase lag exists between them. Out-of-phase loading is characterized by a phase difference between the command signals. Phenomenological observations such as crack growth and crack direction can be used to justify the extension of life prediction models developed for uniaxial and torsional loadings to life prediction for more complex multiaxial loadings.

1.1 Background

1.1.1 Material

In 1913, Harry Brearely of Sheffield, England observed that an experimental steel containing 0.25% carbon and 13% chromium did not rust when exposed to the atmosphere. Because of its resistance to corrosion, this material became known as stainless steel, and was subsequently developed for use in aircraft engine exhaust valves during World War I. Since that time, a variety of stainless steels have been developed with applications ranging from

cutlery to turbine blades [1]. The ASM committee on Wrought Stainless Steels characterizes stainless steel as any ferrous alloy containing a minimum of 10% chromium. Additional alloying elements such as nickel, molybdenum and titanium may be added to enhance the mechanical properties, while maintaining corrosive resistance [2].

It is the resistance to corrosion that makes stainless steel attractive for many specialized uses. The corrosion resistance of stainless steel results from the interaction of chromium and oxygen to form a protective film on the surface of the metal [3]. Within the family of stainless steels there are martensitic, ferritic, austenitic, and precipitation hardenable microstructures which depend on alloying elements and heat treatment. Stainless steels are commonly used in higher temperature environments (400°-1200°C) because of their ability to resist corrosion and scaling. Additionally at these temperatures stainless steel retains a greater percentage of its room temperature mechanical properties than do other materials such as steel and aluminum. For example, at 300°C, the tensile strength of 316 stainless steel is 87% of its tensile strength at room temperature [4].

An austenitic 304 stainless steel was chosen for this investigation. Its chemical composition is reported in Table 1. This can be compared with the ASM specifications for variations in chemical composition that are allowable for the 304 stainless steel category. Type 304 is one of the most commonly used stainless steels because of its relatively low cost and ability to resist corrosion at temperatures up to 400°C without a severe reduction in mechanical properties [3]. Applications of 304 stainless steel include heat exchangers, pressure vessels, and cookware.

1.1.2 Fatigue Testing

Since 1850 it has been documented that components in structures and machinery have failed due to repeated loadings. These failures caused considerable concern among designers and have resulted in much conjecture with regard to their origin [5]. The earliest laboratory experiments involved the examination of varying cyclic stress levels on specimen fatigue life. In 1856 Wohler [6] conducted stress controlled cyclic loading tests on railroad axle steel using a rotating bending test fixture. He reported his data by plotting stress amplitude versus cycles to failure (S-N curve). It was observed that below a certain stress amplitude the material seemed to have an infinite life (greater than 10^6 cycles). This stress level became known as the endurance limit, and was the scope of much of the early research done in fatigue.

In 1910, Basquin [7] proposed the following relation between the fully reversed stress amplitude and the fatigue life:

$$\frac{\Delta\sigma_a}{2} = \sigma_f'(2N_f)^b \qquad (1)$$

Later investigators modified Basquin's relation to correspond to the elastic strain amplitude $\Delta\varepsilon_e/2 = \Delta\sigma_a/(2E)$. This relation is appropriate when the elastic strain amplitude is at least an order of magnitude greater than the plastic strain amplitude. Coffin [8] referred to this regime as high cycle fatigue (HCF).

In 1954, Coffin [9] and Manson [10] introduced a relation between the plastic strain amplitude and the fatigue life, which is similar to Basquin's relation for the stress amplitude.

$$\frac{\Delta\varepsilon_p}{2} = \varepsilon_f'(2N_f)^c \qquad (2)$$

This parameter is applicable for low cycle fatigue (LCF) which is defined by Committee E9 of A.S.T.M. as "...characterized by the presence of macroscopic cyclic plastic strains... as evidenced by a stress strain hysteresis loop" [11]. Manson later argued that the fatigue resistance of a material, which was subjected to an arbitrary strain level, could be characterized by the elastic and plastic strain components. Therefore the above equations were combined and the total strain amplitude was expressed as:

$$\frac{\Delta\varepsilon_t}{2} = \frac{\Delta\varepsilon_e}{2} + \frac{\Delta\varepsilon_p}{2} = \frac{\sigma_f'}{E}(2N_f)^b + \varepsilon_f'(2N_f)^c \qquad (3)$$

As early as 1886 investigators have considered the problems of fatigue due to complex multiaxial cyclic loading. A review of multiaxial fatigue investigations is found in Refs. 12 through 14. One of the earliest investigations was conducted by Lanza [15], who examined the effect of combined torsion and bending on shafts. He compared his experimental data with the existing design criterion and found that these criterion were nonconservative for fatigue loading.

The determination of long life fatigue characteristics was the object of much of the early research in multiaxial fatigue. As with uniaxial fatigue, long life damage analysis for multiaxial fatigue has been based on the cyclic stress excursion. An example of a stress based multiaxial fatigue life estimation criterion is the relation proposed by Guest [16].

$$(\sigma_1 - \sigma_2) + m(\sigma_1 + \sigma_2) = \text{constant} \qquad (4)$$

Later researchers suggested that the fatigue life of ductile materials will be dependent on the maximum shear stress resulting from cyclic loading, while the maximum principal stress will determine the fatigue life for brittle materials [14].

As design criterion became more demanding and the need for component reliability increased, a corresponding need for accurate multiaxial low cycle life prediction models resulted. Both stress based and strain based parameters have been used to analyze low cycle fatigue data. Brown and Miller [17] have suggested that a strain based parameter is most appropriate for multiaxial fatigue correlation. They argue that fatigue crack growth is a localized phenomenon and is constrained by the deformation of the bulk material surrounding the crack tip. As a result bulk strains are assumed to control fatigue crack growth.

Many of the investigations in biaxial fatigue have employed loading paths for which both load channels (e.g., axial and torsional) are applied simultaneously with no difference in phase or frequency. These are denoted as in-phase loading paths. The first out-of-phase fatigue tests were conducted by Mason and Delaney [18] in 1921. They applied bending and torsion stresses with a phase difference of 90° and noted that the fatigue life was less than if each component of the stress was applied separately.

Fatigue failure analysis was greatly enhanced as researchers began to examine crack formation and growth. Ewing and Humphrey [19] were among the earliest investigators to systematically examine and document surface crack formation of a cyclically loaded laboratory specimen. The principal aspect of their research involved the examination of slip lines and their effect on fatigue crack formation. This research and similar investigations have caused many to view fatigue as a two stage process: initiation and propagation.

Forsyth [20] noted that slip band cracking is dependent on the shear stress range acting on the slip plane. Therefore, he predicted that cracks would initiate on planes of maximum shear stress, which he referred to as Stage I cracking. He states "Thus cracks will form on those planes most closely aligned with the maximum shear stress directions in the component fatigue specimen." [20]. Fatigue crack propagation can occur on the same plane as crack initiation or it can occur on planes perpendicular to the maximum principal stress. Forsyth referred to propagation perpendicular to principal stress planes as Stage II crack growth. The characterization of fatigue as a two stage process has required investigators to examine and define crack initiation and propagation. Estimates for initiated cracks have ranged from 10^{-4} mm to 2.5 mm [21].

1.1.3 Purpose and Scope

Both uniaxial and biaxial (in-phase and out-of-phase) fatigue tests were performed. Smooth cylindrical specimens were used for uniaxial testing, while thin walled tubes were employed for all the other tests. Surface fatigue crack development for all tests was monitored via surface replication procedures. Fracture surfaces from uniaxial tests were examined employing scanning electron microscopy. Fatigue life data and cracking observations from uniaxial testing were compared with previous results [22] from fully reversed torsional loading. It was determined that a good correlation between these two tests is possible implementing a damage parameter which employs the product of the maximum principal strain amplitude and the maximum principal stress. This parameter was first proposed by Smith, Watson, and Topper [23]. Similarities in the cracking behavior were used to substantiate the implementation of this damage parameter. This parameter was then employed to analyze more complex biaxial fatigue strain paths. Surface cracking charac-

teristics were used to justify the extension of the Smith, Watson, and Topper parameter (SWT) for 304 Stainless Steel subjected to more complex multiaxial loadings.

2. EXPERIMENTAL PROGRAM

2.1 Test System

Strain controlled tests were conducted on 304 stainless steel uniaxial specimens using a two post axial servo-hydraulic test frame with a 90 KN load cell. An axial clip on extensometer with a 12.7 mm gage length was used to measure strain. Test control and data acquisition were achieved with a microcomputer system. Resolution of the load and strain signals were 20 N (~.7MPa) and 5 X 10^{-6}mm/mm respectively.

A stiffened servo-hydraulic tension-torsion test frame with 222 KN axial capacity and 2.25 KN-m torsional capacity was used to perform biaxial strain controlled tests on tubular specimens. Signal generation and data acquisition were also accomplished with a microcomputer. An internal extensometer was used to measure both axial and torsional strains [24]. Resolution of the axial and torsional loads were 0.01 KN and 0.07 N-m respectively. Axial and torsional strains were resolved to 1.0 x 10^{-4}mm/mm and 2.0 x 10^{-4} mm/mm respectively.

2.2 Specimen Description

Uniaxial fatigue and monotonic test specimens were designed in accordance with ASTM E-606 and ASTM A-370 respectively. A 15 mm gauge length and 6.35 mm gauge diameter were chosen for this investigation. Tubular specimens with a 25.4 mm gage length, 33 mm outer diameter and a 25.4 mm inner diameter were used for all other testing. Specimen details are depicted in Figs. 1 and 2. Specimen surfaces were polished to a 0.3 micron finish to achieve specimen uniformity. This also relieves residual surface stresses induced during machining, and assures a smooth surface to facilitate acetate tape crack replication procedures.

2.3 Test Program

Monotonic tensile tests were performed on two specimens. Baseline material properties from these tests are reported in Table 2. Constant amplitude fully reversed strain controlled tests were performed on eight 304 stainless steel uniaxial specimens. Cyclic data was recorded at logarithmic intervals. Failure was defined as a 50% load drop from the maximum tensile load experienced by the specimen on the last recorded cycle. This failure criteria usually corresponded to complete separation of the specimen. Strain amplitudes and fatigue lives of the uniaxial specimens tested are listed in Table 3. Data from uniaxial tests was compared with previous data from fully reversed torsional tests [22].

Eight tubular specimens were tested in biaxial fatigue using strain as the controlled parameter. Four different biaxial strain paths (C, N, P and Q) were employed and are shown in Fig. 3. For strain amplitudes examined, the resulting fatigue lives were on the order of 10^5 to 10^6 cycles. This was combined with data from a previous investigation in which, for the same biaxial strain paths, the fatigue lives were on the order of 10^3 to 10^4 cycles [22]. Again data was recorded at logarithmic intervals. An axial load drop of 10 percent, from the previously recorded cycle, was used to define specimen failure. This failure criteria corresponded to a failure crack length of at least 3 mm.

2.4 Crack Observations

Surface crack growth was monitored using an acetyl cellulose film replicating procedure to record surface features of the specimen at cyclic intervals corresponding to approximately 10% of estimated fatigue life. Acetate film was dissolved on the specimen surface by applying acetone between the film and specimen surface with a syringe. The film was then allowed to

solidify for approximately 1½ minutes. When removed from the specimen surface, the film was placed between two glass slides to protect the replica. Crack length and surface features were examined with a transmitted light optical microscope. More details of the replication procedure are given by Fash [25]. Fracture surfaces from uniaxial testing were examined with a JEOL Model JSM-25S scanning electron microscope (SEM). The SEM was used because it provided greater resolution than the optical microscope.

3. DISCUSSION

3.1 Uniaxial and Torsional Results

3.1.1 Surface Crack Observations

Using the replication procedure the following surface crack characteristics were observed: 1) crack direction; and 2) the percentage of the life at which cracks were first detected. Typical surface cracks resulting from axial loading are depicted in Figs. 4-5. An examination of the surface crack direction indicates that fatigue cracks primarily occurred on planes perpendicular to the maximum principal stress. Fracture surface observations, presented in Section 3.1.2, further substantiate the presence of stage II type cracking. This is precisely what Forsyth has defined as stage II cracking. Minimal crack initiation or propagation was observed on planes other than the planes of maximum principal stress (i.e. no observable stage I cracking occurred on the surface).

At strain amplitudes of 0.01, 0.0035, and 0.002 cracks were first observed at 77, 63, and 96 percent of the fatigue life respectively. This trend indicates that as the strain amplitude decreases, resulting in longer fatigue lives, the relative importance of macroscopic crack propagation decreases. This observation is not consistent with the trends reported by Dowling [26] for A533B steel, where percentage of life to a given crack size was independent of strain amplitude. However, Dowling suggests that the observed differences may result when different materials are tested. On the basis of data generated by other investigators, Dowling [26] speculates that the transition fatigue life, N_t, where the cyclic elastic and plastic strains are equal ($\Delta\varepsilon_e = \Delta\varepsilon_p$), may demark the change from initiation to propagation dominated cracking behavior. He proposes that at low plastic strain amplitudes initiation behavior will dominate, whereas at high plastic strain amplitudes propagation will dominate. All of Dowling's tests were conducted

at strain levels that resulted in fatigue lives less than N_t. If one considers propagation dominated behavior as accounting for more than fifty percent of the fatigue life, then the present data does not support Dowling's hypothesis. Specifically at a strain amplitude of 0.01, for which $\Delta\varepsilon_p > \Delta\varepsilon_e$, crack nucleation dominated the fatigue life.

3.1.2 Fracture Surface Observations

Examination of fracture surfaces on both a macroscopic and microscopic level has been employed to lend considerable insight and understanding of failure modes. Three fracture surface characteristics were observed in this investigation: On a macroscopic level, 1) the presence of "river markings" indicating the point of crack initiation; on a microscopic level, 2) the existence of micro-voids and 3) fatigue striations were observed. A SEM was used to examine the axial test fracture surfaces. Typical results are illustrated in Figs. 6-7. The first photograph of each series depicts an overall view of the specimen failure surface. The region of fatigue crack initiation is indicated by number 1 and the direction of fatigue crack propagation is indicated by increasing numerical value. Adjacent photographs depict a magnified view of each of these areas. The presence of striations provides much information about the mode of failure and will therefore be the topic of subsequent discussion.

Several investigators have speculated that fatigue striations correspond in a one to one fashion to each stress or strain cycle [27,28]. Forsyth [28] has categorized striations as either brittle or ductile. Brittle striations are observed to propagate along crystallographic planes and therefore are dependent on material microstructure. Ductile striations occur once plastic crack tip deformation occurs. Therefore crack propagation resulting in ductile striations is dependent on the direction of maximum tensile stress.

The presence of ductile striations was observed on all failure surfaces examined. This is particularly evident in regions 2-5 for all but the highest strain amplitude tests (Fig. 8). Brittle striations seem to be present in region 1 for the lower amplitude tests (Fig. 9). One explanation for the change from brittle to ductile striations is the increased stress intensity factor as the crack propagates. As the stress intensity increases, resulting in higher local tensile stresses, ductile striation formation is enhanced. It is noted that ductile striations in region 1 are only present for the highest strain amplitude tests (Fig. 8). This is reasonable because the stress levels required to form this type of striation are most likely to occur at higher strain amplitudes.

Forsyth [28] has also noted that striation spacings will be determined by the stress or strain amplitude. A comparison of striations in the same region for specimens experiencing different strain amplitudes illustrates this phenomenon. The striations observed in the lower amplitude tests are closer together than the striations in the high amplitude tests. This fact supports the assumption that there is a relation between the formation of striations and the number of cycles.

Fracture surfaces were examined for any evidence of stage I cracking. If stage I cracks were present they would be expected to grow at an angle of 45° to the specimen axis for a uniaxial test specimen. No crack growth in this direction was observed. The presence of fatigue striations in region 1 is an indication of stage II cracking.

3.1.3 Selection of Damage Parameter

Fully reversed uniaxial fatigue data is often analyzed via a maximum principal strain amplitude approach employing the Basquin-Coffin/Manson relationship (Eq. 3). Uniaxial data generated in this investigation is pre-

sented in Fig. 10. The solid lines correspond to the elastic, plastic and total strain components of Eq. 3. Uniaxial fatigue data is often employed in the analysis of torsional and other multiaxial fatigue strain states.

In Fig. 11 torsional and axial fatigue data are compared using the maximum principal strain amplitude as suggested by Coffin and Manson. It is noted that the solid lines shown in the figure are intended as an aid in viewing the data and are not derived from Eq. 3. The fully reversed torsional data ($R_\gamma = -1$) was generated from tests conducted on tubular specimens (Table 4). Two of these tube specimens were tested in uniaxial fatigue at strain amplitudes of 0.0035 and 0.0046 at a strain ratio, $R_\varepsilon = -1$ [22]. The lives resulting from these two uniaxial tests agree well with the data from the smooth specimen tests. This indicates that for this material, geometry effects are negligible when comparing uniaxial smooth and tubular specimen data. Using this parameter, torsional fatigue lives for a given principal strain amplitude are greater than axial fatigue lives by a factor of 3.

The shear stress and/or strain amplitude experienced by a material has been suggested as an important factor in determining its fatigue life [24,29,30]. A comparison of axial and torsional fatigue lives using the maximum shear strain amplitude as a damage parameter is illustrated in Fig. 10. Using this shear parameter an order of magnitude difference between axial and torsional fatigue lives is observed.

An explanation of the effectiveness of these two damage criterion can be made with the aid of cracking observations. As discussed previously, uniaxial smooth specimens primarily displayed stage II cracking, which is determined by the maximum principal strain amplitude. Torsional specimens, however, experience both stage I and stage II cracks [22]. Stage II cracking dominated the cracking behavior of the torsional tests, especially at longer fatigue lives (Fig. 13). Therefore, it is expected that the principal strain parameter will

be more effective in correlating torsional and axial fatigue data at longer lives. The discrepancy between axial and torsional data using the shear parameter (Fig. 12) is expected because damage formulations based on principal strain have been shown to be most effective for materials dominated by Stage II cracking.

Socie et al. [30] proposed a modification to the Brown-Miller [17] parameter in the form

$$\hat{\gamma} + \hat{\varepsilon}_n + \hat{\sigma}_{no}/E = \gamma_f' (2N_f)^c + \frac{\tau_f'}{G} (2N_f)^b. \qquad (5)$$

This was used to correlate LCF data for Inconel 718 under various uniaxial and multiaxial cyclic loading conditions. Cracking observations of this material indicate shear crack dominated fatigue lives [24,29,30]. At the strain amplitudes investigated, specimens subjected to both tensile and torsional loading predominantly displayed shear cracking. The suggested damage parameter correlated fatigue lives for Inconel 718 to within a factor of two.

However, using this parameter to correlate axial and torsional 304 stainless steel data (Fig. 14), a factor of 5 difference in life is observed. This correlation is an improvement over the maximum shear strain parameter (Fig. 12), but is still not as effective as the principal strain parameter (Fig. 11). For the torsional strain amplitudes examined here, stage I cracking only occurred during the first 5 to 35 percent of the fatigue life. Lack of observable stage I cracking in uniaxial tests and the presence of limited stage I cracking in torsional tests indicates that a shear based parameter is not appropriate to correlate both sets of data. Examining the two loading conditions more closely it is observed that when applied to fully reversed torsional tests, Socie's parameter will be equivalent to the maximum

shear strain amplitude parameter. However, in uniaxial tests a strain normal to the plane of maximum shear strain results (Fig. 15). Under fully reversed uniaxial conditions, the $\hat{\varepsilon}_n$ term will improve correlations with torsional data in comparison to a simple shear strain amplitude parameter.

Bannantine and Socie [31] have correlated LCF biaxial fatigue data for 304 stainless steel using a modified Smith, Watson and Topper (SWT) parameter [27].

$$\frac{\Delta\varepsilon_1^{max}}{2}\,\sigma_1^{max} = C(N_f)^{\beta} \qquad (6)$$

This parameter has been used to successfully correlate data for materials which predominately display stage II cracking [32,33]. This is similar to the principal strain amplitude parameter, but correlates fatigue lives with the product of the maximum principal strain amplitude and the maximum principal stress on the plane of maximum principal strain amplitude. This approach has been applied to the data generated in this investigation, and used to relate uniaxial data to torsional fatigue lives (Fig. 16). As seen in this figure, the SWT relation provides a good correlation for torsional and axial fatigue data. The largest deviation for any single data point from the fit of both axial and torsional data is within in a factor of two in life.

The examination of cracking characteristics further substantiates implementation of this parameter. The fact that only stage II cracking was observed for uniaxial fatigue tests indicates that the maximum principal stress is an important factor in determining the fatigue lives of these specimens. The presence of both stage I and stage II cracking in torsional tests indicates a diminished role of the maximum principal strain in comparison to the maximum shear strain for these tests when compared with uniaxial tests. Sulfide stringers oriented predominately in the shear

orientation for torsional tests could also be responsible for the observation of shear direction cracks. However, the dominant cracking behavior in these tests is characterized by stage II cracks, except at the highest shear strain amplitude (Fig. 17). This indicates that the maximum principal stress amplitude is eminent in determining the fatigue life.

As seen in Fig. 14 the principal stress for a given shear strain will be greater for a uniaxial test than for a fully reversed torsional test. Therefore, using the product of the principal stress and strain as a damage parameter will improve correlation between axial and torsional fatigue lives. This parameter is similar to the simple principal strain parameter discussed earlier, but it accounts for the differing stress states occurring in torsional and axial tests. The tensile stress for the same tensile strain range is lower in a tension test.

3.2 Multiaxial Results

3.2.1 Analysis of Biaxial Strain Paths

Four biaxial loading histories (path O, N, P, Q) employed in this investigation are depicted in Fig. 5. Each of these biaxial paths have the point $\gamma = \sqrt{3}\ \varepsilon$ in common). Path C is proportional and paths N, P, and Q are non-proportional out-of-phase loadings.

A Mohr's circle analysis, similar to the method used in Ref. 29, has been employed to illustrate differences between these strain states. For the biaxial proportional path, C, (Fig. 16), the points x and y represent planes which are parallel and perpendicular to the specimen axis respectively. It is noted that the two planes of maximum principal strain amplitude will not change orientation with regard to the specimen during a loading cycle. However, the plane of maximum principal strain does change between these two planes during the loading cycle. This is illustrated by examining the state

of strain at points 3 and 5 (Fig. 16). From the Mohr's circle analysis it is seen that the plane of maximum principal strain at point 5 is oriented at an angle of 180° on Mohr's circle from its position at point 3 (this corresponds to a 90° change with regard to the specimen orientation). This change in the principal strain plane is characteristic of any fully reversed loading. The maximum principal strain will occur on one of the two planes for any loading with an axial component. The maximum principal strain experienced during the loading cycle occurs at point 2. This plane is differentiated from the plane of principal strain at point 8 by the fact that the value of the principal stress is greater at point 2 than at point 8. As a result the largest value of the SWT parameter will be on this plane, and physical damage would be expected to occur on this plane.

Non-proportional and out-of-phase path characteristics are visualized by employing the same concepts used for the proportional loading. The 90° out-of-phase path is depicted in this manner in Fig. 17. An important characteristic of out-of-phase loading is that the orientation of the principal strain plane is not constant with regard to the specimen axis, rather it rotates continuously during the loading cycle. Another important characteristic of this type of loading path is that the maximum principal stress and the maximum principal strain do not necessarily occur at the same point during the loading cycle. This type of behavior (Fig. 18) will only be observed when plastic deformation, resulting in stress-strain hysteresis, occurs. When implementing the SWT parameter to analyze this type of deformation behavior, one would choose the plane of maximum principal strain amplitude and use the maximum principal stress experienced by that plane.

Figures 19 through 22 depict the principal and shear strain amplitudes experienced on each plane for the biaxial loading paths examined. Also shown are the values of fatigue damage calculated via Eq. (5) (Socie's shear

parameter) and Eq. (6) (SWT parameter) for these planes. The values of the four parameters depicted in these figures were obtained from an analytical deformation model incorporating out-of-phase strain hardening. This model compared favorably with experimental results. The 0° plane corresponds to the plane which is perpendicular to the specimen axis. For angles less than 0° one would rotate in the clockwise direction from the 0° plane. For proportional in-phase loadings (Fig. 19) the planes of maximum shear strain amplitude and maximum principal strain amplitude are oriented at an angle of 45° with respect to one another. It should be noted that for the 90° out-of-phase and box path (Figs. 20 and 22), planes of maximum shear strain amplitude can occur at an angle which is less than 45° from the plane of maximum principal strain amplitude. This is a deformation characteristic sometimes displayed by out-of-phase loadings. The two box path (Fig. 21) does not display this phenomenon, even though it is an out-of-phase loading. Additionally, for in-phase loadings the plane experiencing either the maximum principal strain amplitude or maximum shear strain amplitude correspond to the maximum value of fatigue damage calculated by Eqs. (5) and (6), respectively (Fig. 19). Examination of Figs. 20 through 22 reveals that this is not always the case for out-of-phase loadings, and the interpretation of the damage parameters is not as straightforward. Cracking behavior will be employed to clarify this difference in the subsequent discussion.

3.2.2 Biaxial Surface Crack Observations

The replication procedure previously described was used to monitor surface crack growth and crack direction which occurred in biaxial fatigue tests (Sec. 2.4). Initial crack growth occurred near the plane of maximum principal strain amplitude for the proportional path C. It is also noted that the shear strain amplitude on this plane is zero (Fig. 19). After initiation

on this plane the crack changes direction and grows on a new plane which is oriented at approximately 10° degrees from the $\Delta\varepsilon_1^{max}$ plane (Fig. 23). This new plane experiences a principal strain amplitude, $\Delta\varepsilon_1'$, which is nearly the same magnitude as $\Delta\varepsilon_1^{max}$ ($\Delta\varepsilon_1' \sim 0.9\ \Delta\varepsilon_1^{max}$). This secondary plane is distinguished from the plane of initiation by the presence of a shear strain amplitude that is approximately equal to 1/2 $\Delta\gamma^{max}$ for the entire cycle, as opposed to no shear strain on the $\Delta\varepsilon_1^{max}$ plane. Fatigue life predictions were made on the basis of stress-strain response on the plane of maximum principal strain amplitude. This is considered to be the most damaging plane for this material. The fact that long crack growth for path C occurred on a plane which experiences a principal strain amplitude that is less than $\Delta\varepsilon_1^{max}$ may account for the slight increase in experimentally observed lives when compared to SWT predicted lives. Mixed mode fracture mechanics type crack growth may dominate the "long" crack direction and growth rate [34], but since crack formation dominates the fatigue life for these tests no effort will be made to elaborate on "long" crack growth. The quote marks on "long" result from the lack of consensus in defining long and short cracks.

Cracks nucleate on the plane of maximum principal strain amplitude for the 90° out-of-phase, Box, and Two Box (N, P, Q, respectively). Crack propagation from the Two Box path, Q, (Fig. 24) appears to take place during the nominal fully reversed tensile part of the loading cycle with no shear strain, even though it is not the plane of maximum principal strain amplitude. As seen in Fig. 20, the maximum principal strain amplitude is essentially constant on all planes for the 90° out-of-phase path, which indicates numerous specimen orientations could experience similar fatigue damage. Therefore a distinct cracking direction is not as likely to occur for this loading path. A change in cracking directions was observed for paths N, P, and Q, (Figs. 24-26). A possible explanation for the change in crack direc-

tion also could cite mixed mode fracture mechanics longer crack growth. The fact that less than 10 percent of the life was spent in crack propagation on a plane other than the plane of initial crack growth (Figs. 27 and 28) indicates that it will have a minimal effect on the fatigue life for the tests conducted.

From the previously discussed torsional and axial tests it was determined that the cracking behavior of this material is characterized by Stage II cracking. This is further substantiated by the observation that in biaxial fatigue tests cracks nucleated on maximum principal strain amplitude planes. This cracking behavior appears to dominate damage accumulation for the range of fatigue lives investigated. Appendix A contains documentation of crack growth versus number of cycles obtained from the acetate tape replicas. Photos providing similar data, as presented in Figs. 23-26, of the crack direction for all tests are summarized in Appendix B.

3.2.3 Biaxial Fatigue Life Predictions

Fatigue Life predictions for multiaxial loading conditions should account for the variation of stress-strain response uniquely associated with each loading path. Additionally, life prediction parameters should coincide with physical damage observations. Specifically, an appropriate parameter should take into account crack initiation and growth direction. The previous examination of fully reversed torsional and axial cracking behavior established that cracking in 304 stainless steel occurs in the direction perpendicular to the maximum principal strain amplitude (Stage II). Correlation of fatigue lives with the maximum principal strain amplitude was deemed appropriate because this was in agreement with the observed physical damage, which was dominated by Stage II cracking.

This concept is now extended to the prediction of the multiaxial fatigue lives resulting from the loading paths under examination. Socie [35] has generalized the Smith-Watson-Topper parameter for multiaxial loading as follows:

$$\frac{\Delta\varepsilon_1}{2}\sigma_1^{max} = \sigma_f'\,\varepsilon_f'(2N_f)^{b+c} + \frac{\sigma_f'^2}{E}(2N_f)^{2b} \qquad (7)$$

It is important to note that the coefficients and exponents on the right hand side of the equation are material constants and can be obtained from the axial smooth specimen strain-life data. The terms on the left hand side of the equation are interpreted as the maximum principal strain amplitude and the maximum stress normal to that plane. For out-of-phase loadings this does not always imply the maximum value of the damage parameter.

McDowell et al. [36] has investigated the stress-strain response of 304 stainless steel under conditions of multiaxial out-of-phase cyclic loading. He observed that this material displays cyclic hardening resulting from out-of-phase loadings. The degree of hardening is more pronounced than the cyclic hardening experienced during in-phase loading as is illustrated in Fig. 29. In other words, the stable cyclic stress strain response for out-of-phase tests differs from that of in-phase tests and is dependent on the degree of nonproportionality in the path under consideration.

The SWT parameter has been employed to predict fatigue lives for both the in-phase and out-of-phase paths under investigation. The cyclic loading conditions investigated display shorter lives for out-of-phase tests. This parameter is deemed appropriate for two reasons: 1) Correlation of fatigue lives with the maximum principal strain amplitude is consistent with the observed physical damage. Specifically, as previously discussed, initial crack formation resulting from both in-phase and out-of-phase tests displayed

Stage II characteristics. 2) The degree of cyclic hardening, which is dependent on the degree of non-proportionality, is taken into account with the maximum principal stress term. The correlation of the fatigue life data, generated in this investigation, with the SWT parameter is illustrated in Fig. 30. The theoretical life predictions resulting from both forms of the SWT parameter, Eqs. 6 and 7, are displayed in this figure (linear and bilinear respectively). It is noted, that for the range of fatigue lives under consideration, that both forms of the SWT parameter give very similar life predictions. Fully reversed uniaxial data was used to fit Eqs. 4 and 7.

The implementation of the SWT parameter for these various biaxial loading conditions illustrates the importance of accurately modeling the stress-strain response which results from various biaxial cyclic loadings. This parameter provides a good life prediction model for 304 stainless steel, a material which fails in a tensile manner, when the stress strain response of out-of-phase loadings is taken into account.

4. CONCLUSIONS

1. Uniaxial strain controlled tests were conducted on 304 stainless steel. Axial fatigue lives and cracking observations were compared with previous data for torsional tests.

   a. Stage II cracking dominated fatigue lives for uniaxial specimens at all strain amplitudes tested. Crack growth data from previous research [23] indicates that except for LCF torsional tests (i.e. < 10,000 cycles) only 5 to 35 percent of the fatigue life was spent initiating and propagating stage I cracks.

   b. Macroscopic crack propagation accounted for a greater percentage of the fatigue life as strain amplitude increased.

   c. Macroscopic cracking behavior indicates that a damage parameter based on principal strain amplitude is most appropriate for this material.

   d. The Smith, Watson, Topper parameter, a modification to the principal strain amplitude theory, correlates axial and torsional fatigue lives, to within a factor of two.

2. Biaxial strain controlled fatigue tests were conducted on 304 stainless steel. Observed physical damage was used to substantiate th extension of the SWT damage parameter to multiaxial fatigue life predictions.

   a. Stage II type cracking dominated the fatigue lives for both the in-phase and out-of-phase biaxial tests.

   b. At the strain amplitudes investigated, fatigue lives were dominated by crack nucleation.

   c. The stable cyclic stress-strain response differed for proportional and out-of-phase loadings. A higher stable stress response for a given strain amplitude was observed for the out-of-phase tests in comparison to proportional loadings.

d. Correlation of both in-phase and out-of-phase testing with the SWT parameter to within a factor of 2½ with regard to life is possible due to the observed damage mechanism (i.e., crack direction) being consistent with prior data and consideration of the stress-strain response which is dependent on the type of loading (i.e. in-phase or out-of-phase).

e. Longer crack growth directions change for the biaxial loadings considered, and for components or specimens where "long" crack growth dominates the fatigue life, alternate damage assessment may be appropriate.

REFERENCES

1. Elliott, D., and Tupholine, S. M., An Introduction to Steel Selection: Part 2, Stainless Steels, Oxford University Press, 1981.

2. Metals Handbook, Ninth Edition, Vol. 3, Properties and Selection: Stainless Steels, Tool Materials and Special Purpose Metals, The American Society for Metals, 1980, pp. 882.

3. Source Book on Stainless Steels, ASM, American Society for Metals, 1980, pp. 408.

4. Peckner, Donald, and Berstein, I. M., Handbook of Stainless Steels, McGraw-Hill Inc., 1977, pp. 800.

5. Peterson, R. E., "Discussions of a Century Ago Concerning the Nature of Fatigue and Review of Some of the Subsequent Researches Concerning the Mechanism of Fatigue," ASTM Bulletin, American Society for Testing and Materials, 1950, pp. 50-56.

6. Wolher, A., Zeitschrift für Bauwesan, Vol. 8, 1858, p. 641.

7. Basquin, O. H., "The Exponential Law of Endurance Tests," Proc. ASTM, 1910, pp. 625-630.

8. Coffin, L. F., Jr., "Fatigue at High Temperature - Prediction and Interpretation," Proceedings The Institute of Mechanical Engineers, Vol. 188, 1974, pp. 109-127.

9. Coffin, L. F. Jr., " A Study of Cyclic Thermal Stresses on a Ductile Metal," Transactions: ASME, Vol. 76, 1954, pp. 931-950.

10. Manson, S. S., "Behavior of Materials Under Conditions of Thermal Stresses," Proc., Heat Transfer Symposium, University of Michigan Research Institute, 1953, pp. 9-10.

11. Coffin, L. F., Jr., "Fatigue at High Temperature-Prediction and Interpretation," James Clayton Lecture, Proceedings of the Institute of Mechanical Engineers, Vol. 188, 1974, pp. 109-127.

12. Findley, W. N., "Fatigue of Metals under Combinations of Stresses," Trans. ASME, Vol. 79, 1957, pp. 1337-1348.

13. Garud, Y. S., "Multiaxial Fatigue: A Survey of the State of the Art," Journal of Testing and Evaluation, Vol. 9, No. 3, May 1981, pp. 165-178.

14. Krempl, E. "The Influence of State of Stress on Low-Cycle Fatigue of Structural Materials: A Literature Survey and Interpretive Report," ASTM STP549, American Society of Testing Materials, 1974, pp. 46.

15. Lanza, G., "Strength of Shafting Subjected to Both Twisting and Bending," Transactions ASME, Vol. 8, 1886, pp. 130-144.

16. Guest, J. J., "Recent Research on Combined Stress," Proceedings Institution of Automobile Engineers, Vol. 35, Dec. 1940, pp. 33-72 and 146-171.

17. Brown, M. W., and Miller, K. J., "A Theory for Fatigue Under Multiaxial Stress-Strain Condition," Proc., Inst. Mech. Engrs., Vol. 187, 1973.

18. Mason, W., and Delaney, W. J., "Alternating Combined Stress Experiments," Reports British Association for the Advancement of Science, London, 1921, pp. 329-341.

19. Ewing, J. A., and J. C. W. Humphrey, "The Fracture of Metals and Repeated Alterations of Stress," Philosophical Trans. of the Royal Society of London, Series A, Vol. 200, 1903, Part 1, pp. 241-250.

20. Forsyth, P. J. E., "A Two Stage Process of Fatigue Crack Growth," Proceedings of the Symposium on Crack Propagation, Cranfield, England, 1961, pp. 76-94.

21. Kurath, P., Socie, D. F., and Morrow, J., "A Nonarbitrary Fatigue Crack Size Concept to Predict Total Fatigue Lives," Technical Report AFDL-TR-79-3144, Air Force Flight Dynamics Laboratory, Wright-Patterson AFB, Ohio, Dec. 1979, pp. 53.

22. Bannantine, J. A., "Observations of Tension and Torsion Fatigue Cracking Behavior and the Effect on Multiaxial Damage Correlations," M.S. Thesis, Department of Mechanical Engineering, University of Illinois at Urbana-Champaign, Urbana, IL, 1986.

23. Smith, K. N., Watson, P., and Topper, T. H., "A Stress-Strain Function for the Fatigue of Metals," Journal of Materials, Vol. 5, No. 4, Dec. 1970, pp. 767-778.

24. Waill, L. E., "Crack Observations in Biaxial Fatigue," M.S. Thesis, Department of Mechanical Engineering, University of Illinois at Urbana-Champaign, Urbana, IL, 1983, pp. 61.

25. Fash, J. W., "Fatigue Crack Initiation and Growth in Gray Cast Iron," Fracture Control Program, Report No. 35, College of Engineering, University of Illinois, 1980, pp. 47-50.

26. Dowling, N. E., "Crack Growth during Low-Cycle Fatigue of Smooth Axial Specimens," Cyclic Stress-Strain and Plastic Deformation Aspects of Fatigue Crack Growth, ASTM STP 637 Ed., American Society for Testing and Materials, 1977, pp. 97-112.

27. Jacquelin, B., Hourlier, F., and Pineau, A., "Crack Initiation Under Low-Cycle Multiaxial Fatigue in Type 316L Stainless Steel," Transactions ASME, Vol. 105, 1983, pp. 138-143.

28. Forsyth, P. J. E., "Fatigue Damage and Crack Growth in Aluminum Alloys," ACTA Metallurgica, Vol. 11,f 1963, pp. 703-715.

29. Koch, J. L., "Proportional and Non-Proportional Biaxial Fatigue of Inconel 718," M.S. Thesis, Department of Mechanical Engineering, University of Illinois at Urbana-Champaign, Urbana, Il, 1985, pp. 146.

30. Socie, D. F., and Shield, T. W., "Mean Stress Effects in Biaxial Fatigue of Inconel 718," J. of Engineering Materials and Technology, Vol. 106, 1984, pp. 227-232.

31. Bannantine, J. A., and Socie, D. F., "Observations of Cracking Behavior in Tension and Torsion Low Cycle Fatigue," Presented at ASTM Conference on Low Cycle Fatigue: Directions for the Future (to be published as an ASTM STP) Bolton Landing, NY, Sept. 30 - Oct. 4, 1985.

32. Socie, D. F., Fash, J. W., Downing, S. D., "Fatigue of Grey Cast Iron," Fracture Control Program No. 44, University of Illinois at Urbana-Champaign, October, 1982.

33. Furman, Peter J., "Fatigue of Grey Cast Iron under Axial and Bending Loads," M.S. Thesis, Department of Mechanical Engineering, University of Illinois at Urbana-Champaign, Urbana, IL, 1983, pp. 50.

34. Hua, C. T., "Fatigue Damage and Small Crack Growth During Biaxial Loading," Ph.D. Thesis, Department of Mechanical and Industrial Engineering, University of Illinois at Urbana-Champaign, 1983, 158 pp.

35. Socie, D. F., "Multiaxial Fatigue Damage Models," submitted to Journal of Engineering Materials and Technology, 1986.

36. McDowell, D. L., and Socie, D. F., "Transient and Deformation Behavior Under Cyclic Nonproportional Loading," Multiaxial Fatigue ASTM STP 853, K. J. Miller and M. W. Brown, Eds., American Society for Testing and Materials, Philadelphia, 1985, pp. 64-87.

Table 1
Composition of 304 Stainless Steel

Element	Actual	Min	Max
Chromium	19.2	18.0	20.00
Nickel	10.8	8.0	10.50
Manganese	1.6		2.00
Silicon	0.40		1.00
Phosphorous	< 0.01		0.045
Carbon	0.057		0.08
Sulfur	0.023		0.03

Table 2

Baseline Material Properties

Monotonic Tensile Properties		
E,	Elastic Modulus	183 GPa
σ_y2%,	.2% Offset Yield Strength	325 MPa
σ_u,	Ultimate Strength	650 MPa
σ_f,	True Fracture Strength	1400 MPa
ε_f,	True Fracture Strain	1.61
%RA,	% Reduction in Area	80
K	Strain Hardening Coefficient	1210 MPa
n,	Strain Hardening Exponent	0.193
R_b	Rockwell Hardness	72
Axial Cyclic Properties ($R_\varepsilon = -1$)		
E,	Elastic Modulus	185 GPa
σ_f'	Fatigue Strength Coefficient	1000 MPa
b	Fatigue Strength Exponent	-0.114
ε_f'	Fatigue Ductility Coefficient	0.171
c	Fatigue Ductility Exponent	-0.402
K'	Cyclic Strain Hardening Coefficient	1660 MPa
n'	Cyclic Strain Hardening Exponent	0.287
Torsional Cyclic Properties ($R_\gamma = -1$)		
G	Torsional Modulus	82.8 GPa
τ_f'	Fatigue Strength Coefficient	709 MPa
b	Fatigue Strength Exponent	-0.121
γ_f'	Fatigue Ductility Coefficient	0.315
c	Fatigue Ductility Exponent	-0.353
K'	Cyclic Strength Coefficient	785
n'	Cyclic Strain Hardening Exponent	0.295

Table 3
Uniaxial Constant Amplitude Fatigue Data
Material: 304 Stainless Steel

Spec. No.	$\Delta\varepsilon/2$	R_ε	E (GPa)	Stable Half Life Response $\Delta\varepsilon_p/2$	$\Delta\sigma/2$ (MPa)	σ_o (MPa)	N_f (cycles)
03	0.0100	-1	--	0.0080	383	2.0	1,070
09	0.0100	-1	191	0.0078	426	-1.4	1,167
06	0.0060	-1	172	0.0038	379	-21.9	6,080
06*	0.0046	-1	--	0.0031	279	0	10,300
01	0.0035	-1	--	0.0021	261	5.8	30,700
10	0.0035	-1	186	0.0021	258	-9.1	33,530
11	0.0035	-1	194	0.0021	266	8.4	29,000
15*	0.0035	-1	--	0.0022	240	-2.2	38,500
12	0.0020	-1	192	0.0008	230	16.5	286,400
2	0.0020	-1	172	0.0008	206	2.9	333,100

*Tubular Specimen Data [22]

Table 4

Torsional Constant Amplitude Fatigue Data

Material: 304 Stainless Steel [22]

				Stable Half Life Response			
Spec I.D.	$\frac{\Delta\gamma}{2}$	R_γ	G (GPa)	$\frac{\Delta\gamma_p}{2}$	$\frac{\Delta\tau}{2}$ (MPa)	τ_o	N_f
08	0.01700	-1	---	0.01370	248	1.2	4,090
05	0.00800	-1	---	0.00580	191	1.9	48,500
21	0.00793	-1	76.4	0.00590	156	0.4	32,100
22	0.00800	-1	---	0.00580	157	0	33,900
07	0.00600	-1	---	0.00420	156	0	133,000
16	0.00609	-1	83.3	0.00439	140	0	83,400
09	0.00340	-1	---	0.00190	138	0	1.10×10^6
20	0.00342	-1	80.0	0.00186	125	0	824,200

Note: Surface Shear Strains are 13% Greater

Table 5
Biaxial Constant Amplitude Fatigue Data
Material: 304 Stainless Steel

PATH CODE	SPEC I.D.	MIDSECTION VALUES CONTROL PARAMETERS $\Delta\varepsilon/2$	ε_o	$\Delta\gamma/2$	γ_o	STEADY STATE STRESSES (MPa) $\Delta\sigma/2$	σ_o	$\Delta\tau/2$	τ_o	$N_{1.0}$ (cycles)	N_f (cycles)
C	SS-02	0.0025	0	0.0043	0	184	2.7	109	0.3	44,300	53,000
	SS-12	0.0025	0	0.0043	0	176	-3.7	101	0.7	44,000	52,900
	SS-25	0.00145	0	0.0023	0	161	0.6	89	1.2	420,000	440,000
	SS-26	0.00145	0	0.0023	0	157	0.8	90	- 2.9	340,000	356,000
N	SS-10	0.0035	0	0.0061	0	477	2.6	267	- 4.4	3,340	3,560
	SS-13	0.0035	0	0.0061	0	457	-4.5	256	1.3	3,600	3,730
	SS-28	0.0020	0	0.0035	0	300	18.6	168	- 2.1	38,600	50,000
	SS-29	0.0020	0	0.0033	0	307	29.3	176	- 3.5	35,300	45,000
P	SS-03	0.0025	0	0.0043	0	420	0	226	0	5,110	5,110
	SS-11	0.0025	0	0.0043	0	380	0	218	0	6,000	6,200
	SS-30	0.0014	0	0.0024	0	230	20.6	139	1.8	82,100	89,312
	SS-31	0.0014	0	0.0024	0	234	17.1	137	2.2	90,100	100,000
Q	SS-01	0.0025	0	0.0043	0	365	32	199	-13.2	-----	11,080
	SS-04	0.0025	0	0.0043	0	347	35	209	-21.8	7,340	9,800
	SS-32	0.0014	0	0.0024	0	210	47.7	114.7	-17.0	182,000	200,000
	SS-33	0.0014	0	0.0024	0	210	44.5	115.6	-15.7	192,200	205,000

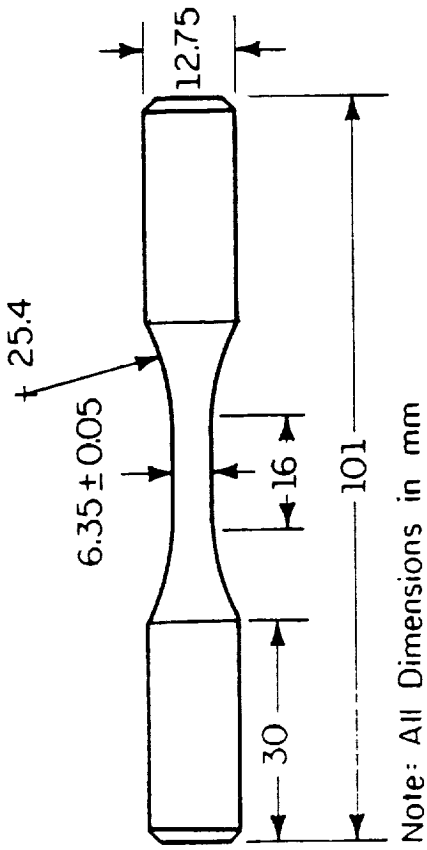

Figure 1 Uniaxial Specimen Dimensions

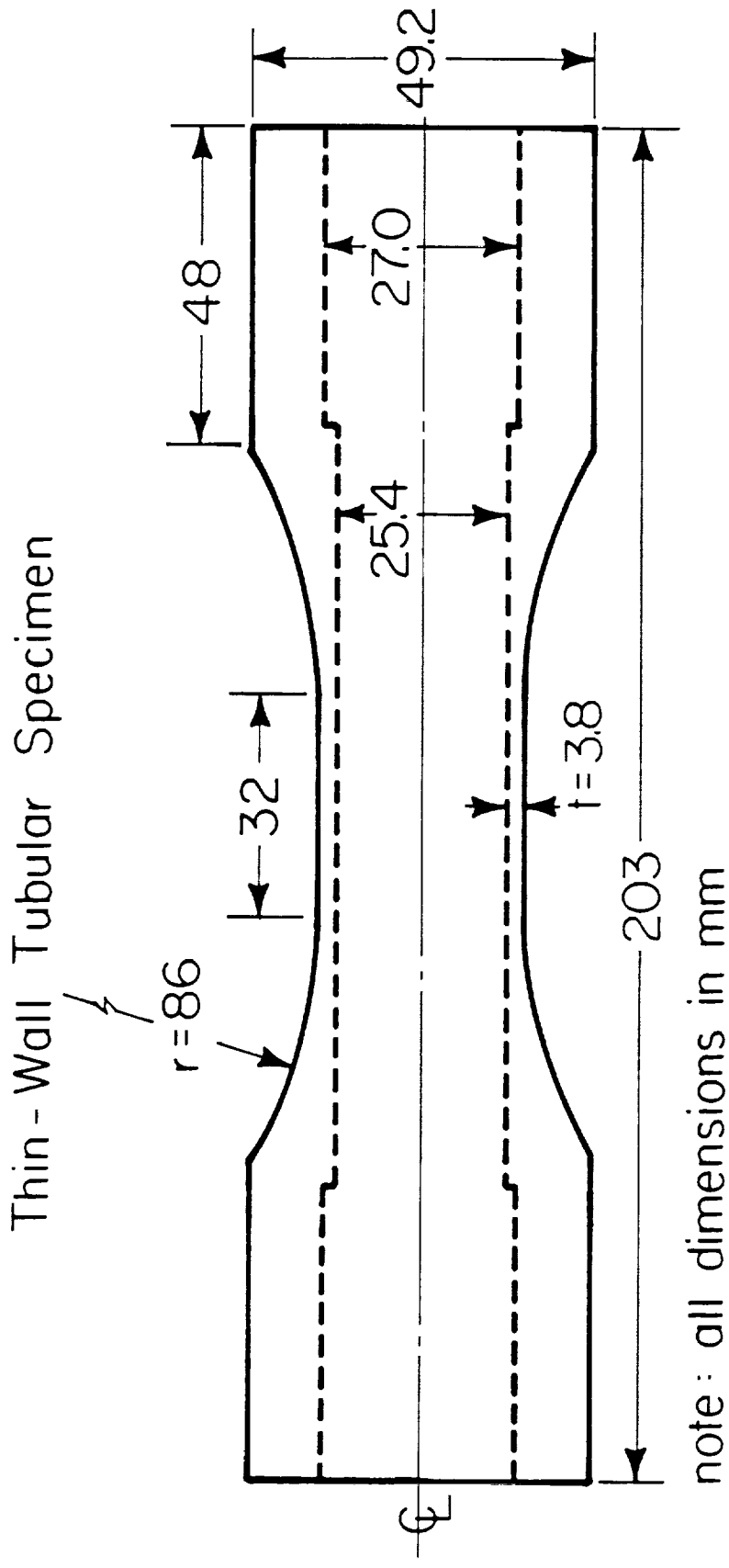

Figure 2 Biaxial Specimen Dimensions

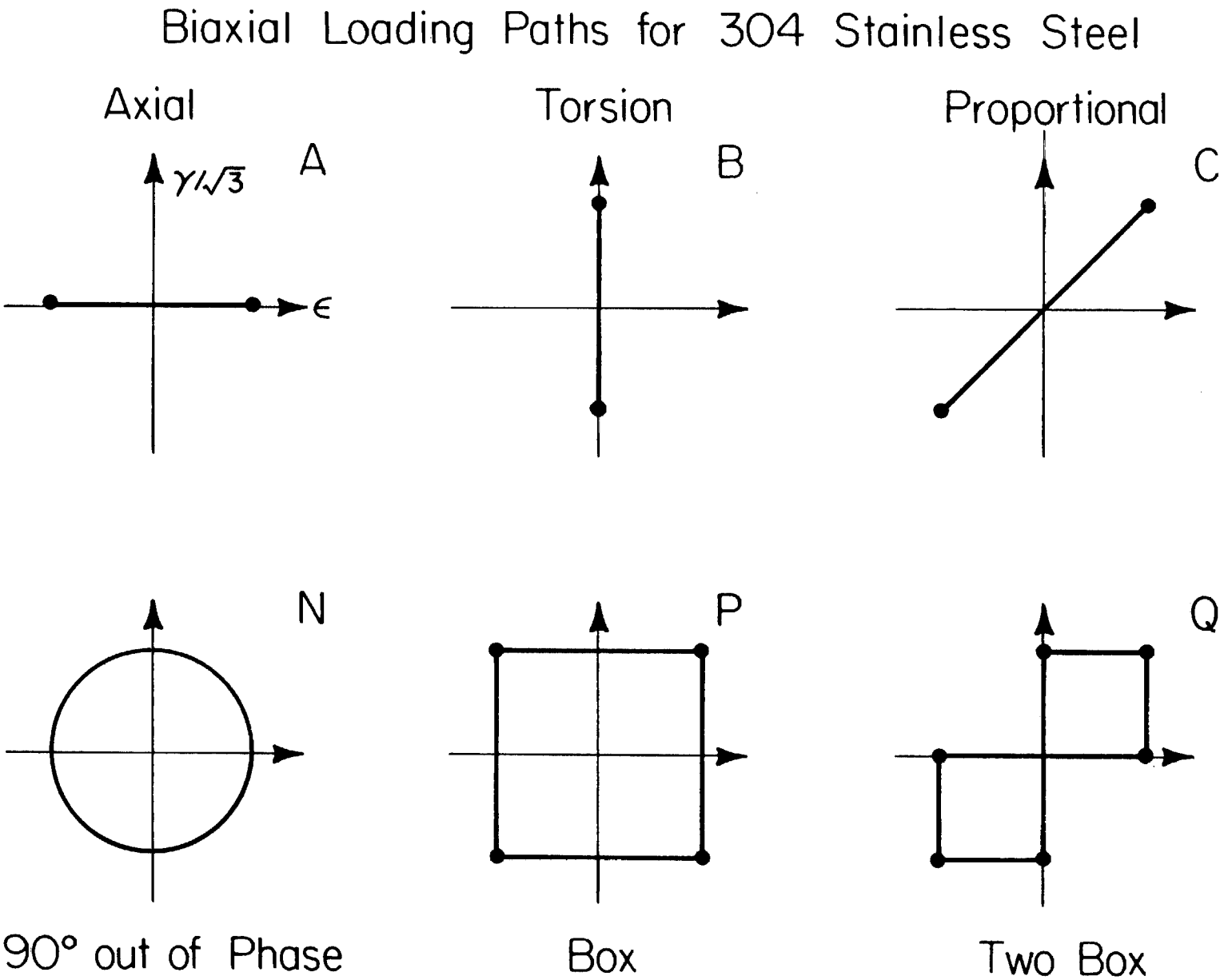

Figure 3 Biaxial Loading Paths for 304 Stainless Steel

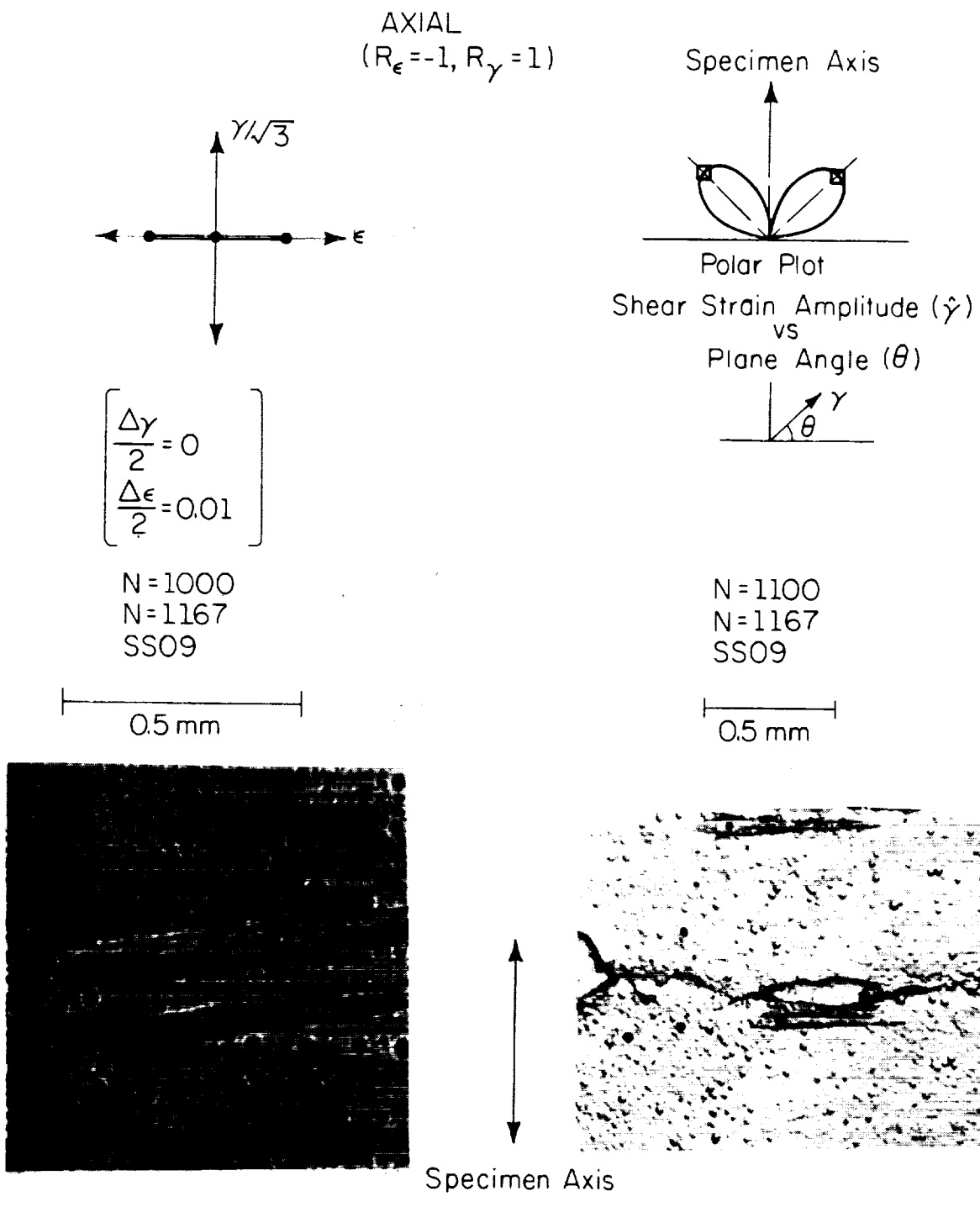

Figure 4 Typical Surface Crack Features, $\frac{\Delta\epsilon}{2}$ = 0.01

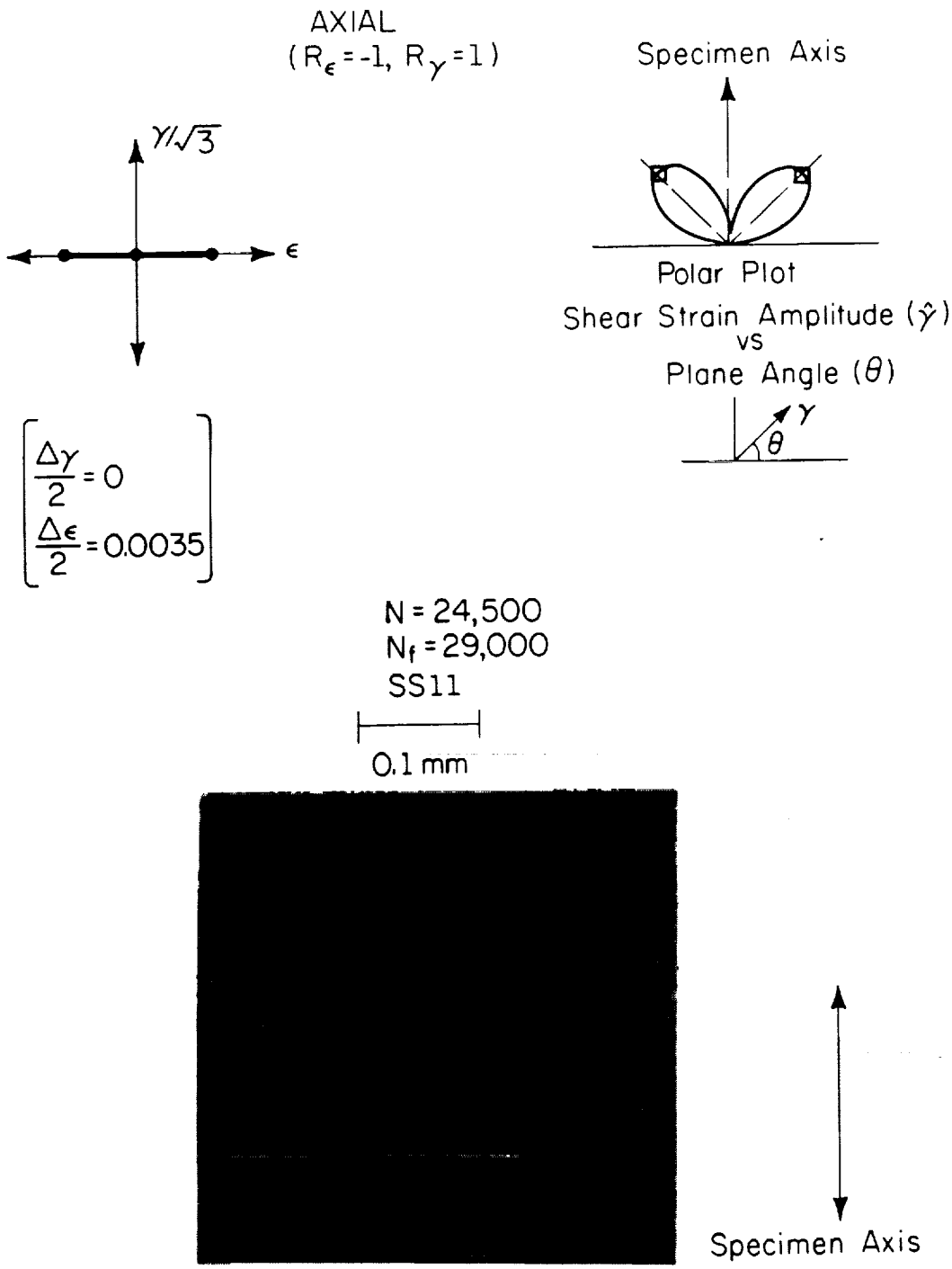

Figure 5 Typical Surface Crack Features, $\frac{\Delta\epsilon}{2} = 0.0035$

Axial Fatigue Fracture Surface of SS-09, $\Delta\varepsilon/2=0.0100$

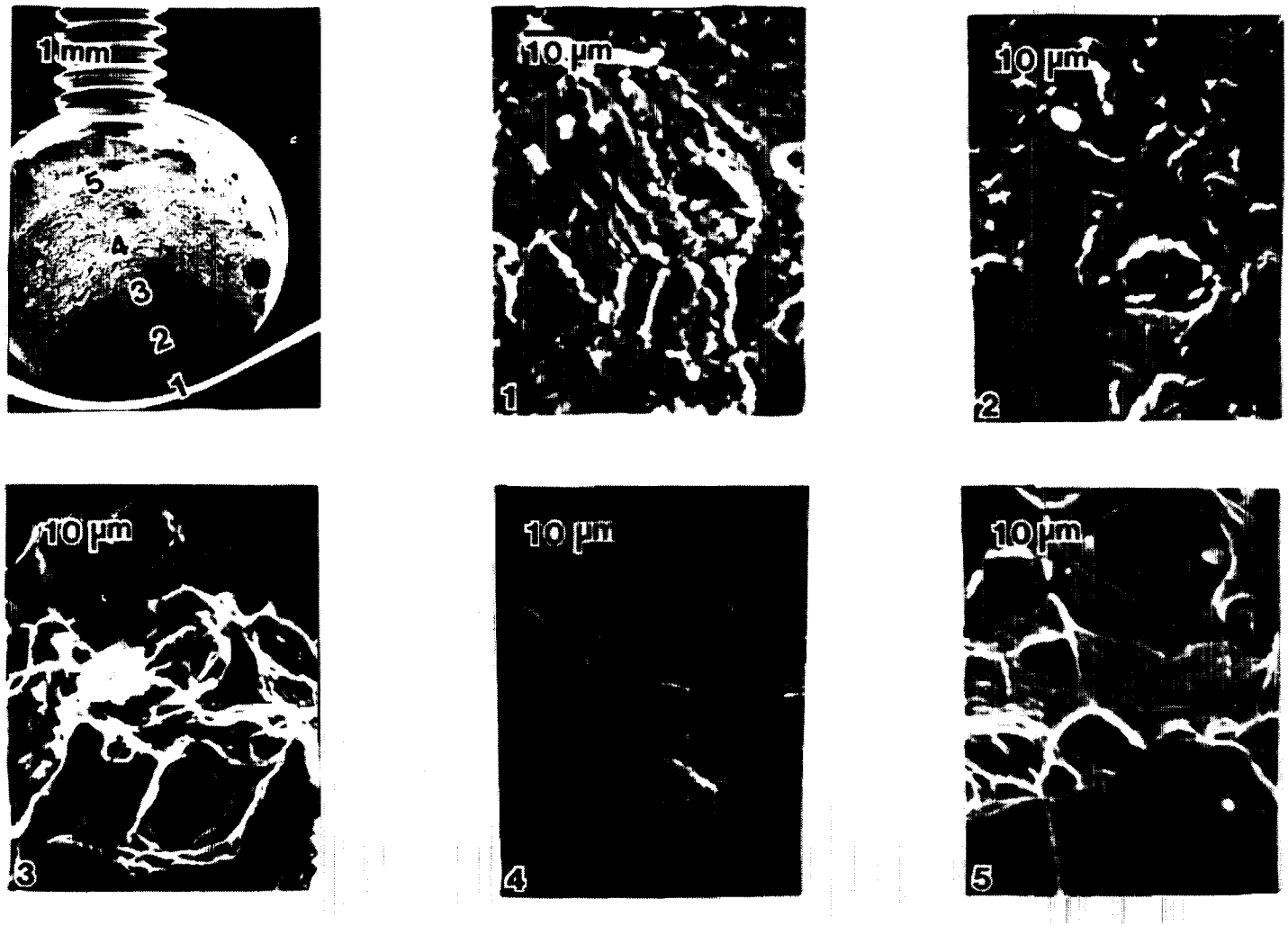

Figure 6 Fatigue Failure Surface Micrographs, $\frac{\Delta\varepsilon}{2}$ = 0.01

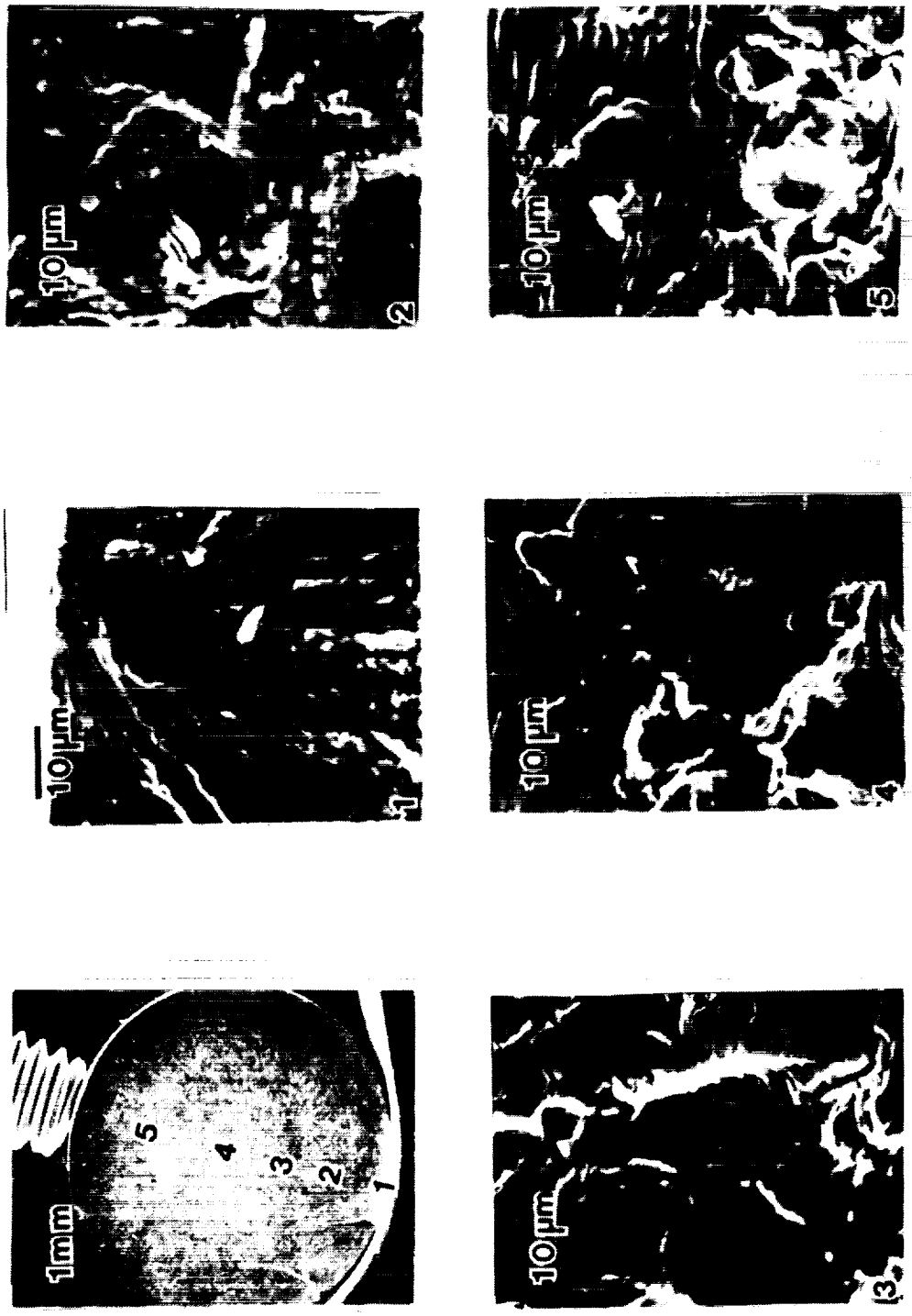

Figure 7 Fatigue Failure Surface Micrographs, $\frac{\Delta\varepsilon}{2} = 0.0035$

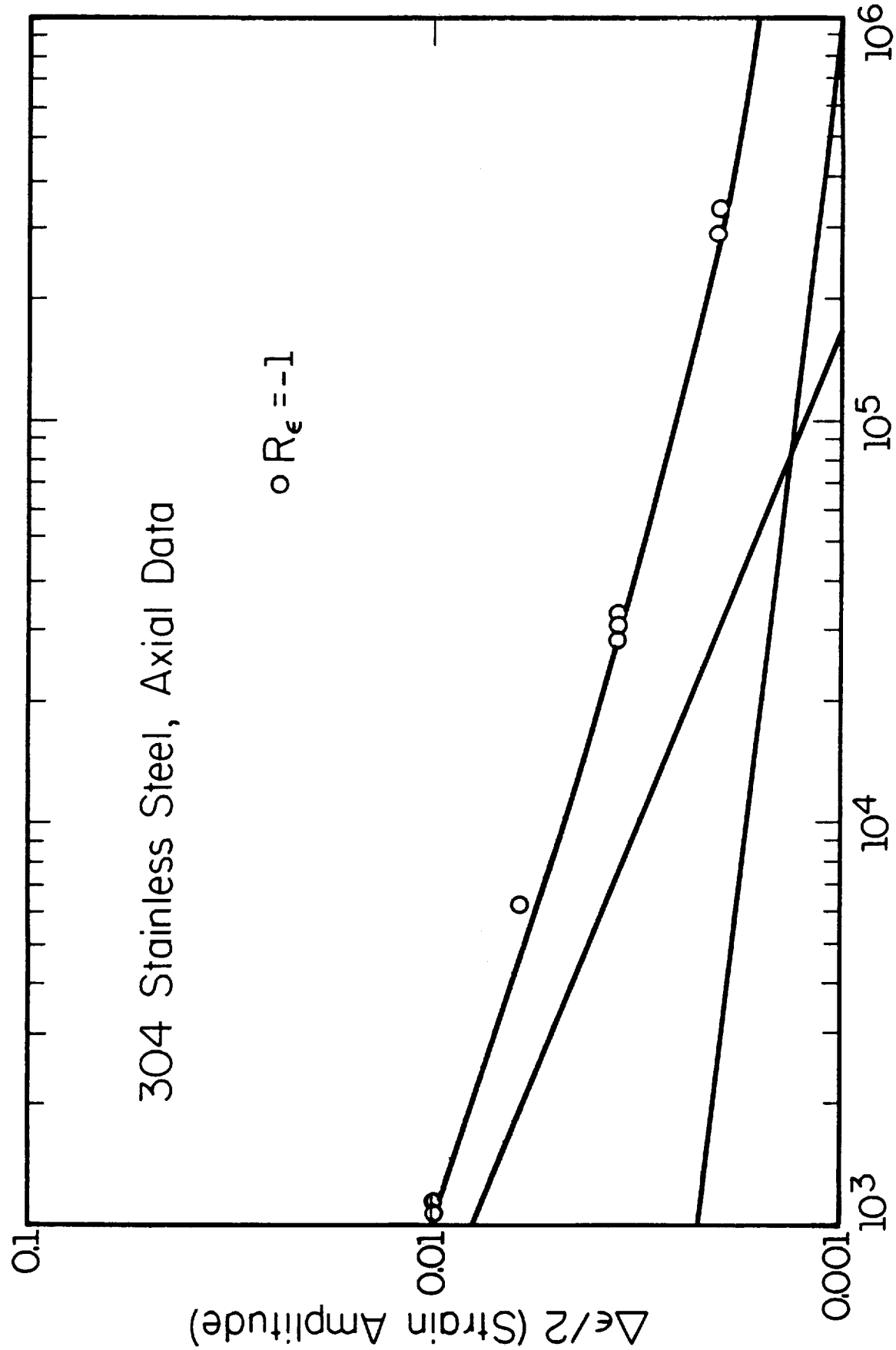

Figure 8 Strain Life Curve for 304 Stainless Steel

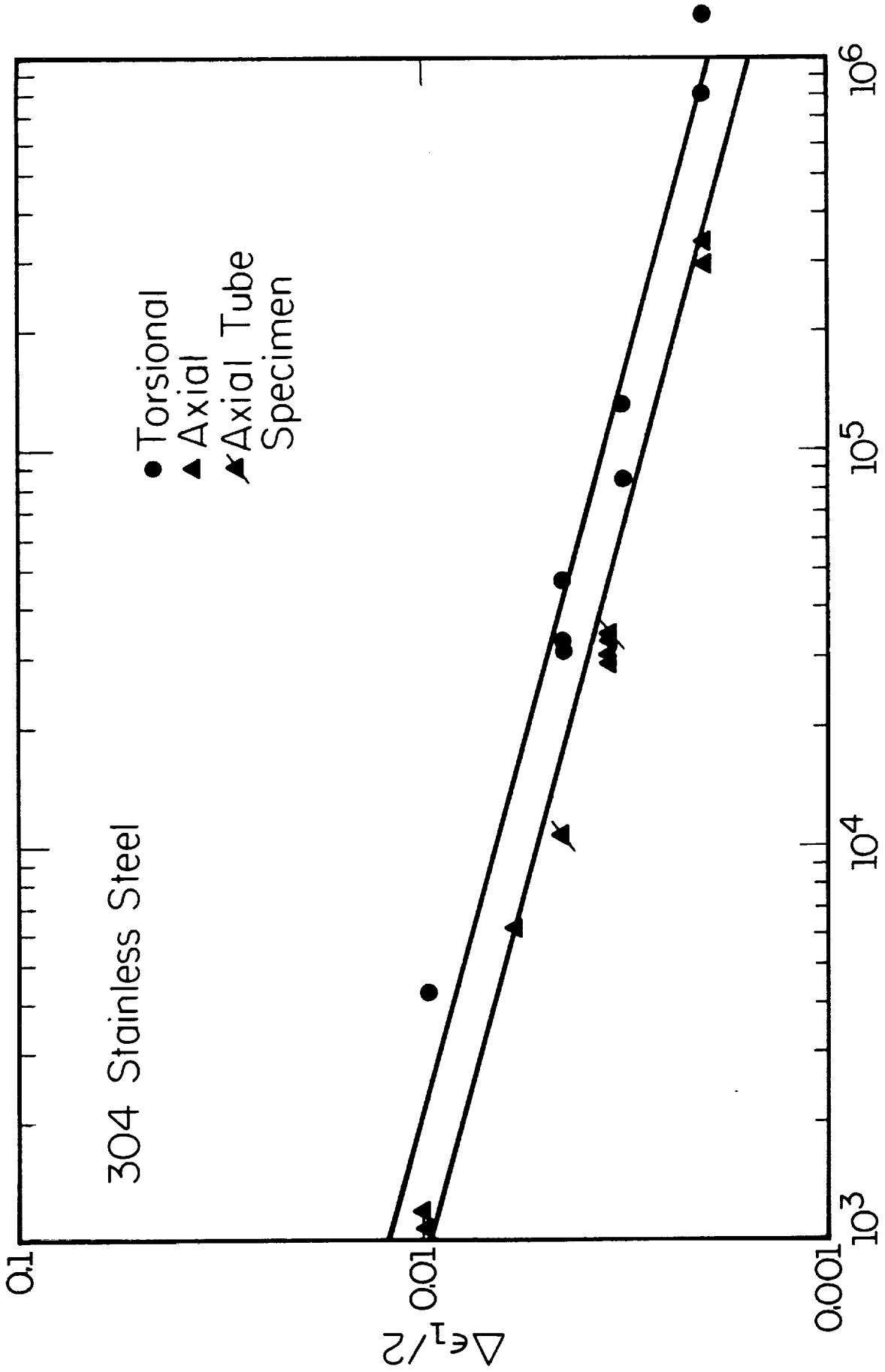

Figure 9 Comparison of Axial and Torsional Data using Maximum Principal Strain Amplitude

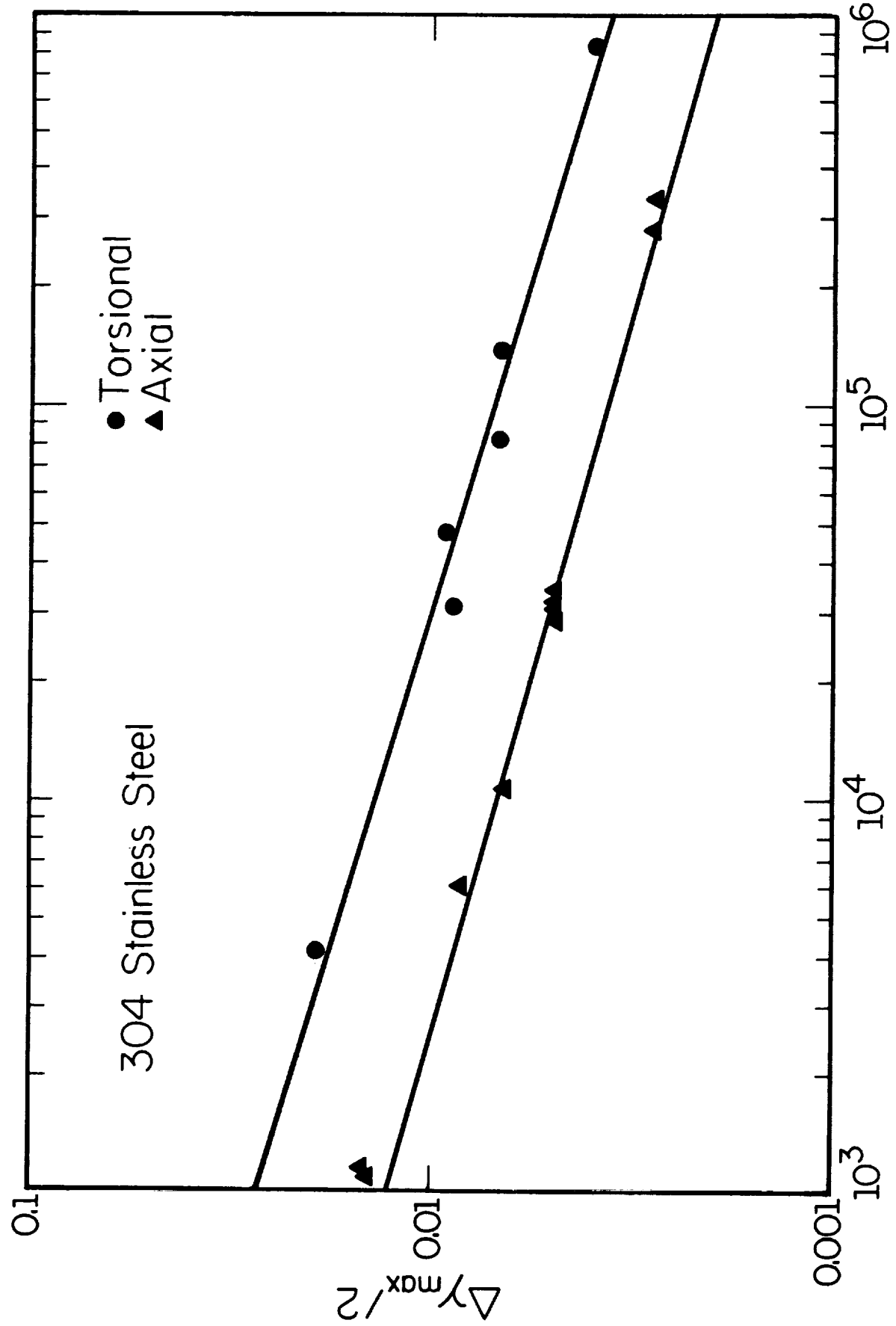

Figure 10 Comparison of Axial and Torsional Data using Maximum Shear Strain Amplitude

TORSION

$(R_\epsilon = 1,\ R_\gamma = -1)$

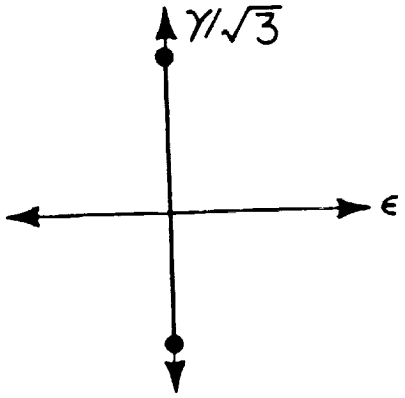

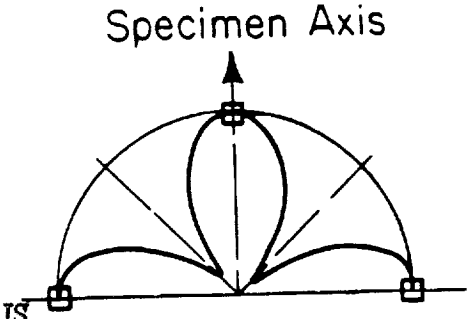

Polar Plot

Shear Strain Amplitude ($\dot{\gamma}$)

vs

Plane Angle (θ)

$$\begin{bmatrix} \frac{\Delta\gamma}{2} = 0.008 \\ \frac{\Delta\epsilon}{2} = 0 \end{bmatrix}$$

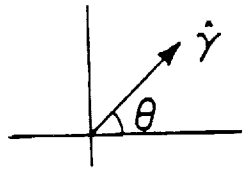

N = 48,000

$N_{1.0}$ = 42,000

SS-05

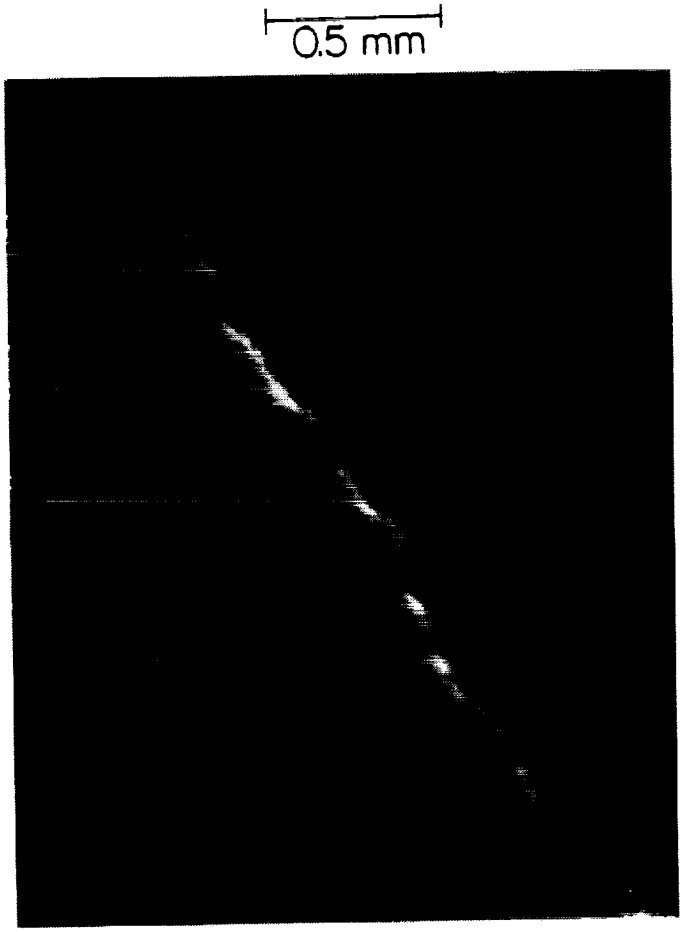

Specimen Axis

Figure 11 Typical Surface Crack Features, $\frac{\Delta}{2}\gamma = 0.008$

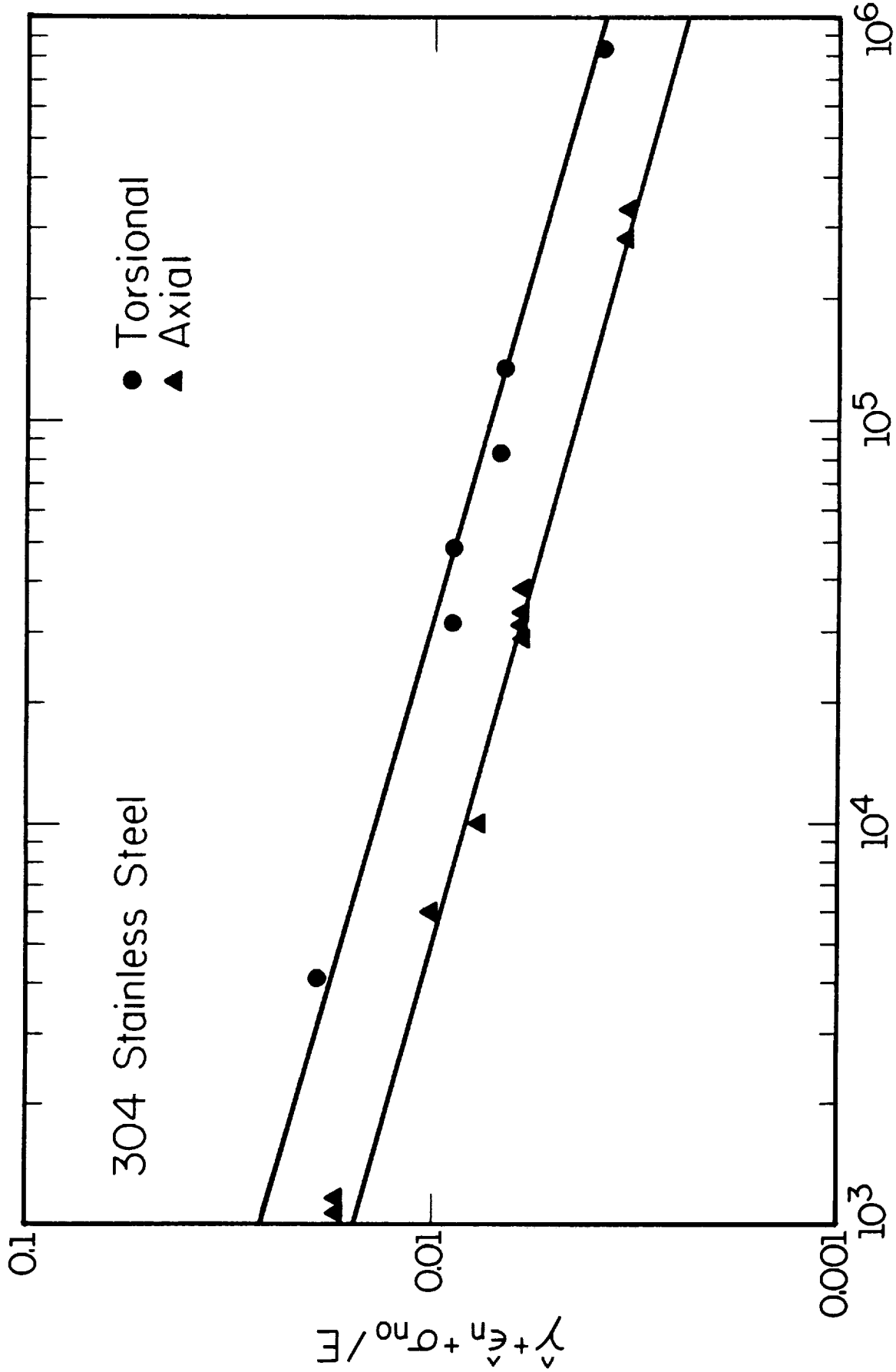

Figure 12 Comparison of Axial and Torsional Data using Socie's Parameter

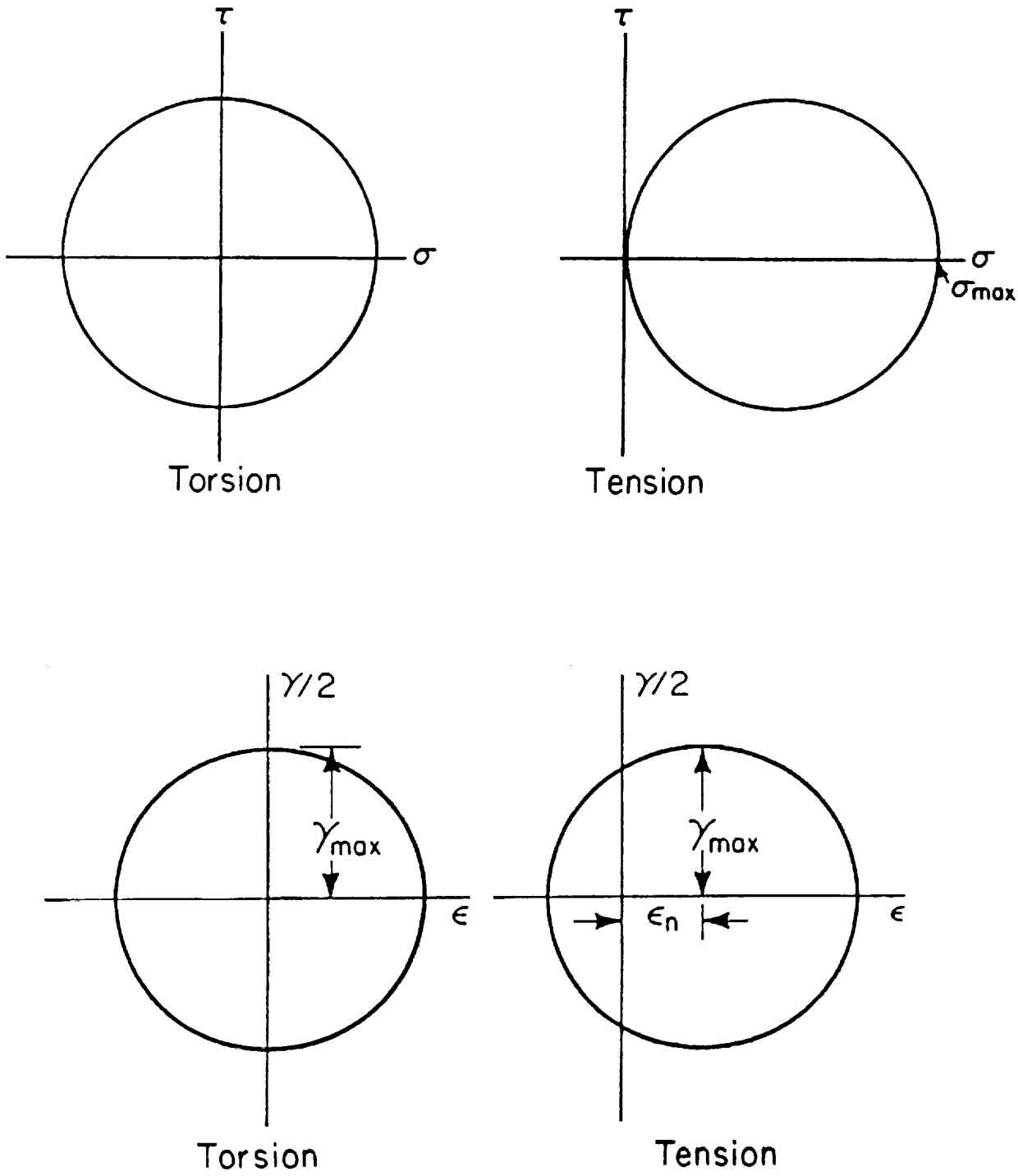

Figure 13 Comparison of Axial and Torsional Stress and Strain States

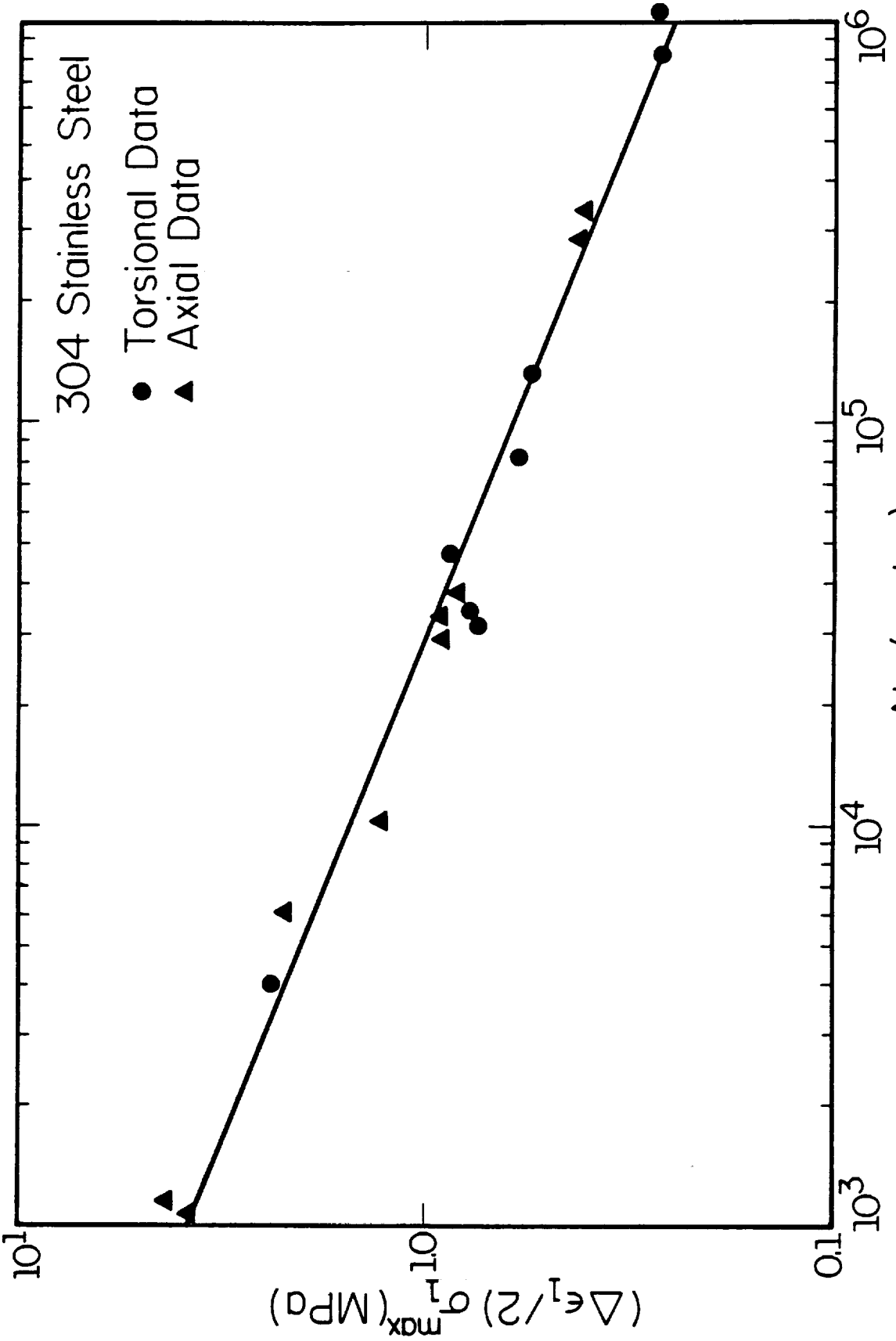

Figure 14 Comparison of Axial and Torsional Data using Smith, Watson, Topper Parameter

TORSION

$(R_\epsilon = 1,\ R_\gamma = -1)$

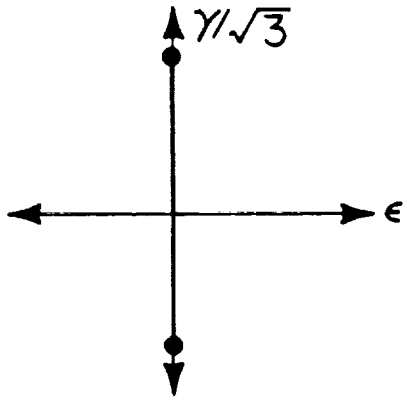

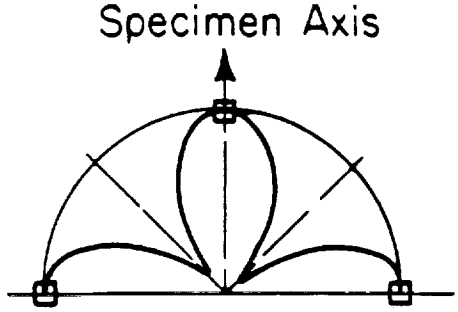

Polar Plot

Shear Strain Amplitude ($\dot{\gamma}$)

vs

Plane Angle (θ)

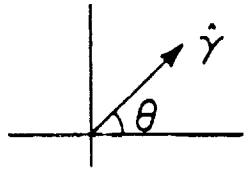

$$\left[\begin{array}{l} \frac{\Delta\gamma}{2} = 0.017 \\ \frac{\Delta\epsilon}{2} = 0 \end{array}\right]$$

N = 800

N_{10} = 1,370

SS-08

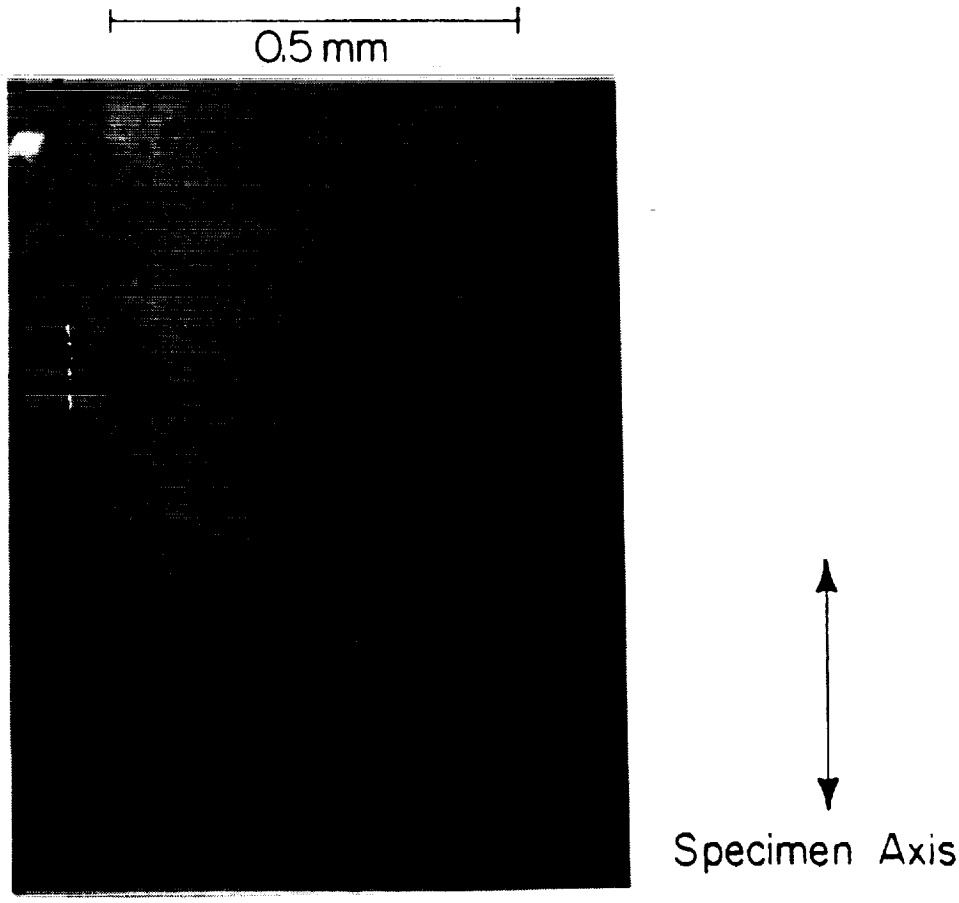

Figure 15 Typical Surface Crack Features, $\frac{\Delta\gamma}{2} = 0.017$

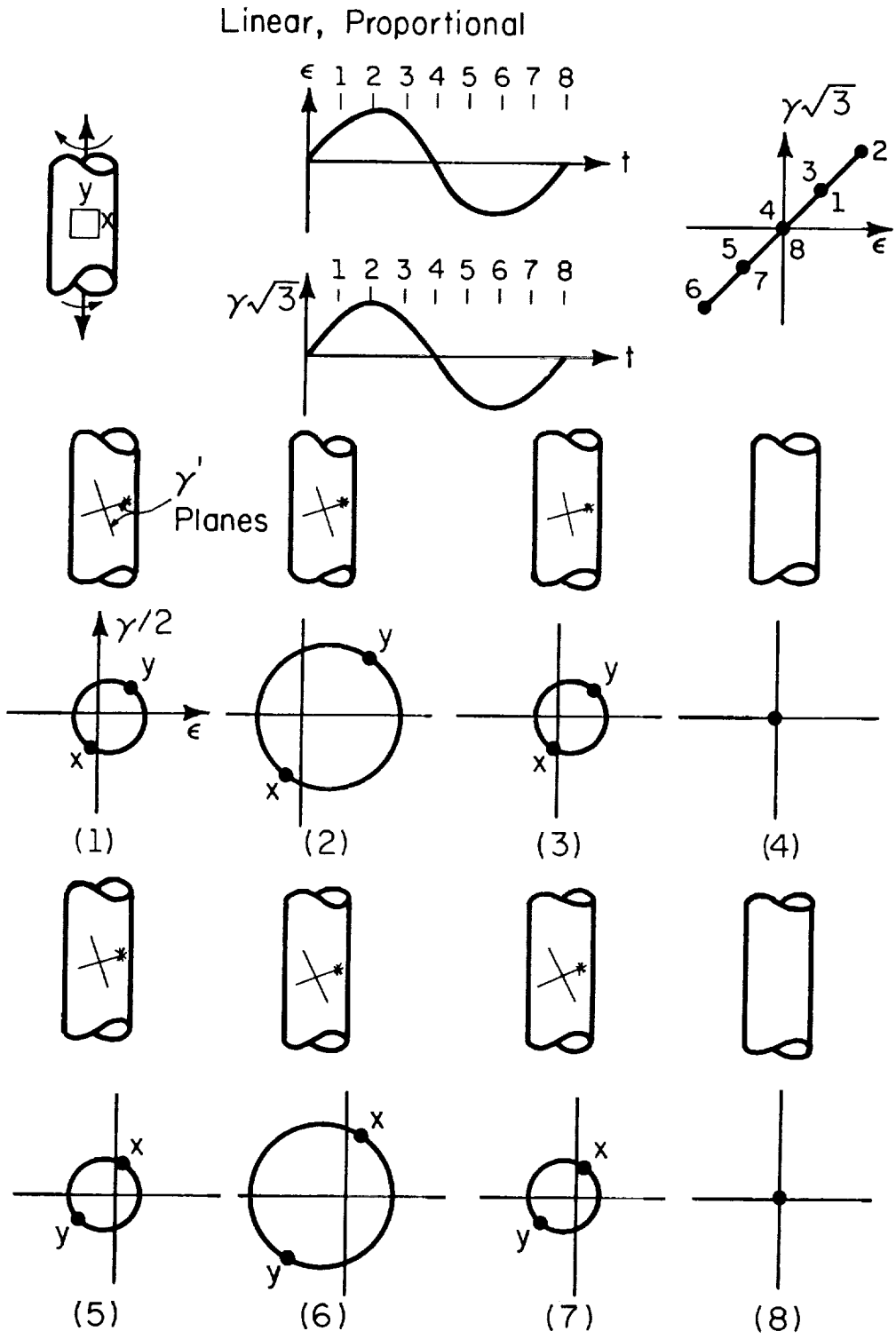

Figure 16 Illustration of the State of Strain for Proportional Path

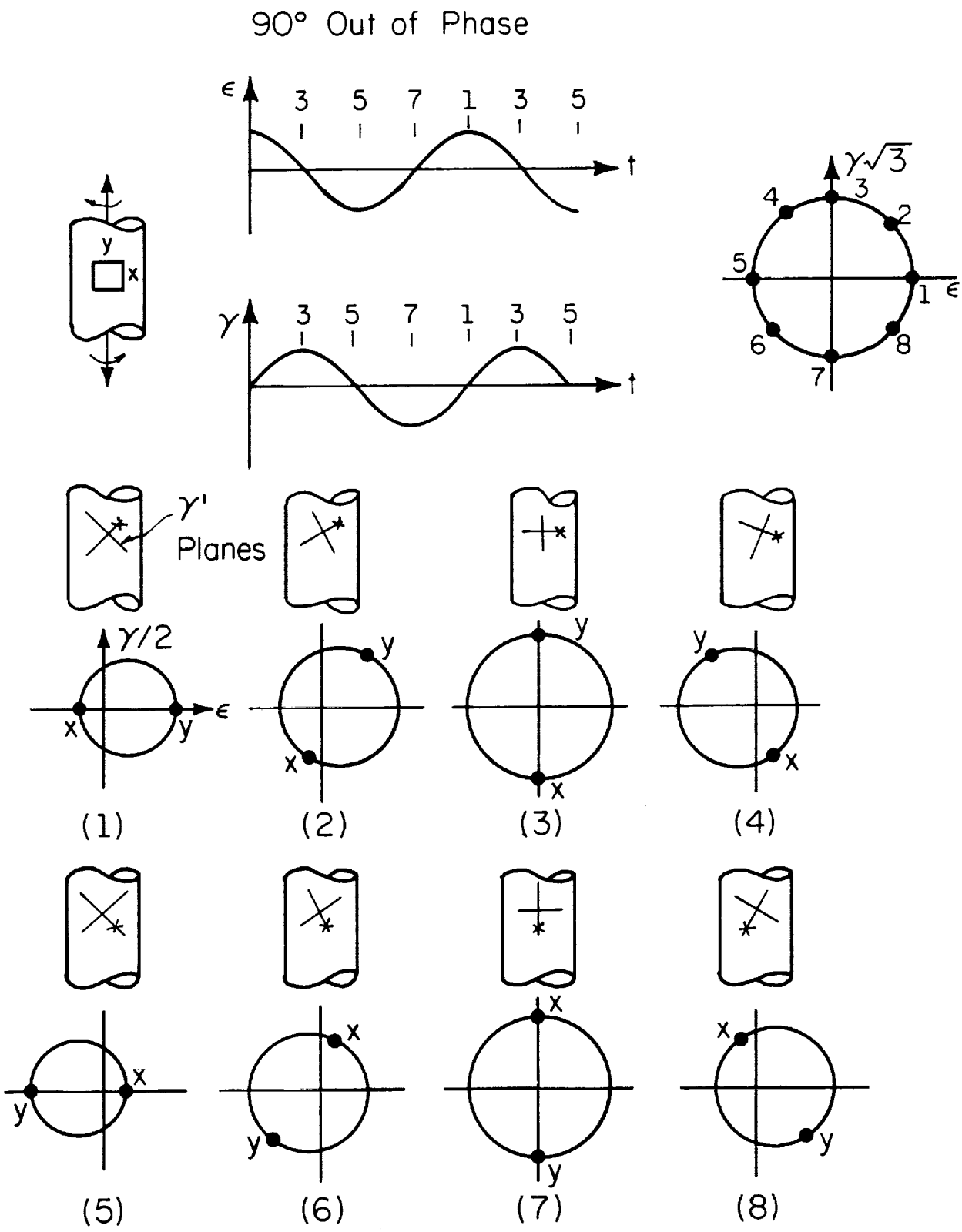

Figure 17 Illustration of the State of Strain for 90° Out-of-Phase Path

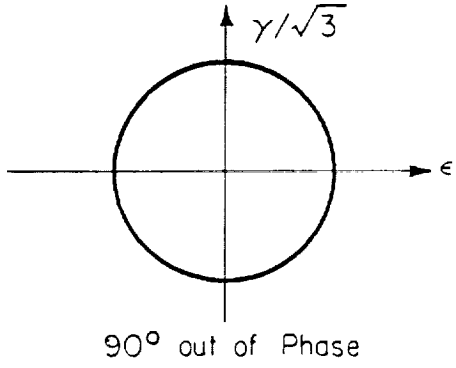

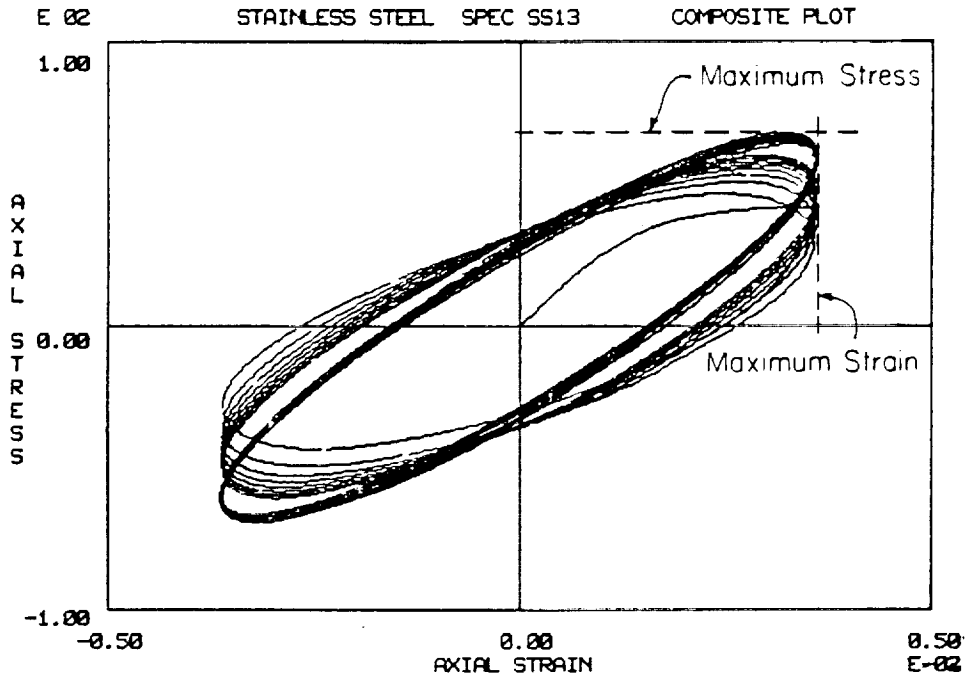

Figure 18 Stress Strain Response for Out-of-Phase Loading

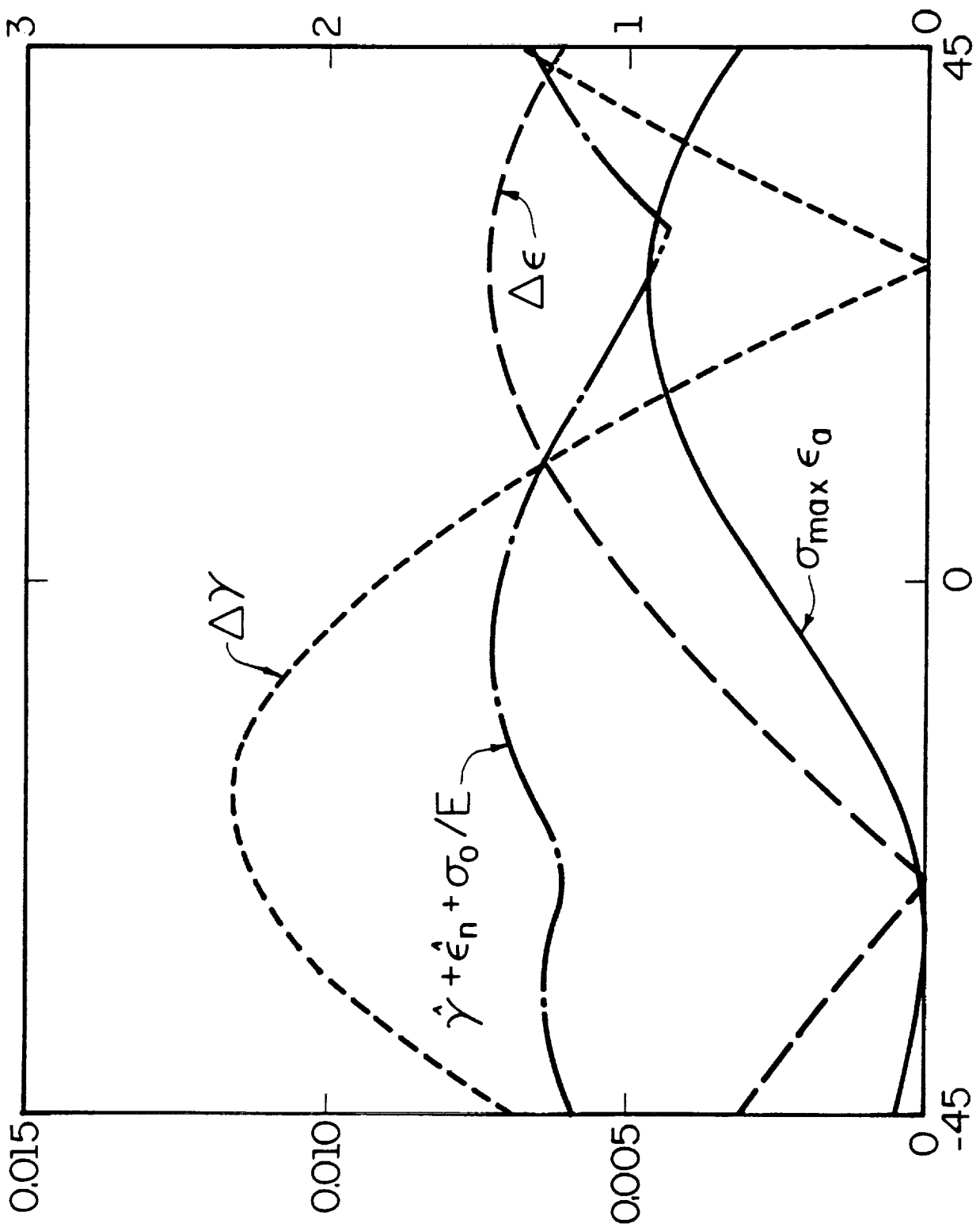

Figure 19 Variation of Strain Amplitudes, Proportional Path

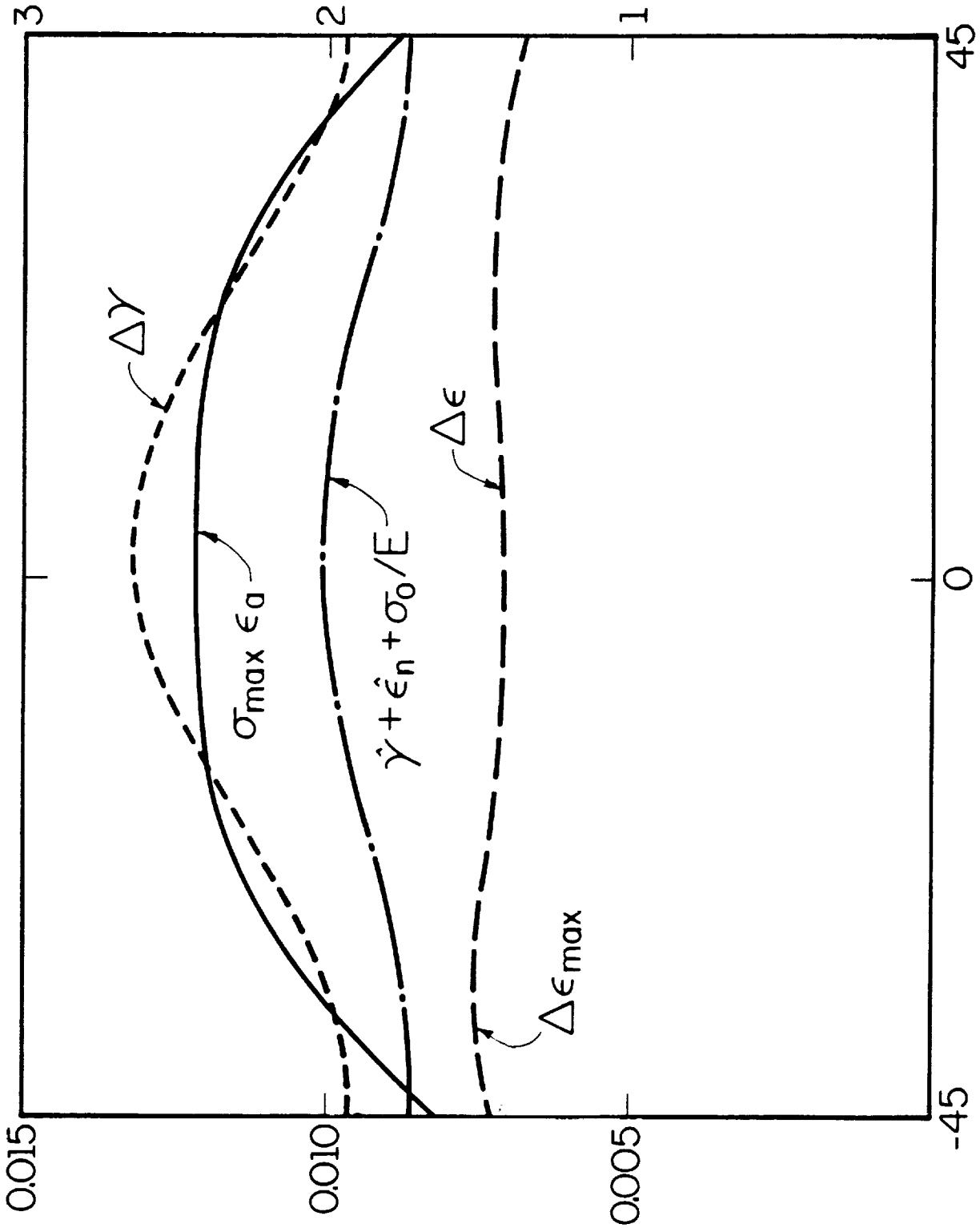

Figure 20 Variation of Strain Amplitudes, 90° Out-of-Phase Path

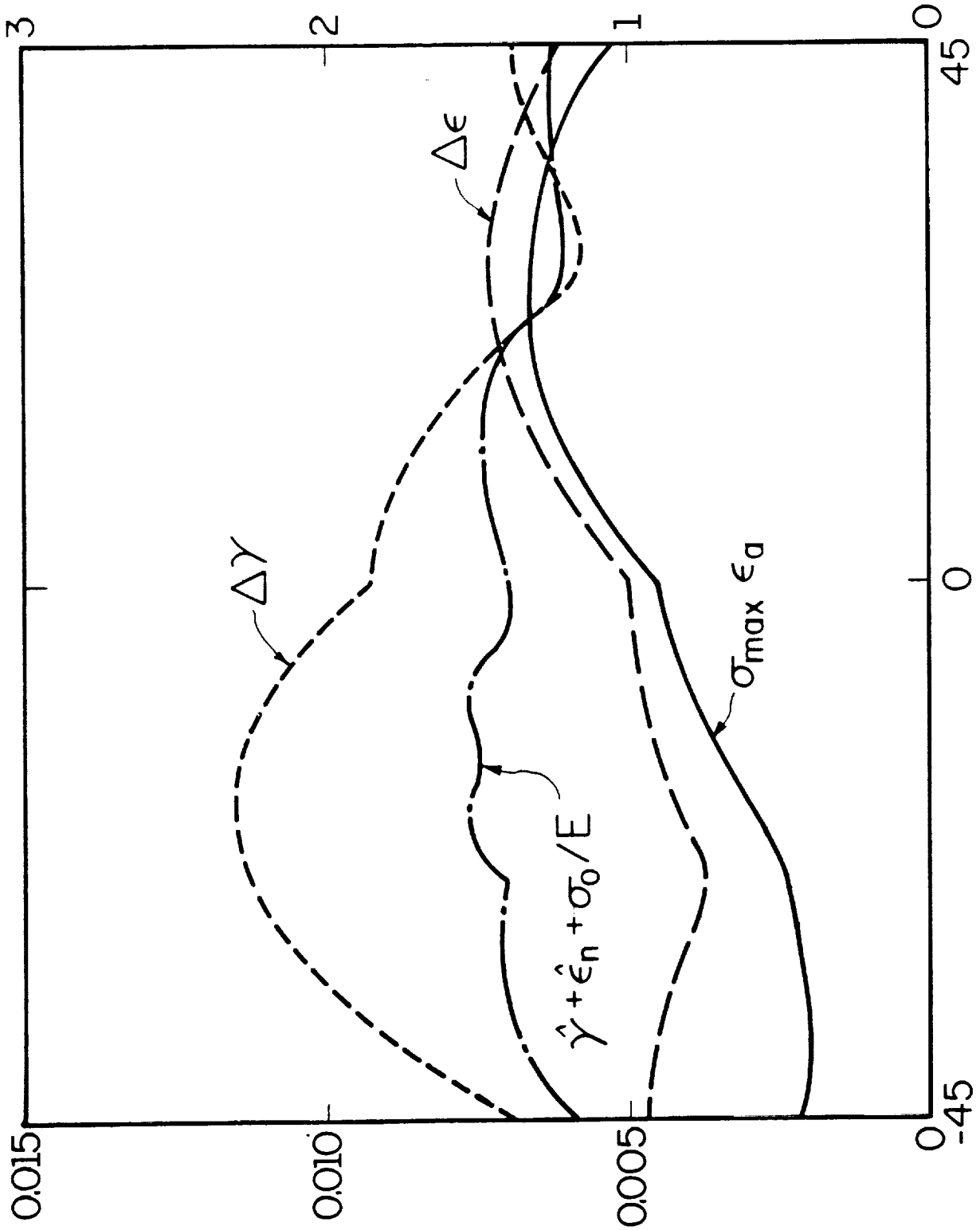

Figure 21 Variation of Strain Amplitudes, Two Box Path

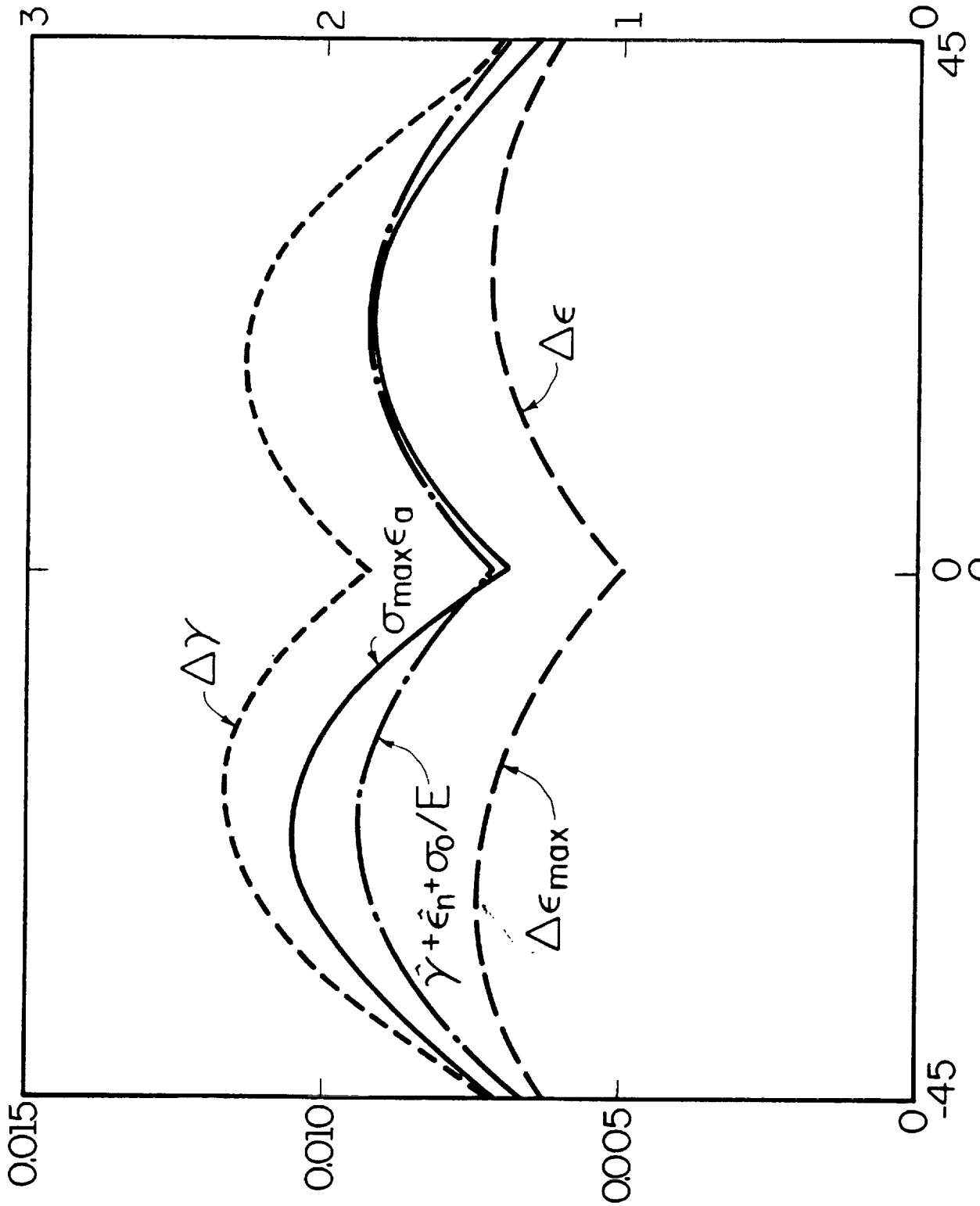

Figure 22 Variation of Strain Amplitudes, Box Path

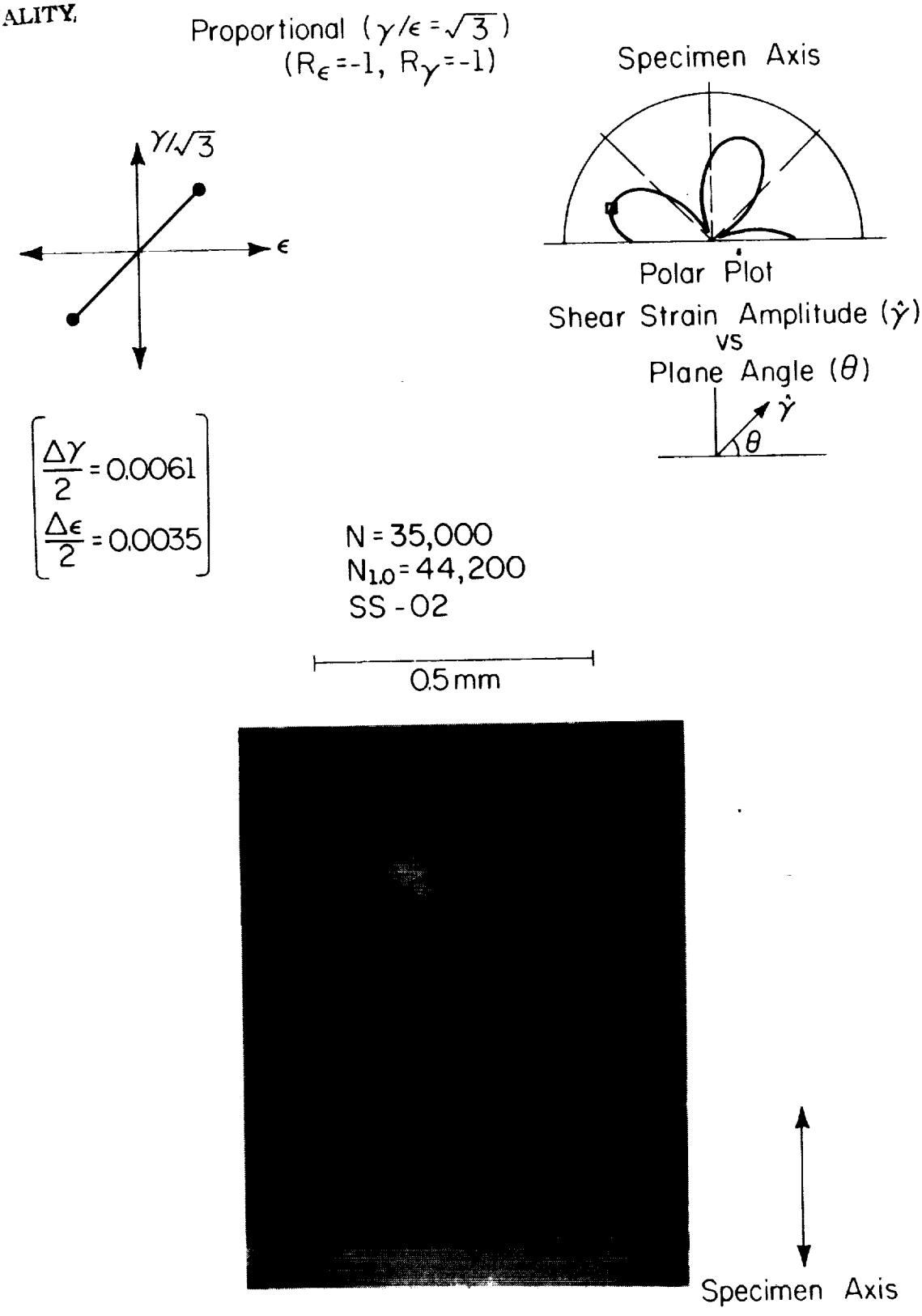

Figure 23 Typical Surface Crack for Proportional Paths

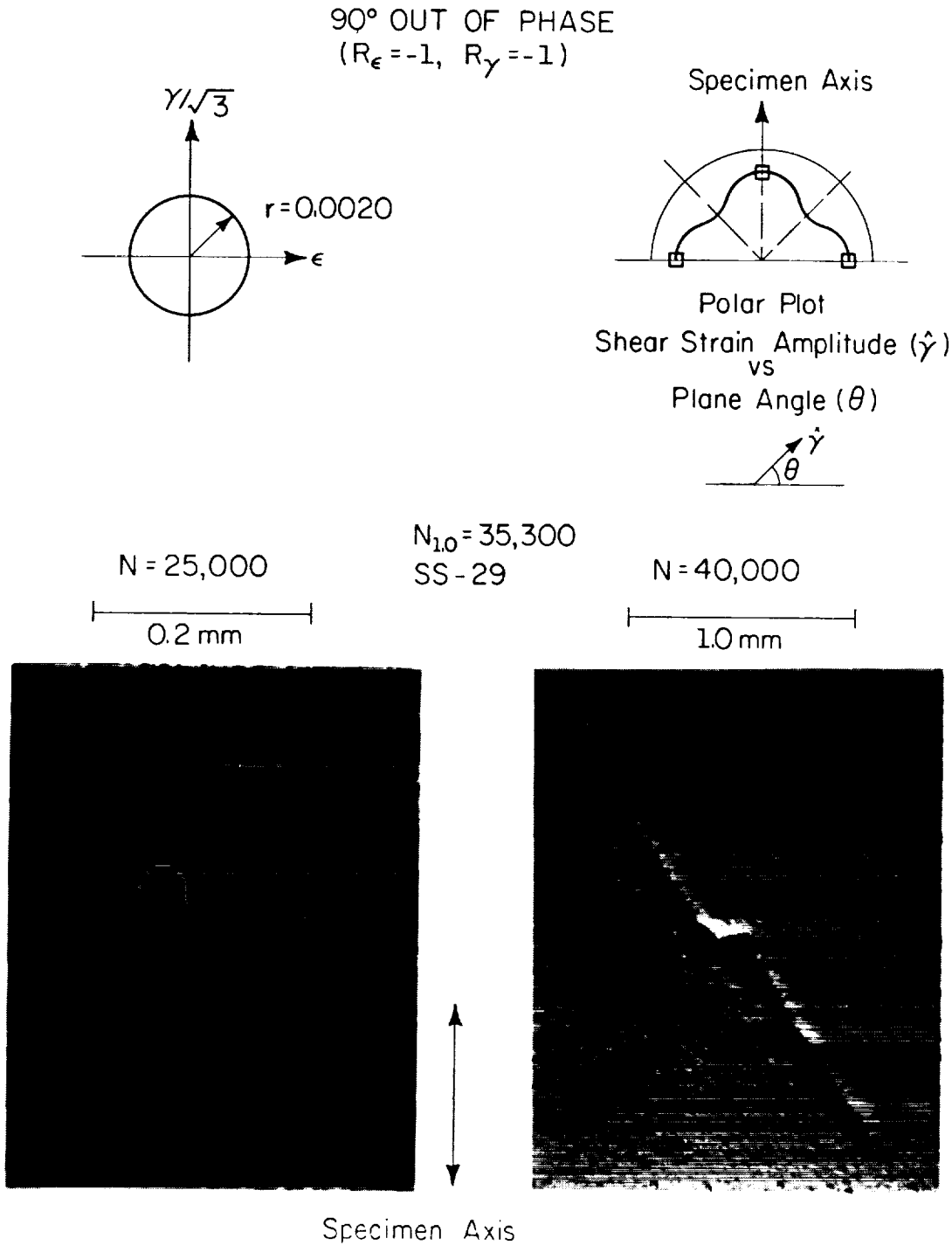

Figure 24 Typical Surface Crack for 90° Out-of-Phase Path

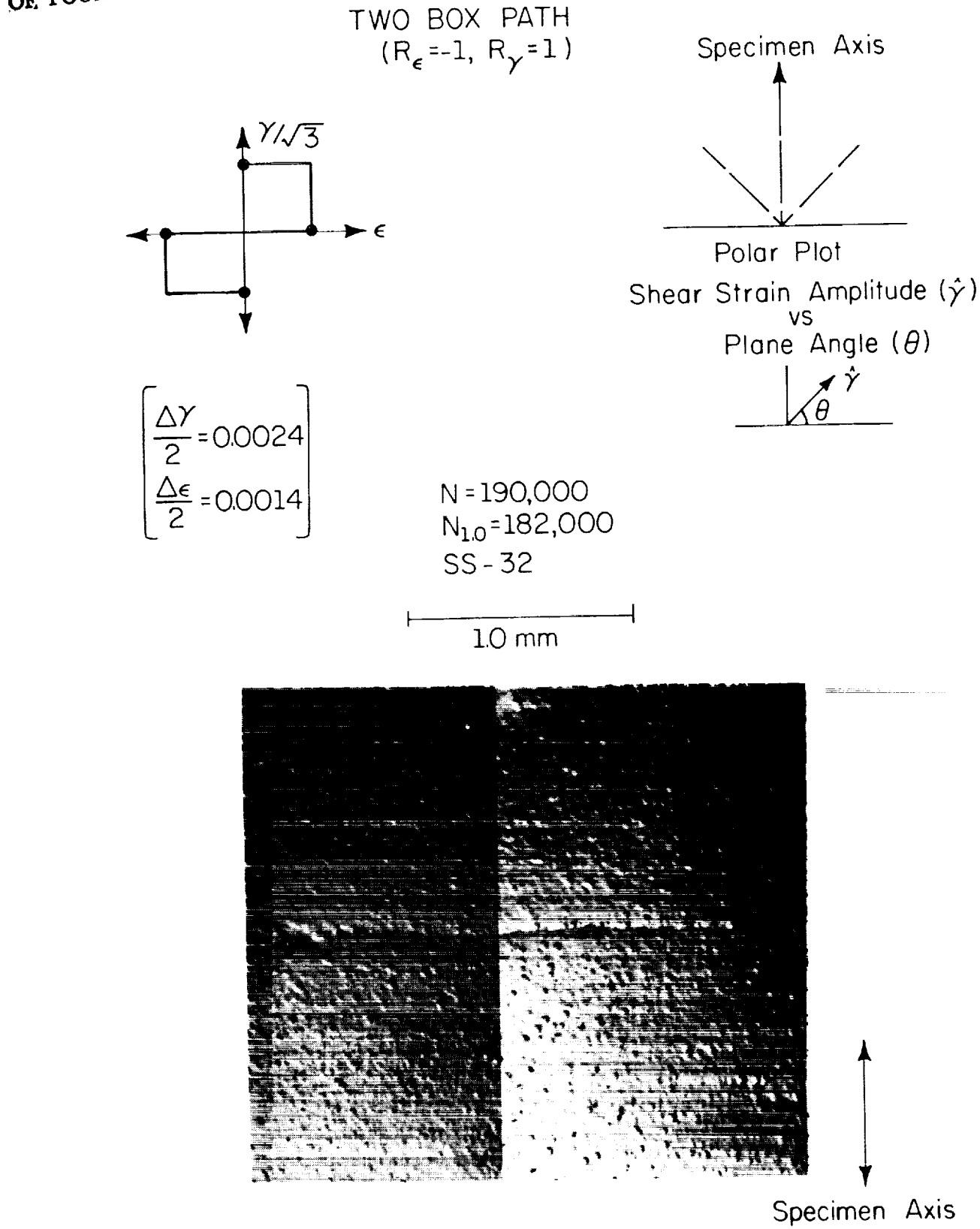

Figure 25 Typical Surface Crack for Two Box Path

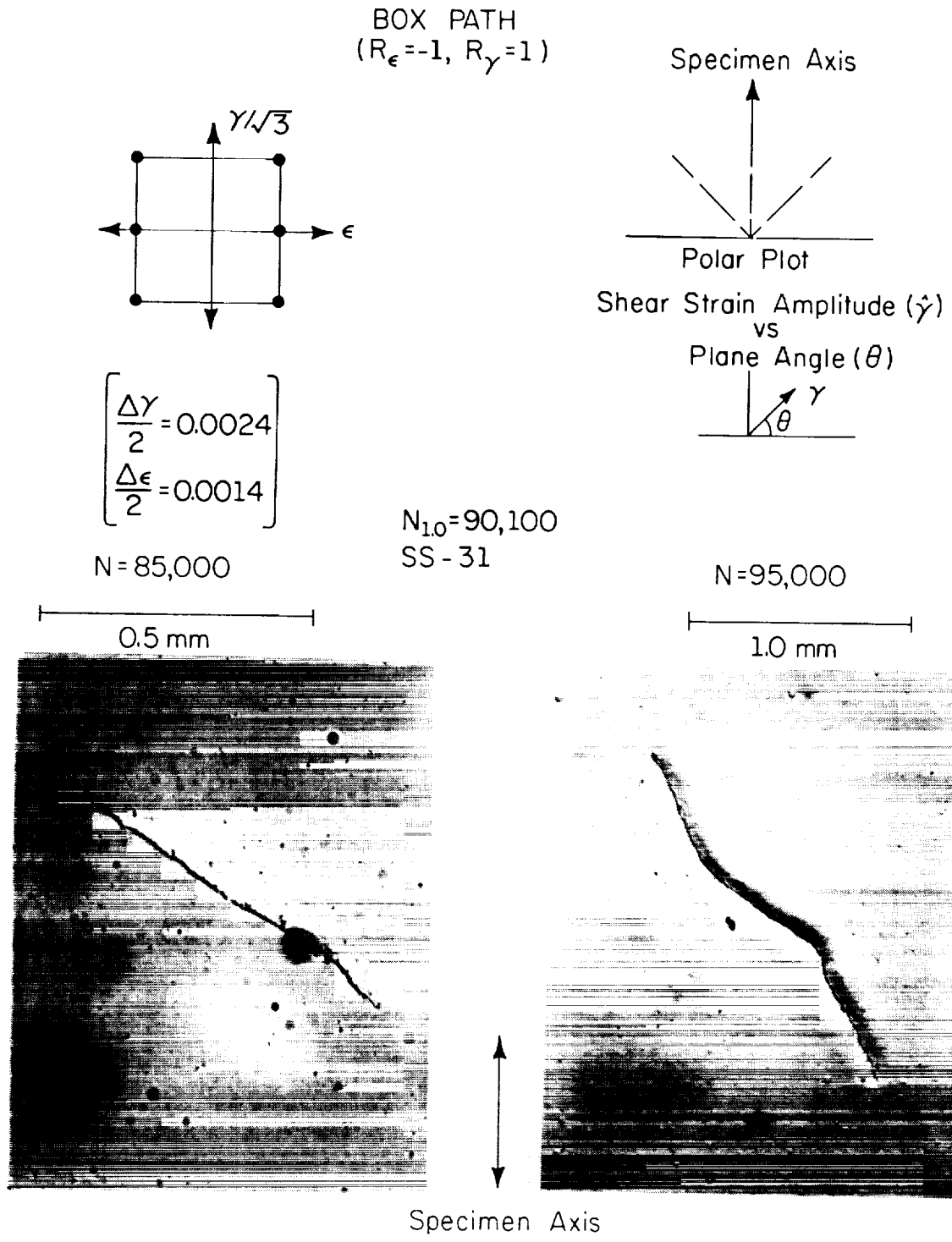

Figure 26 Typical Surface Crack for Box Path

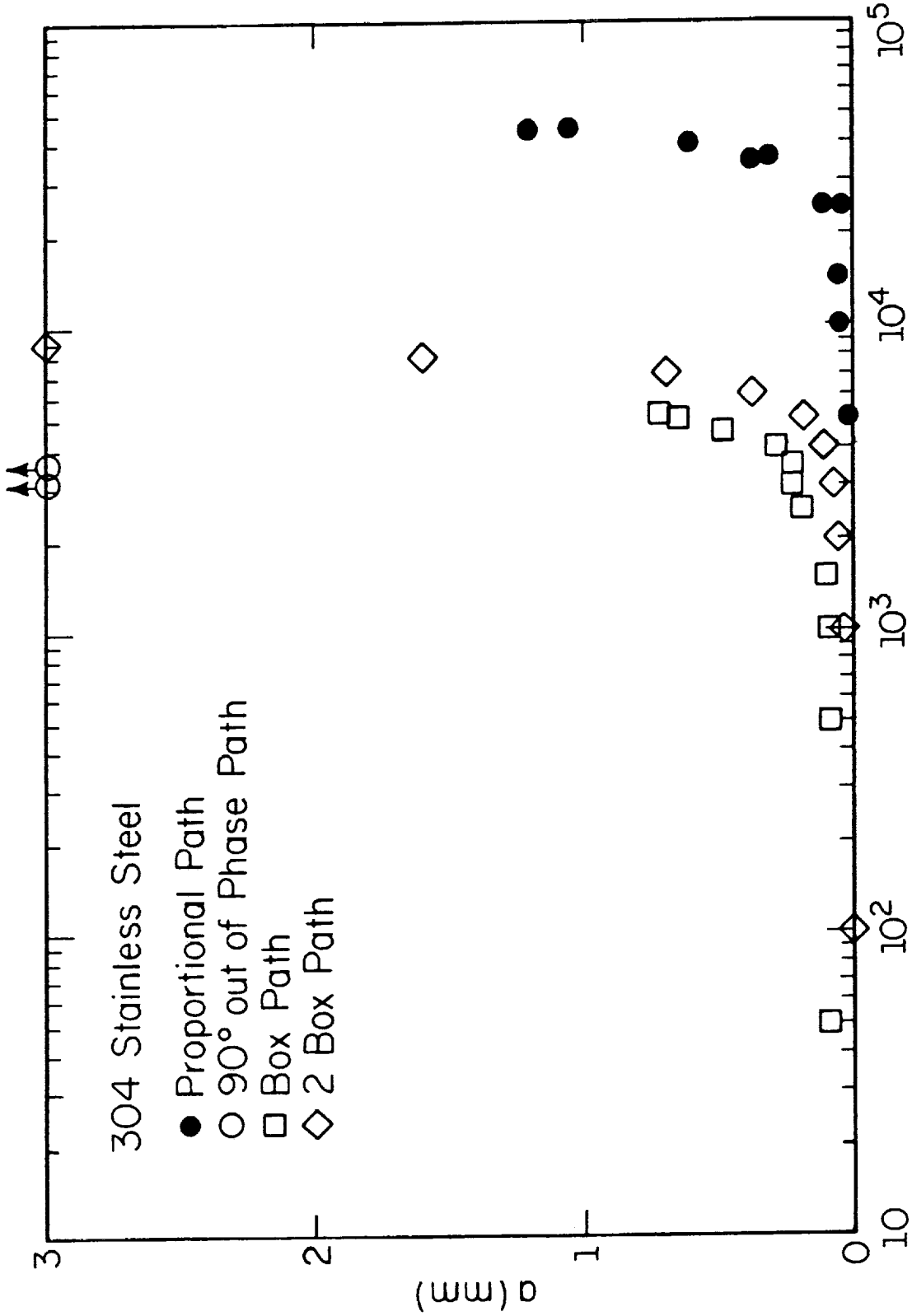

Figure 27 Crack Growth Data for Short Life Biaxial Tests

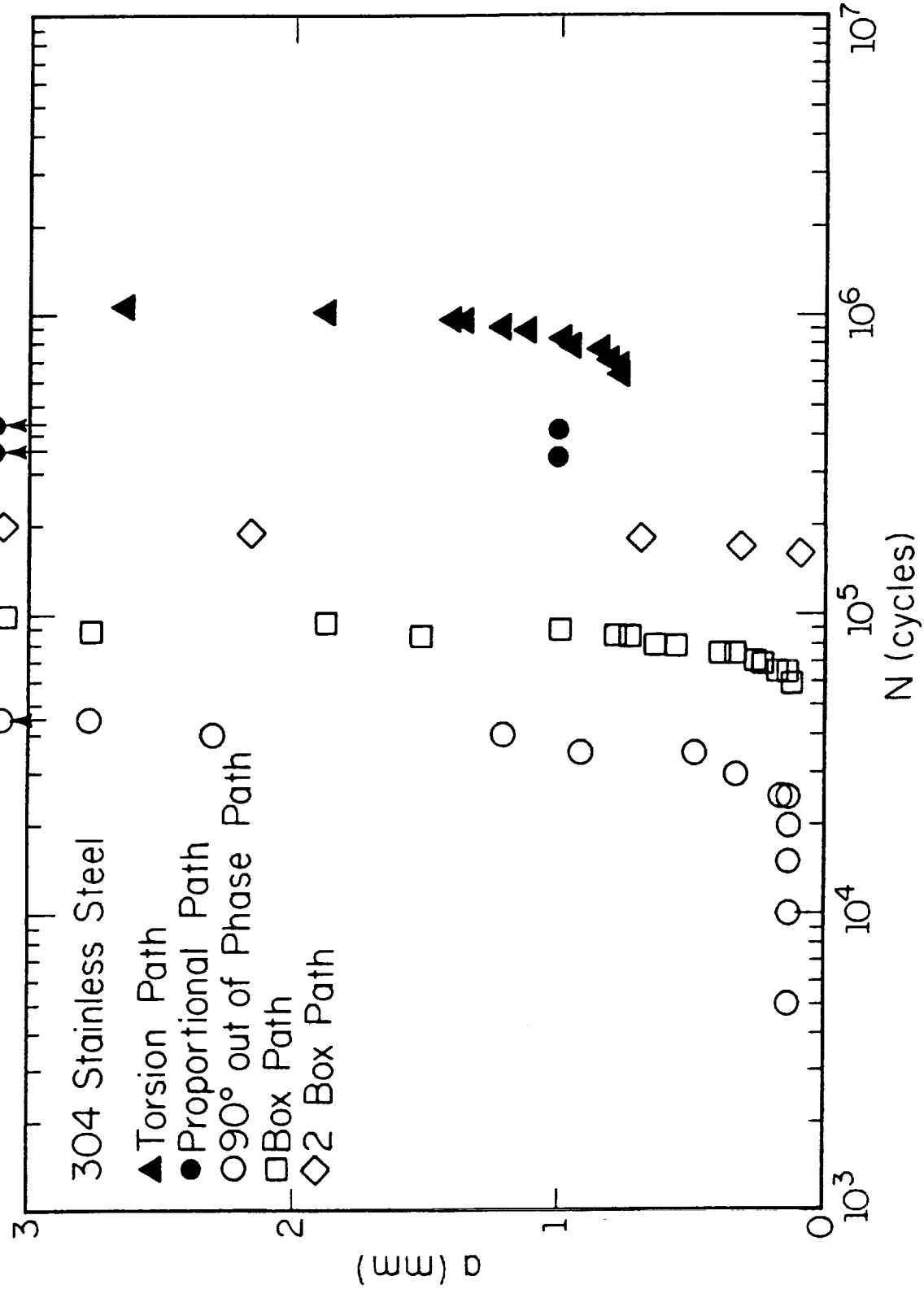

Figure 28 Crack Growth Data for Intermediate Life Biaxial Tests

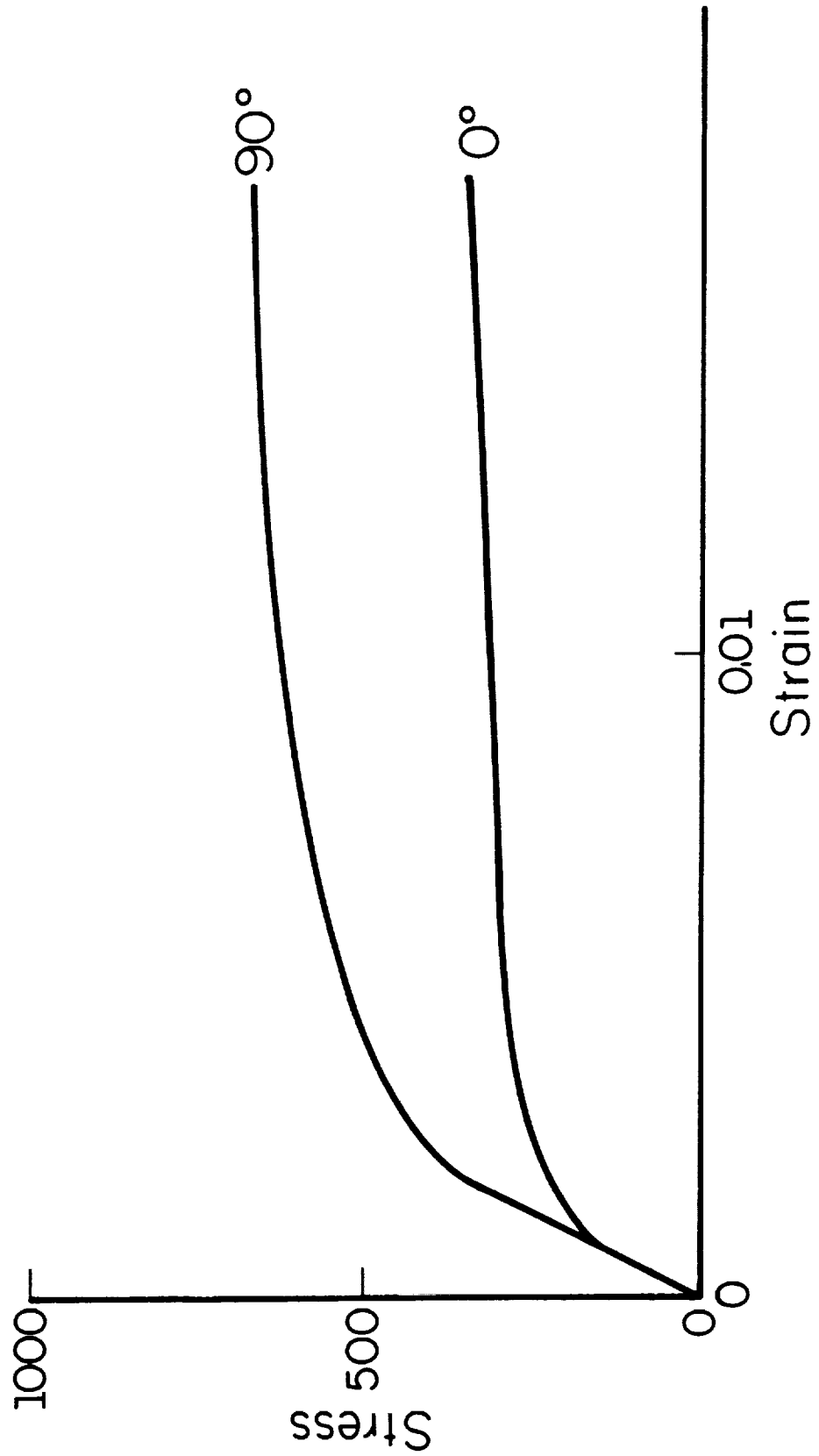

Figure 29 Comparison of Cyclic Hardenings for In-Phase and Out-of-Phase Loading

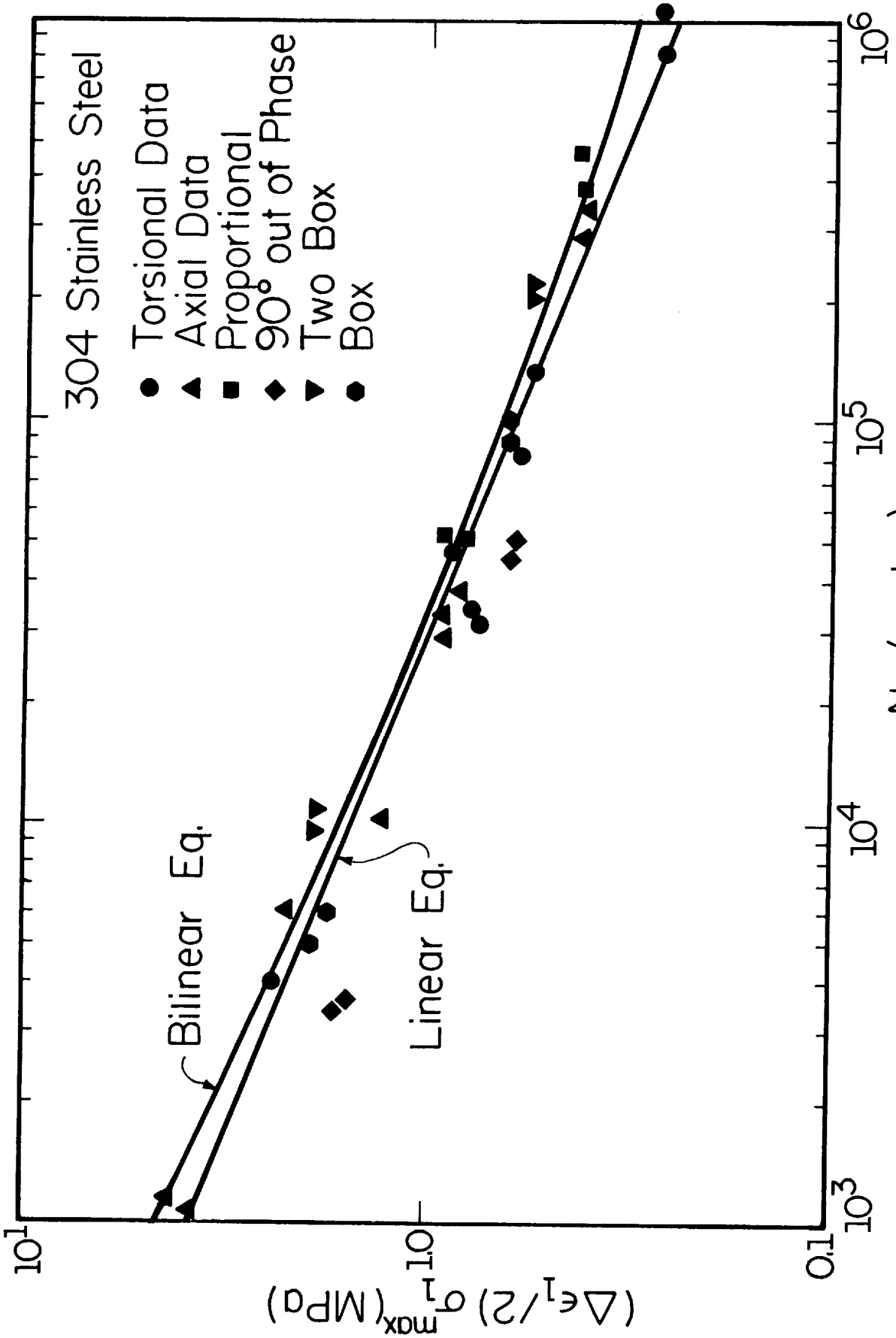

Figure 30 Comparison of Axial Torsional and Biaxial Data Using Modified Smith, Watson, Topper Parameter

APPENDIX A: CRACK GROWTH DATA

LIST OF TABLES

TABLE PAGE

A.1 Proportional, $\frac{\Delta\epsilon}{2}$ = 0.0025, $\frac{\Delta\gamma}{2}$= 0.00432 65

A.2 Proportional, $\frac{\Delta\epsilon}{2}$ = 0.0025, $\frac{\Delta\gamma}{2}$ = 0.00432 66

A.3 Proportional, $\frac{\Delta\epsilon}{2}$ = 0.0014, $\frac{\Delta\gamma}{2}$ = 0.0024 67

A.4 Proportional, $\frac{\Delta\epsilon}{2}$ =0.0014, $\frac{\Delta\gamma}{2}$ = 0.0024 68

A.5 Torsional, $\frac{\Delta\epsilon}{2}$ = 0, $\frac{\Delta\gamma}{2}$ = 0.0035.....69

A.6 90° Out-of-Phase, $\frac{\Delta\epsilon}{2}$ = 0.00353, $\frac{\Delta\gamma}{2}$ = 0.00612.....70

A.7 90° Out-of-Phase, $\frac{\Delta\epsilon}{2}$ = 0.00353, $\frac{\Delta\gamma}{2}$ = 0.00612.....71

A.8 90° Out-of-Phase, $\frac{\Delta\epsilon}{2}$ = 0.062, $\frac{\Delta\gamma}{2}$ = 0.0035.....72

A.9 90° Out-of-Phase, $\frac{\Delta\epsilon}{2}$ = 0.002, $\frac{\Delta\gamma}{2}$ =0.0035.....73

A.10 Box, $\frac{\Delta\epsilon}{2}$ = 0.0025, $\frac{\Delta\gamma}{2}$ = 0.00432.....74

A.11 Box, $\frac{\Delta\epsilon}{2}$ = 0.0025, $\frac{\Delta\gamma}{2}$ = 0.00432.....75

A.12 Box, $\frac{\Delta\epsilon}{2}$ = 0.0014, $\frac{\Delta\gamma}{2}$ = 0.0024.....76

A.13 Box, $\frac{\Delta\epsilon}{2}$ = 0.0014, $\frac{\Delta\gamma}{2}$ = 0.0024.....77

A.14 Two Box, $\frac{\Delta\epsilon}{2}$ = 0.0025, $\frac{\Delta\gamma}{2}$ = 0.0043.....78

A.15 Two Box, $\frac{\Delta\epsilon}{2}$ = 0.0014, $\frac{\Delta\gamma}{2}$ = 0.0024.....79

A.16 Two Box, $\frac{\Delta\epsilon}{2}$ = 0.0014, $\frac{\Delta\gamma}{2}$ = 0.0024.....80

Table A.1
Stainless Steel 304
Crack Growth Data
Specimen I.D. SS12 (Path C)

$R_\varepsilon = -1$ $R_\gamma = -1$
$\Delta\varepsilon/2 = 0.0025$ $\Delta\gamma/2 = 0.00432$

N (cycles)	L (mm)	a_1 (mm)	a_2 (mm)	a_3 (mm)	Comments
50,000	3.769	0	3.769	0	
45,000	1.225	0	1.225	0	
40,000	0.612	0	0.612	0	
35,000	0.319	0	0.319	0	
30,000	0.175	0	0.175	0	
25,000	0.047	0	0.047	0	Note: High crack density; failure is caused by crack linkage

Table A.2
Stainless Steel 304
Crack Growth Data
Specimen I.D. SS02 (Path C)

$R_\varepsilon = -1$ $R_\gamma = -1$
$\Delta\varepsilon/2 = 0.0025$ $\Delta\gamma/2 = 0.00432$

N (cycles)	L (mm)	a_1 (mm)	a_2 (mm)	a_3 (mm)	Comments
53,031	9.08	0	9.08	0	
45,000	1.05	0	1.05	0	
35,000	0.37	0	0.37	0	
25,000	0.12	0	0.12	0	
15,000	0.05	0	0.05	0	
10,000	0.05	0	0.05	0	
5,000	0.02	0	0.02	0	

Table A.3
Stainless Steel 304
Crack Growth Data
Specimen I.D. SS25 (Path C)

$R_\varepsilon = -1$ $R_\gamma = -1$
$\Delta\varepsilon/2 = 0.0014$ $\Delta\gamma/2 = 0.0024$

N (cycles)	L (mm)	a_1 (mm)	a_2 (mm)	a_3 (mm)	Comments
Failure	12.15	1.89	0.612	10.08	No visible cracks before failure.

Table A.4
Stainless Steel 304
Crack Growth Data
Specimen I.D. SS26 (Path C)

$R_\varepsilon = -1$ $R_\gamma = -1$
$\Delta\varepsilon/2 = 0.0014$ $\Delta\gamma/2 = 0.0024$

N (cycles)	L (mm)	a_1 (mm)	a_2 (mm)	a_3 (mm)	Comments
Failure	18.9	11.0	1.35	6.41	No visible cracks before failure.

Table A.5
Stainless Steel 304
Crack Growth Data
Specimen I.D. SS27 (Path B)

$R_\varepsilon = 1$ $R_\gamma = -1$
$\Delta\varepsilon/2 = 0$ $\Delta\gamma/2 = 0.0035$

N (cycles)	L (mm)	a_1 (mm)	a_2 (mm)	a_3 (mm)	Comments
Failure	5.58	2.93	2.30	2.29	
1,090,000	2.64	1.31	2.30	0.81	
1,040,000	1.87	0.86	2.30	0.50	
990,000	1.39	0.57	2.30	0.38	
960,000	1.35	0.48	2.30	0.35	
930,000	1.20	0.38	2.30	0.29	
900,000	1.12	0.27	2.30	0.28	
870,000	1.08	0.26	2.30	0.21	
840,000	0.98	0.25	2.30	0.20	
810,000	0.95	0.24	2.30	0.15	
780,000	0.84	0.17	2.30	0.14	
720,000	0.80	0.15	2.30	0.09	
690,000	0.76	0.12	2.30	0.08	
660,000	0.76	0.10	2.30	0.04	
630,000	0	0.07	2.30	0	a_3 bifurcates
600,000	0	0.07	2.30	0	Crack starts at stringer inclusion
0	0	0	2.30	0	

Table A.6
Stainless Steel 304
Crack Growth Data
Specimen I.D. SS10 (Path N)

$R_\varepsilon = -1$ $R_\gamma = -1$
$\Delta\varepsilon/2 = 0.00353$ $\Delta\gamma/2 = 0.00612$

N (cycles)	L (mm)	a_1 (mm)	a_2 (mm)	a_3 (mm)	Comments
3,562	9.57	0	9.57	0	
3,000	0	0	0	0	

Table A.7
Stainless Steel 304
Crack Growth Data
Specimen I.D. SS13 (Path N)

$R_\varepsilon = -1$ $R_\gamma = -1$
$\Delta\varepsilon/2 = 0.00353$ $\Delta\gamma/2 = 0.00612$

N (cycles)	L (mm)	a_1 (mm)	a_2 (mm)	a_3 (mm)	Comments
3,733	5.46	0	5.46	0	
3,600	0	0	0	0	

Table A.8
Stainless Steel 304
Crack Growth Data
Specimen I.D. SS28 (Path N)

$R_\varepsilon = -1$ $R_\gamma = -1$
$\Delta\varepsilon/2 = 0.002$ $\Delta\gamma/2 = 0.0035$

N (cycles)	L (mm)	a_1 (mm)	a_2 (mm)	a_3 (mm)	Comments
49,818	~9.61	~4.85	~0.176	~4.80	Cracks are too thick for accurate measurement.
45,000	2.770	1.330	0.171	1.380	
40,000	1.196	0.522	0.171	0.554	
35,000	0.487	0.200	0.171	0.130	
30,000	0.277	0.059	0.171	0.060	Bifurcation
25,000	0.139	0	0.139	0	
20,000	0.134	0	0.134	0	
15,000	0.130	0	0.130	0	
10,000	0.130	0	0.130	0	
5,000	0.129	0	0.129	0	

Table A.9
Stainless Steel 304
Crack Growth Data
Specimen I.D. SS29 (Path N)

$R_\varepsilon = -1$ $R_\gamma = -1$
$\Delta\varepsilon/2 = 0.002$ $\Delta\gamma/2 = 0.0035$

N (cycles)	L (mm)	a_1 (mm)	a_2 (mm)	a_3 (mm)	Comments
45,000	~10.08	4.420	~0.120	5.770	
40,000	2.350	1.147	~0.114	1.149	
35,000	0.910	0.422	0.111	0.430	
30,000	0.335	0.152	0.111	0.119	
25,000	0.152	0.040	0.111	0.038	Crack is very thin
20,000	0	0	0	0	

Table A.10
Stainless Steel 304
Crack Growth Data
Specimen I.D. SS03 (Path P)

$R_\varepsilon = -1$ $R_\gamma = -1$
$\Delta\varepsilon/2 = 0.0025$ $\Delta\gamma/2 = 0.00432$

N (cycles)	L (mm)	a_1 (mm)	a_2 (mm)	a_3 (mm)	Comments
5,013	0.72	0.130	0.601	0.110	
5,000	0.65	0.123	0.601	0.059	Change in crack direction
4,500	0.48	0	0.48	0	
4,000	0.28	0	0.28	0	
3,500	0.22	0	0.22	0	
3,000	0.22	0	0.22	0	
2,500	0.18	0	0.18	0	
1,500	0.10	0	0.10	0	
1,000	0.08	0	0.08	0	
500	0.08	0	0.08	0	
50	0.08	0	0.08	0	
0	0.08	0	0.08	0	Scratch on specimen

Table A.11
Stainless Steel 304
Crack Growth Data
Specimen I.D. SS11 (Path P)

$R_\varepsilon = -1$ $R_\gamma = -1$

$\Delta\varepsilon/2 = 0.0025$ $\Delta\gamma/2 = 0.00432$

N (cycles)	L (mm)	a_1 (mm)	a_2 (mm)	a_3 (mm)	Comments
6,202	10.00	0	10.00	0	
6,000	0	0	0	0	
6,000	0.923	0	0.923	0	Non-failure crack
5,500	0.444	0	0.444	0	
5,000	0.241	0	0.241	0	
4,560	0.141	0	0.141	0	
4,000	0.125	0	0.125	0	
3,500	0.119	0	0.119	0	
3,000	0.063	0	0.063	0	

Table A.12
Stainless Steel 304
Crack Growth Data
Specimen I.D. SS30 (Path P)

$R_\varepsilon = -1$ $R_\gamma = -1$
$\Delta\varepsilon/2 = 0.0014$ $\Delta\gamma/2 = 0.0024$

N (cycles)	L (mm)	a_1 (mm)	a_2 (mm)	a_3 (mm)	Comments
89,312	2.760	1.389	~0.084	1.424	
85,000	1.516	0.783	0.077	0.658	
80,000	0.641	0.315	0.077	0.283	
75,000	0.393	0.143	0.077	0.116	
70,000	0.235	0.132	0.077	0.042	a_3 bifurcates
65,000	0.147	0.079	0.077	0	
60,000	0	0	0	0	

Table A.13
Stainless Steel 304
Crack Growth Data
Specimen I.D. SS31 (Path P)

$R_\varepsilon = -1$ $R_\gamma = -1$
$\Delta\varepsilon/2 = 0.0014$ $\Delta\gamma/2 = 0.0024$

N (cycles)	L (mm)	a_1 (mm)	a_2 (mm)	a_3 (mm)	Comments
100,000	3.010	1.264	0.740	1.135	
95,000	1.853	0.661	0.740	0.574	
90,000	0.982	0.254	0.740	0.160	Bifurcation
86,638	0.789	0.025	0.740	0.059	
85,000	0.727	0	0.727	0	
80,000	0.506	0	0.506	0	
75,000	0.339	0	0.339	0	
70,000	0.246	0	0.246	0	
65,000	0.177	0	0.177	0	
60,000	0.128	0	0.128	0	

Table A.14
Stainless Steel 304
Crack Growth Data
Specimen I.D. SS04 (Path Q)

$R_\varepsilon = -1$ $R_\gamma = -1$
$\Delta\varepsilon/2 = 0.0025$ $\Delta\gamma/2 = 0.0043$

N (cycles)	L (mm)	a_1 (mm)	a_2 (mm)	a_3 (mm)	Comments
9,000	3.00	1.07	0.938	1.18	
8,000	1.60	0.36	0.938	0.395	Change in crack direction
7,000	0.69	0	0.69	0	
6,000	0.37	0	0.37	0	
5,000	0.18	0	0.18	0	
4,000	0.11	0	0.11	0	
3,000	0.07	0	0.07	0	
2,000	0.06	0	0.06	0	
1,000	0.03	0	0.03	0	
100	0.01	0	0.01	0	

Table A.15
Stainless Steel 304
Crack Growth Data
Specimen I.D. SS32 (Path Q)

$R_\varepsilon = -1$ $R_\gamma = -1$
$\Delta\varepsilon/2 = 0.0014$ $\Delta\gamma/2 = 0.0024$

N (cycles)	L (mm)	a_1 (mm)	a_2 (mm)	a_3 (mm)	Comments
200,000	25.4	17.7	0.44	7.7	
190,000	2.16	2.16	0	0	
180,000	0.69	0.69	0	0	
170,000	0.304	0.304	0	0	
160,000	0.09	0.09	0	0	Crack is extremely thin

Table A.16
Stainless Steel 304
Crack Growth Data
Specimen I.D. SS33 (Path Q)

$R_\varepsilon = -1$ $R_\gamma = -1$
$\Delta\varepsilon/2 = 0.0014$ $\Delta\gamma/2 = 0.0024$

N (cycles)	L (mm)	a_1 (mm)	a_2 (mm)	a_3 (mm)	Comments
205,000	5.52	0	5.52	0	
200,000	2.54	0	2.54	0	
195,000	1.34	0	1.34	0	
190,000	0.727	0	0.727	0	
185,000	0.384	0	0.384	0	
180,000	0.195	0	0.195	0	Crack is extremely thin

APPENDIX B: TYPICAL SURFACE CRACK FEATURES

LIST OF FIGURES

FIGURE PAGE

B.1 Proportional Path, $\frac{\Delta\varepsilon}{2} = 0.0035$, $\frac{\Delta\gamma}{2} = 0.0061$.....82

B.2 Proportional Path, $\frac{\Delta\varepsilon}{2} = 0.0014$, $\frac{\Delta\gamma}{2} = 0.0024$.....83

B.3 Proportional Path, $\frac{\Delta\varepsilon}{2} = 0.0014$, $\frac{\Delta\gamma}{2} = 0.0024$.....84

B.4 90° Out-of-Phase, $\frac{\Delta\varepsilon}{2} = 0.00353$, $\frac{\Delta\gamma}{2} = 0.00612$.....85

B.5 90° Out-of Phase, $\frac{\Delta\varepsilon}{2} = 0.002$, $\frac{\Delta\gamma}{2} = 0.0035$ 86

B.6 90° Out-of-Phase, $\frac{\Delta\varepsilon}{2} = 0.002$, $\frac{\Delta\gamma}{2} = 0.0035$ 87

B.7 Box Path, $\frac{\Delta\varepsilon}{2} = 0.0025$, $\frac{\Delta\gamma}{2} = 0.0043$ 88

B.8 Box Path, $\frac{\Delta\varepsilon}{2} = 0.0014$, $\frac{\Delta\gamma}{2} = 0.0024$ 89

B.9 Box Path, $\frac{\Delta\varepsilon}{2} = 0.0014$, $\frac{\Delta\gamma}{2} = 0.0024$ 90

B.10 Two Box Path, $\frac{\Delta\varepsilon}{2} = 0.0025$, $\frac{\Delta\gamma}{2} = 0.0043$.....91

B.11 Two Box Path, $\frac{\Delta\varepsilon}{2} = 0.0014$, $\frac{\Delta\gamma}{2} = 0.0024$.....92

B.12 Two Box Path, $\frac{\Delta\varepsilon}{2} = 0.0014$, $\frac{\Delta\gamma}{2} = 0.0024$.....93

Proportional ($\gamma/\epsilon = \sqrt{3}$)
(R_ϵ=-1, R_γ=-1)

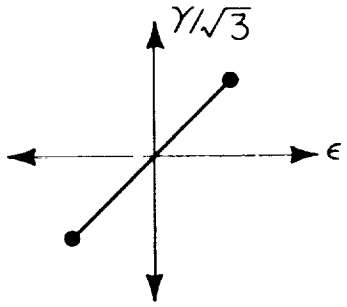

$$\left[\begin{array}{l}\frac{\Delta\gamma}{2} = 0.0061 \\ \frac{\Delta\epsilon}{2} = 0.0035\end{array}\right]$$

Specimen Axis

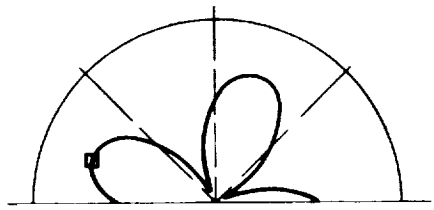

Polar Plot
Shear Strain Amplitude ($\dot{\gamma}$)
vs
Plane Angle (θ)

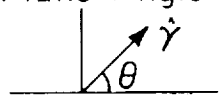

N = 35,000
$N_{1.0}$ = 44,200
SS - 02

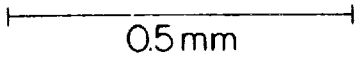

Specimen Axis

Figure B.1 Proportional Path, $\frac{\Delta\epsilon}{2}$ = 0.0035, $\frac{\Delta\gamma}{2}$ = 0.0061

Proportional ($\gamma/\epsilon = \sqrt{3}$)
($R_\epsilon = -1$, $R_\gamma = -1$)

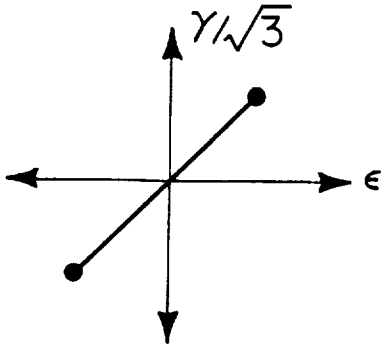

Specimen Axis

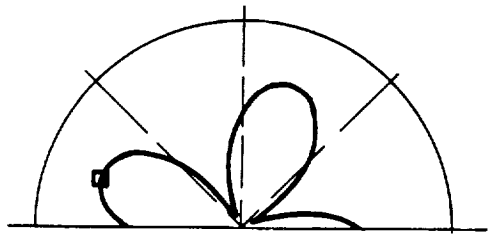

Polar Plot
Shear Strain Amplitude ($\hat{\gamma}$)
vs
Plane Angle (θ)

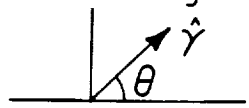

$$\left[\begin{array}{l}\frac{\Delta\gamma}{2} = 0.0023 \\ \frac{\Delta\epsilon}{2} = 0.0015\end{array}\right]$$

N = 356,000
$N_{1.0}$ = 340,000
SS - 26

5.0 mm

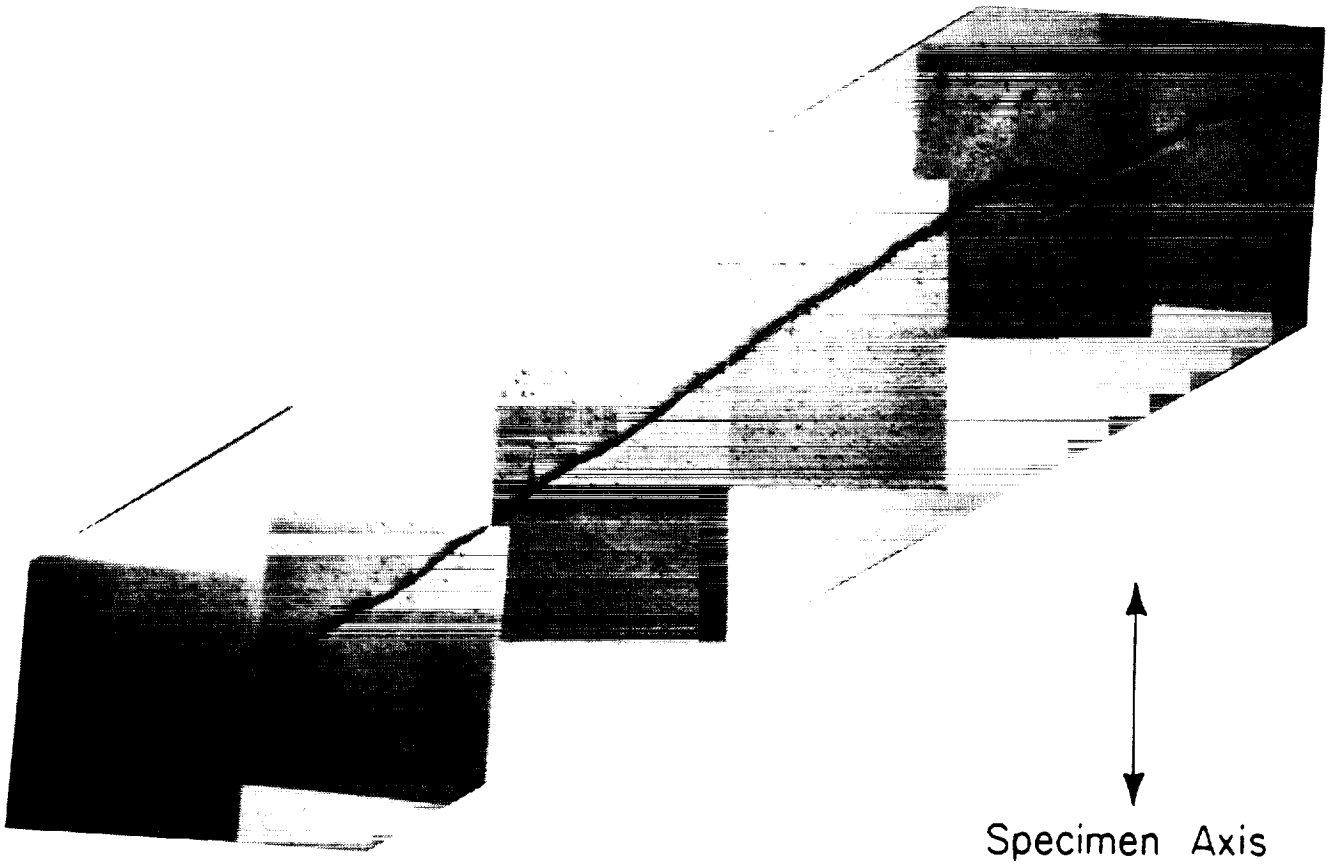

Specimen Axis

Figure B.2 Proportional Path, $\frac{\Delta\epsilon}{2} = 0.0014$, $\frac{\Delta\gamma}{2} = 0.0024$

Proportional ($\gamma/\epsilon = \sqrt{3}$)
($R_\epsilon = -1$, $R_\gamma = -1$)

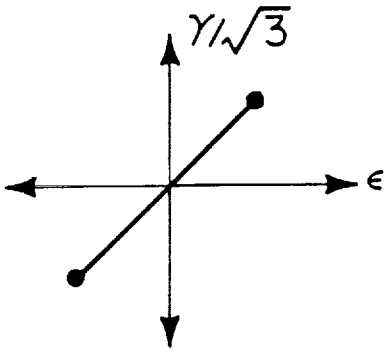

Specimen Axis

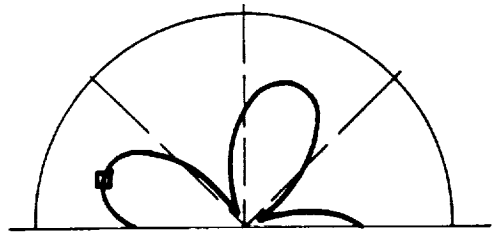

Polar Plot
Shear Strain Amplitude ($\hat{\gamma}$)
vs
Plane Angle (θ)

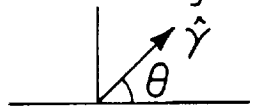

$$\left[\frac{\Delta\gamma}{2} = 0.0023\right]$$
$$\left[\frac{\Delta\epsilon}{2} = 0.0015\right]$$

$N = 440{,}000$
$N_{1.0} = 420{,}000$
SS - 25

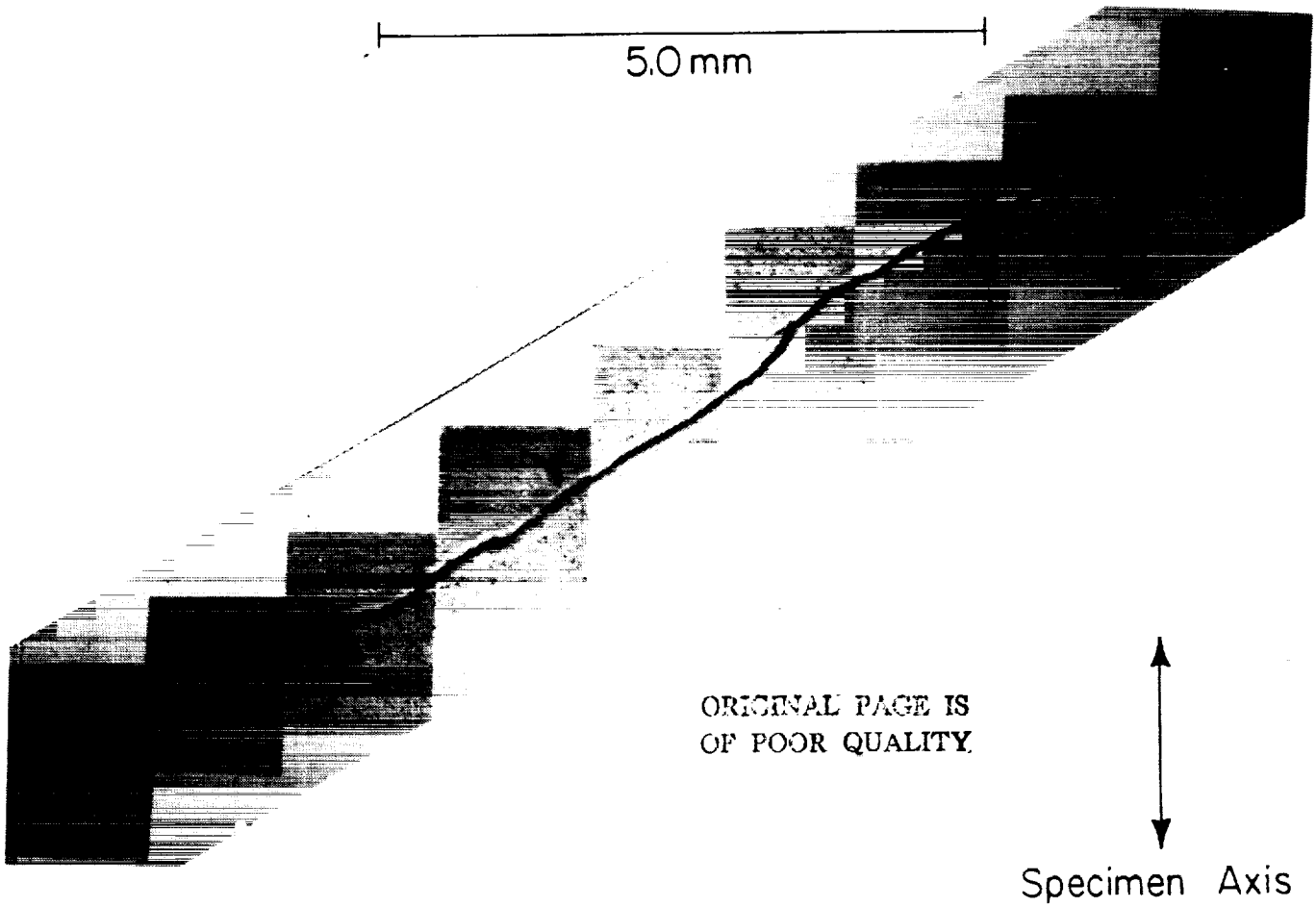

Figure B.3 Proportional Path, $\frac{\Delta\epsilon}{2} = 0.0014$, $\frac{\Delta\gamma}{2} = 0.0024$

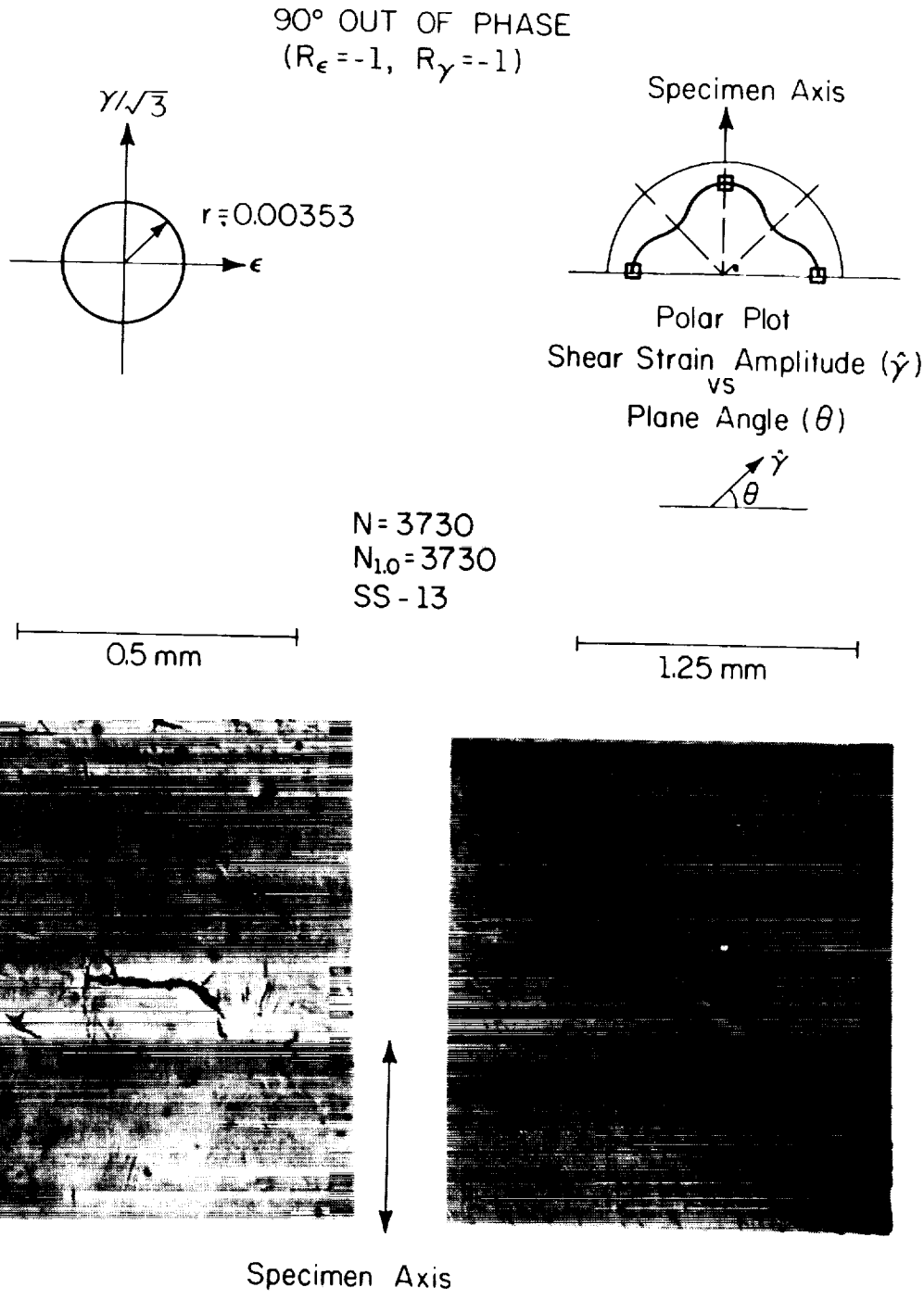

Figure B.4 90° Out-of-Phase, $\frac{\Delta\epsilon}{2}$ = 0.00353, $\frac{\Delta\gamma}{2}$ = 0.00612

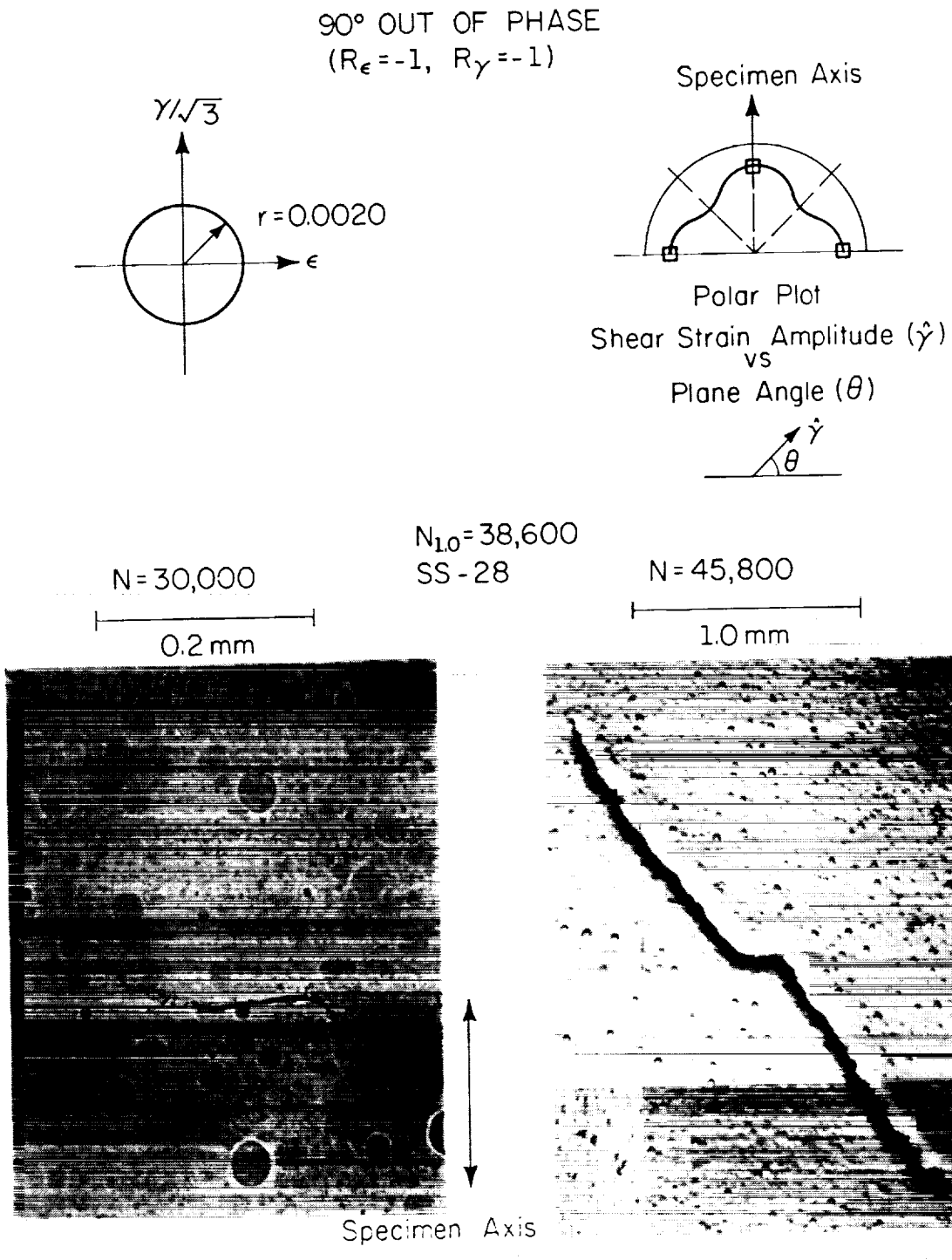

Figure B.5 90° Out-of Phase, $\frac{\Delta\epsilon}{2}$ = 0.002, $\frac{\Delta\gamma}{2}$ = 0.0035

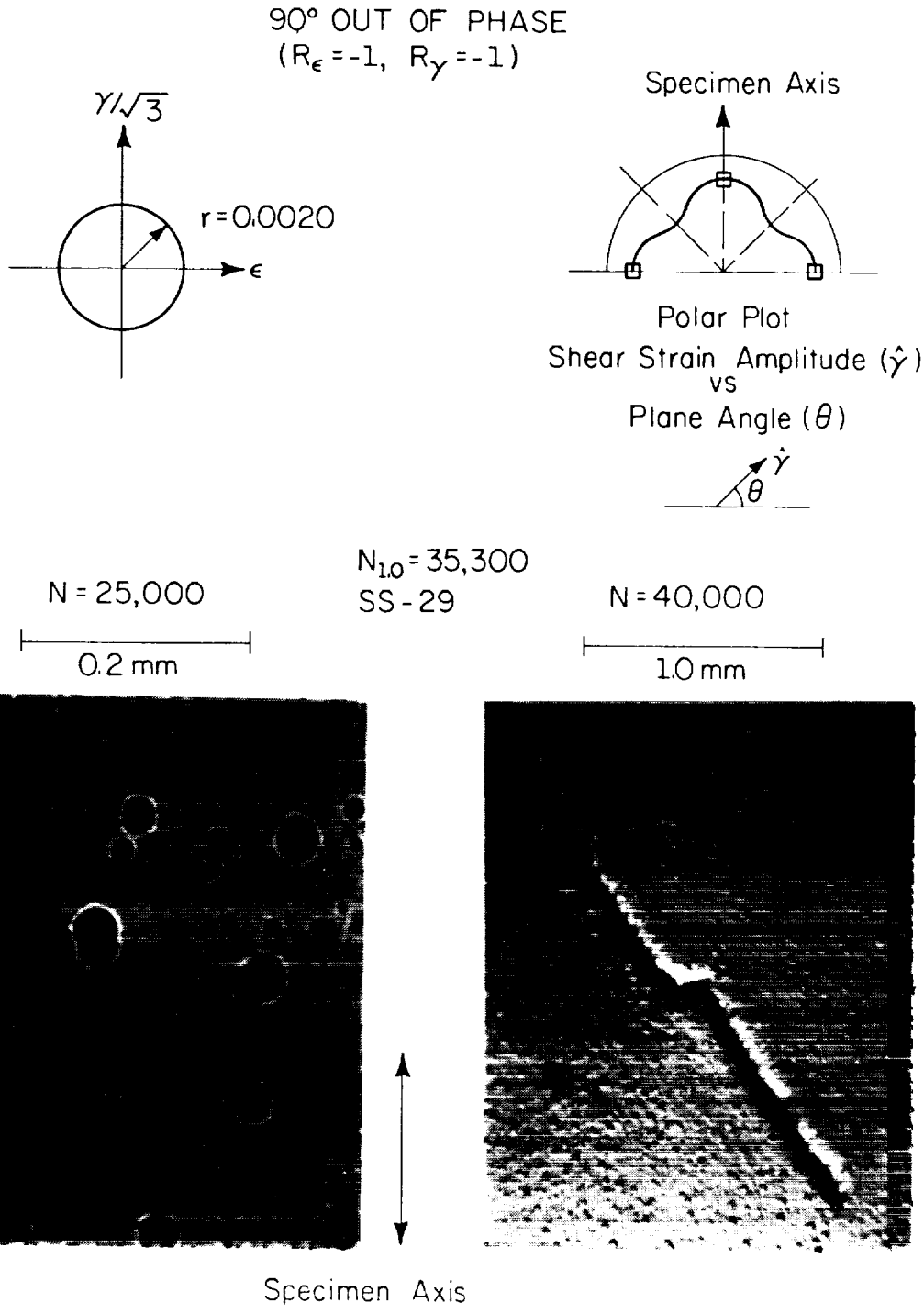

Figure B.6 90° Out-of-Phase, $\frac{\Delta\epsilon}{2}$ = 0.002, $\frac{\Delta\gamma}{2}$ = 0.0035

BOX PATH
(R_ϵ=-1, R_γ=1)

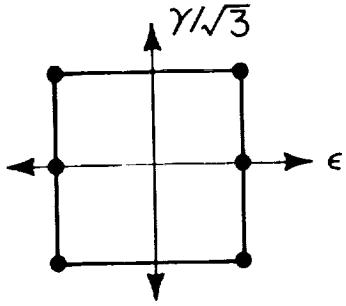

$$\left[\begin{array}{l}\frac{\Delta\gamma}{2}=0.0043\\ \frac{\Delta\epsilon}{2}=0.0025\end{array}\right]$$

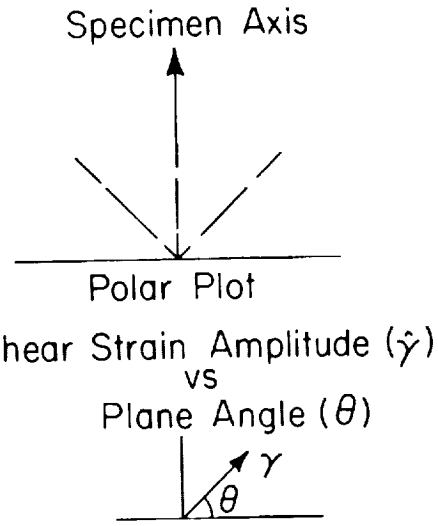

N = 5500
$N_{1.0}$= 6200
SS - 11

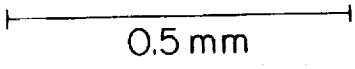

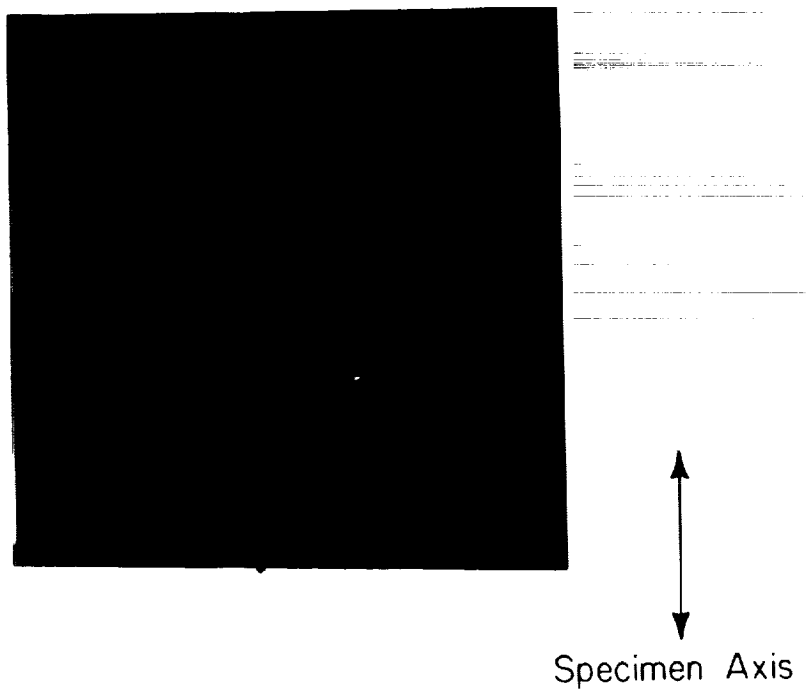

Figure B.7 Box Path, $\frac{\Delta\epsilon}{2}$ = 0.0025, $\frac{\Delta\gamma}{2}$ = 0.0043

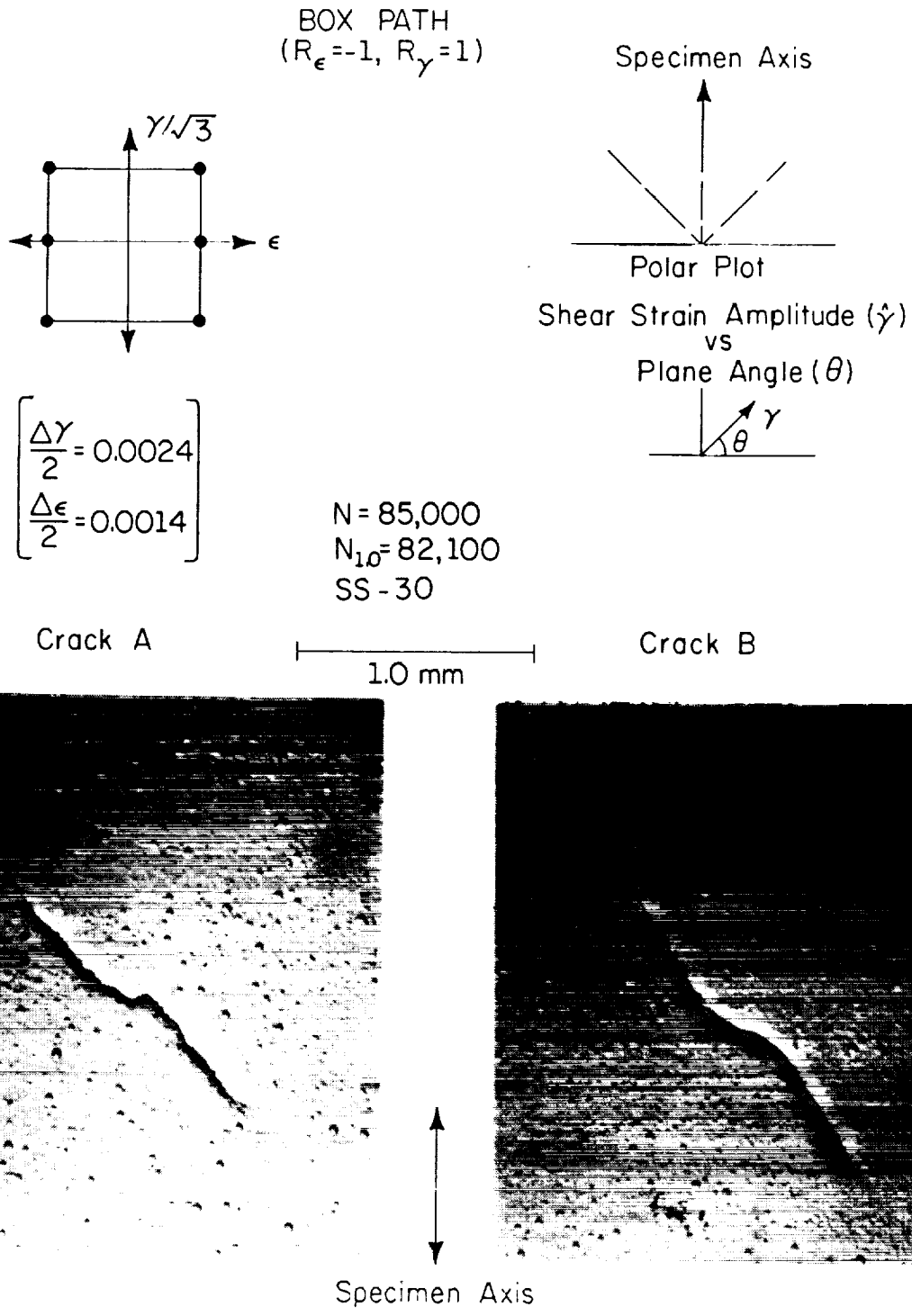

Figure B.8 Box Path, $\frac{\Delta\epsilon}{2}$ = 0.0014, $\frac{\Delta\gamma}{2}$ = 0.0024

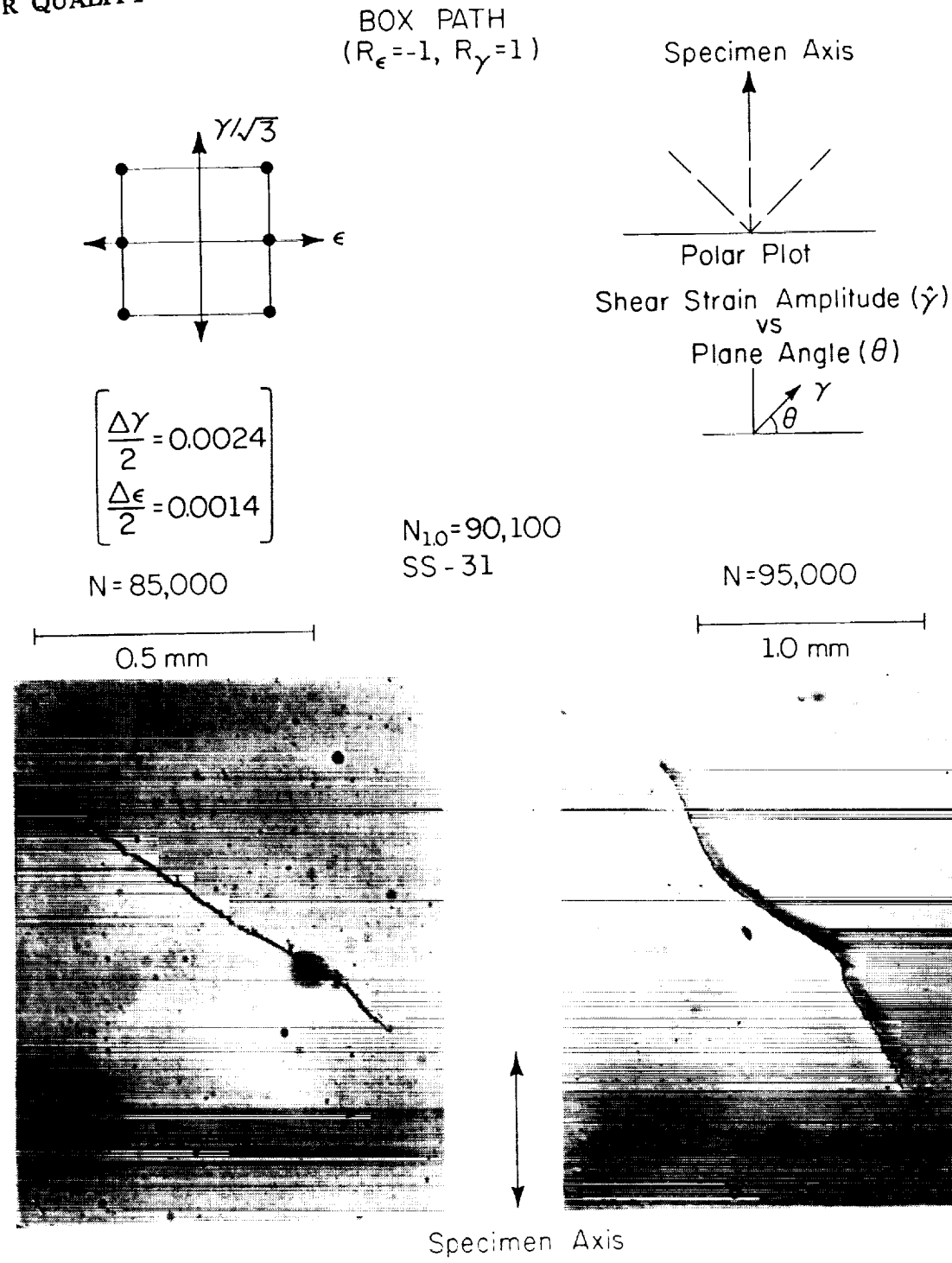

Figure B.9 Box Path, $\frac{\Delta\epsilon}{2}$ = 0.0014, $\frac{\Delta\gamma}{2}$ = 0.0024

TWO BOX PATH
(R_ϵ=-1, R_γ=1)

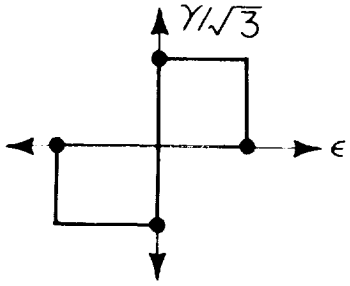

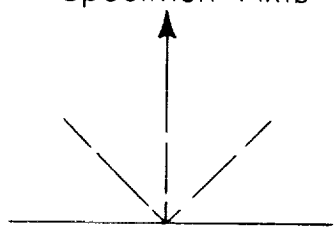

Polar Plot
Shear Strain Amplitude ($\dot{\gamma}$)
vs
Plane Angle (θ)

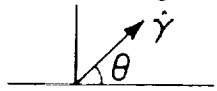

$\frac{\Delta\gamma}{2}$ = 0.0043
$\frac{\Delta\epsilon}{2}$ = 0.0025

N = 6000
$N_{1.0}$ = 7340
SS - 04

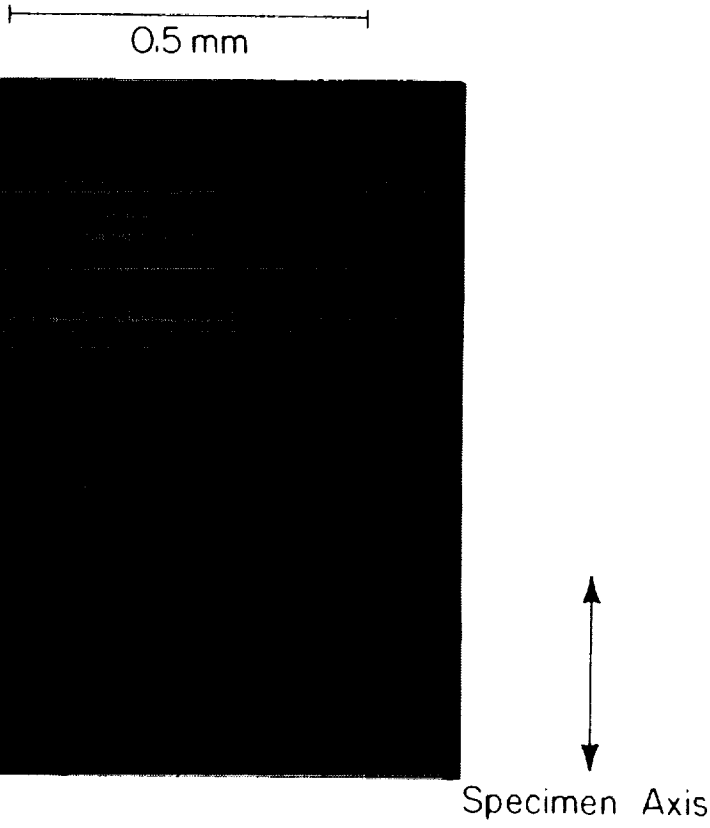

Figure B.10 Two Box Path, $\frac{\Delta\epsilon}{2}$ = 0.0025, $\frac{\Delta\gamma}{2}$ = 0.0043

TWO BOX PATH
(R_ϵ=-1, R_γ=1)

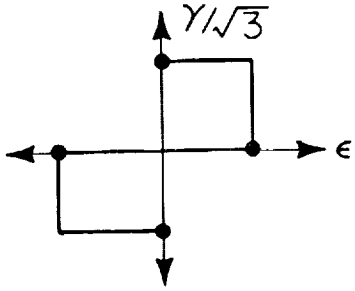

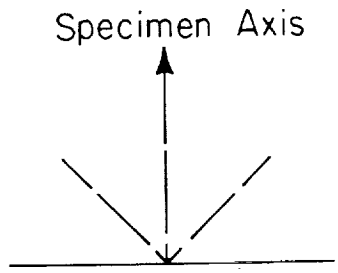

Polar Plot
Shear Strain Amplitude ($\dot{\gamma}$)
vs
Plane Angle (θ)

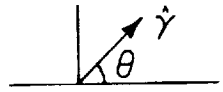

$$\left[\begin{array}{l}\frac{\Delta\gamma}{2}=0.0024\\ \frac{\Delta\epsilon}{2}=0.0014\end{array}\right]$$

N = 190,000
$N_{1.0}$ = 182,000
SS - 32

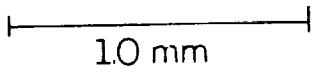

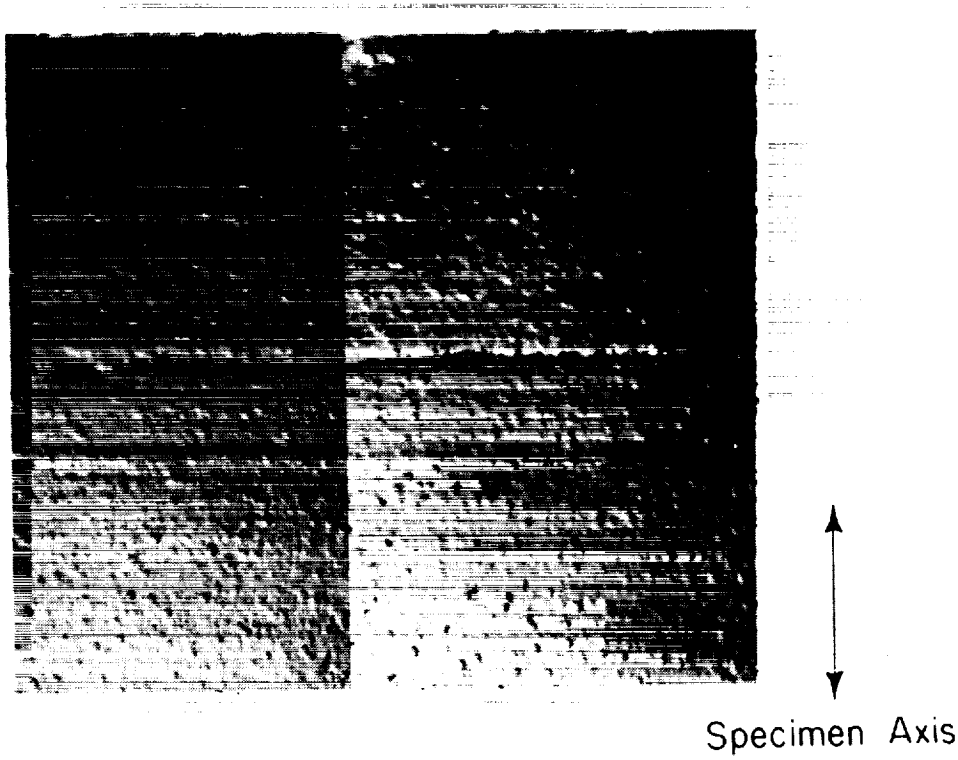

Figure B.11 Two Box Path, $\frac{\Delta\epsilon}{2}$ = 0.0014, $\frac{\Delta\gamma}{2}$ = 0.0024

C-2

TWO BOX PATH
(R_ϵ=-1, R_γ=1)

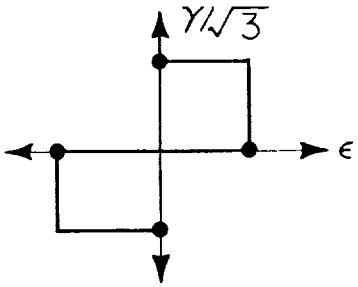

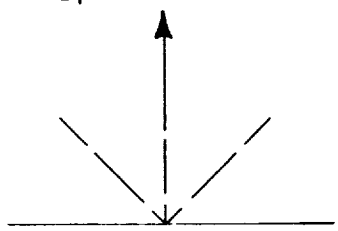

Polar Plot
Shear Strain Amplitude ($\hat{\gamma}$)
vs
Plane Angle (θ)

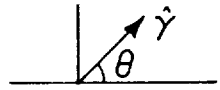

$\frac{\Delta\gamma}{2}$ = 0.0024

$\frac{\Delta\epsilon}{2}$ = 0.0014

N = 180,000
$N_{1.0}$ = 192,200
SS-33

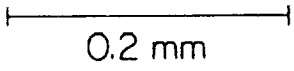

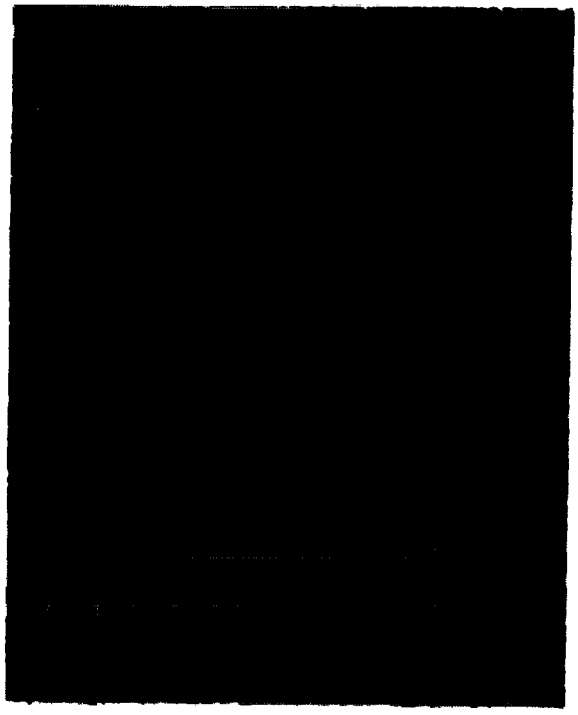

Specimen Axis

Figure B.12 Two Box Path, $\frac{\Delta\epsilon}{2}$ = 0.0014, $\frac{\Delta\gamma}{2}$ = 0.0024

NASA
National Aeronautics and Space Administration

Report Documentation Page

1. Report No.	2. Government Accession No.	3. Recipient's Catalog No.
NASA CR-182126		

4. Title and Subtitle	5. Report Date
Cyclic Fatigue Damage Characteristics Observed for Simple Loadings Extended to Multiaxial Life Prediction	June 1988
	6. Performing Organization Code
7. Author(s)	8. Performing Organization Report No.
David J. Jones and Peter Kurath	None
	10. Work Unit No. 506-60-12
9. Performing Organization Name and Address	11. Contract or Grant No.
University of Illinois Dept. of Mechanical Engineering Urbana, Illinois	NAG3-465
	13. Type of Report and Period Covered
12. Sponsoring Agency Name and Address	Technical Memorandum
National Aeronautics and Space Administration Lewis Research Center Cleveland, Ohio 44135-3191	14. Sponsoring Agency Code

15. Supplementary Notes

Project Manager, Alan D. Freed, Structures Division, NASA Lewis Research Center.

16. Abstract

Fully reversed uniaxial strain controlled fatigue tests were performed on smooth cylindrical specimens made of 304 stainless steel. Fatigue life data and cracking observations for uniaxial tests were compared with life data and cracking behavior observed in fully reversed torsional tests. It was determined that the product of maximum principal strain amplitude and maximum principal stress (Smith, Watson, Topper parameter) provided the best correlation of fatigue lives for these two loading conditions. Implementation of this parameter is in agreement with observed physical damage and it accounts for the variation of stress-strain response, which is unique to specific loading conditions. Biaxial fatigue tests were conducted on tubular specimens employing both in-phase and out-of-phase tension-torsion cyclic strain paths. Cracking observations indicated that the physical damage which occurred in the biaxial tests was similar to the damage observed in uniaxial and torsional tests. The Smith, Watson, and Topper parameter was then extended to predict the fatigue lives resulting from the more complex loading conditions. The correlation of the biaxial fatigue lives with experimental data was within a factor of 2½, when strain hardening due to out-of-phase loading was incorporated into the life estimation analysis.

17. Key Words (Suggested by Author(s))	18. Distribution Statement
Metal fatigue Crack initiation Damage maps Multiaxial fatigue	Unclassified - Unlimited Subject Category 39

19. Security Classif. (of this report)	20. Security Classif. (of this page)	21. No of pages	22. Price*
Unclassified	Unclassified	99	A05

NASA FORM 1626 OCT 86

*For sale by the National Technical Information Service, Springfield, Virginia 22161

o U.S. GOVERNMENT PRINTING OFFICE: 1988 548-157/60435